

PENTAFLUOROPHENYL-BASED SINGLE-CHAIN POLYMER NANOPARTICLES

Jan-Willem Detmer Paats

PENTAFLUOROPHENYL-BASED SINGLE-CHAIN POLYMER NANOPARTICLES

DISSERTATION

to obtain
the degree of doctor at the University of Twente,
on the authority of the rector magnificus,
prof.dr.ir. A. Veldkamp,
on account of the decision of the Doctorate Board,
to be publicly defended
on Wednesday the 11th of October 2023 at 14.45 hours

by

Jan-Willem Detmer Paats

This dissertation has been approved by:

Promotor: Prof. dr. J.J.L.M. Cornelissen

Co-promotor: dr. ir. J.M.J. Paulusse

This thesis was supported by the funding from Health–Holland, Top Sector Life Science & Health and Alzheimer Netherlands. The research in this dissertation has been conducted in the Biomolecular Nanotechnology (BNT) group at the MESA+ institute, Faculty of Science and Technology, University of Twente, the Netherlands.

Cover design: Nina van Tuikwerd

Printed by: Gildeprint

ISBN: 978-90-365-5765-8

DOI: 10.3990/1.9789036557665

© 2023 Jan-Willem Detmer Paats, The Netherlands. All rights reserved. No parts of this thesis may be reproduced, stored in a retrieval system or transmitted in any form or by any means without permission of the author. Alle rechten voorbehouden. Niets uit deze uitgave mag worden vermenigvuldigd, in enige vorm of op enige wijze, zonder voorafgaande schriftelijke toestemming van de auteur.

Graduation committee:

Chair/secretary	Prof. dr. J.L. Herek University of Twente
Promotor	Prof. dr. J.J.L.M. Cornelissen University of Twente
Co-promotor	dr. ir. J.M.J. Paulusse University of Twente
Committee members	Prof. dr. D.W. Grijpma University of Twente dr. D. Klinger Free University Berlin dr. ir. S. Lindhoud University of Twente Prof. dr. E. Mastrobattista Utrecht University Prof. dr. ir. A. Palmans Eindhoven University of Technology

Table of Contents

Chapter 1	1
Preface	
Chapter 2	13
Pentafluorophenyl-based single-chain polymer nanoparticles as a modular platform for controlling cellular uptake	
Chapter 3	39
Transport of single-chain polymer nanoparticles across the blood-brain barrier	
Chapter 4	59
Controlled drug delivery by subcellular targeting with single-chain polymer nanoparticles	
Chapter 5	83
Dual-reactive single-chain polymer nanoparticles for orthogonal functionalization through active ester and click chemistry	
Chapter 6	117
Future outlook and additional findings	
Samenvatting	131
Summary	133
Dankwoord	135

Chapter 1

Preface

1.1 Introduction

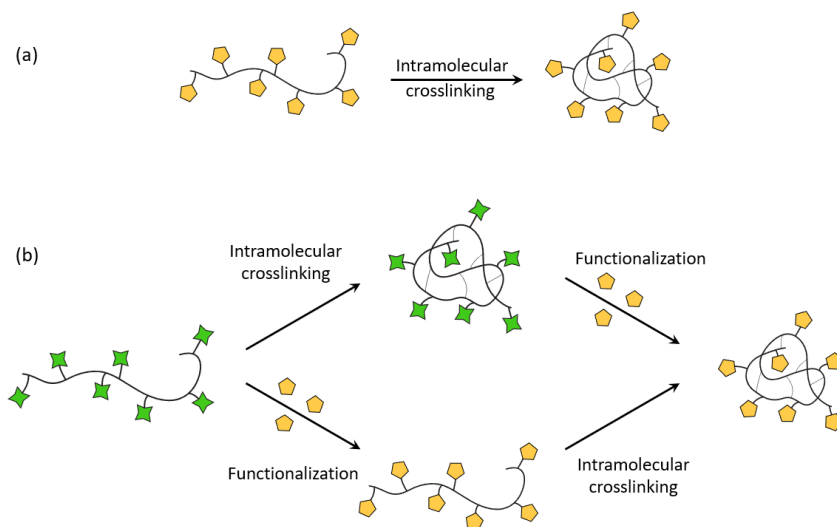
Engineering nanomaterials offers the opportunity to enhance disease diagnosis and improve its treatment efficacy. Nanomaterials have the capability to address the shortcomings associated with traditional drug delivery methods, such as inadequate biodistribution profiles or impaired intracellular trafficking.¹ One commonly employed type of nanomaterials are polymeric nanoparticles (NPs). Polymeric NPs exhibit unique properties based on their high surface to volume ratio and similar dimensions as observed in biological systems.²⁻³ Owing to these characteristics, these nanomaterials have found widespread use in biomedical applications, not only in the field of drug delivery, but also in a wider context, ranging from biosensing⁴⁻⁵ to imaging.⁶ For NPs to be effective, they need to be able to interact in a controlled manner with target sites within the body. For example, the negatively charged cell membrane can be targeted by equipping the NPs surface with cationic groups.⁷ Alternatively, recognition of NPs can be promoted by specific elements present on the cell surface, such as a transporter proteins or receptors. Coating NPs with appropriate ligands can therefore improve local retention and subsequent endocytosis.⁸ A key advantage of using NPs is the aspect of multivalency, where multiple ligands bind simultaneously to a cell surface, thereby increasing the NP's affinity for the target.⁹ Multivalency depends on many factors, including binding strength between ligand and receptor, as well as the number of ligands able to participate in binding events.¹⁰ Careful tuning of the surface properties of NPs is therefore of utmost important to achieving selective and specific binding to cell surfaces. Furthermore, NP size, shape and flexibility play an important role in cellular uptake.¹¹ An increase in cellular association of organic polymeric NPs was shown in cancer (HeLa) cells with decreasing particle size, with a factor 3 difference between 40 nm and 7 nm particles.¹² Flexible particles potentially allow for more ligand-receptor binding interactions. However, this comes with the downside of self-limiting behavior, where the construct crowds the surface with inert parts. Therefore, a structure inbetween solid and flexible could potentially provide an optimum for specific cellular targeting.¹³

An interesting type of small NPs are single-chain polymer nanoparticles (SCNPs).¹⁴⁻¹⁵ SCNPs are soft and semi-flexible particles in the size range of proteins, formed by intramolecular crosslinking of a single polymer chain. In effect, NP size is directly dependent on the length of the precursor polymer,¹⁶ which is readily controlled by controlled polymerization techniques that have become available over the past decades¹⁷⁻¹⁸ and on the employed crosslinking density.¹⁹ The first intramolecular crosslinking of polymers was already performed in 1962,²⁰ but it was not until 2002 that the process became well-controlled at higher scales.²¹ Since then, a wide variety of different methods have been developed to intramolecularly crosslink precursor polymer chains to form functional SCNPs. The

formation and biomedical applications of SCNPs have been reviewed multiple times over the (recent) years.^{15-16, 22-25} Examples of SCNPs in a biomedical setting include cell targeting,²⁶⁻²⁷ catalysis,²⁸⁻²⁹ enzyme mimicry³⁰⁻³¹ and antimicrobial activity.³²⁻³³ For SCNPs to be effective in a biomedical setting, for example drug delivery or imaging, the particle surface functionalization needs to be carefully tuned and optimized towards the desired application. In this preface Chapter, the focus lies on the different functionalization methods currently available to equip SCNPs with functional ligands. In Chapter 6, we subsequently reflect on how to proceed to advance the field of functional SCNPs towards attaining more resolution in functionalization degree, as well as improving the screening efficiency.

1.2 Post-formation functionalization of SCNPs

Introduction of surface functionality on SCNPs has been achieved by direct polymerization of functional monomers, followed by intramolecular crosslinking of the functional precursor polymers (Scheme 1.1a). For example, glucose-functional methacrylate monomers were directly co-polymerized with a crosslinkable group and subsequently intramolecularly folded to form functional glyco-SCNPs.³⁴ This pathway does require the monomers to be compatible both with the (controlled) polymerization technique, as well as the crosslinking chemistry. This severely limits the scope of ligands that can be introduced.



Scheme 1.1. Intramolecular crosslinking of a precursor polymer chain to yield well-defined single-chain polymer nanoparticles (SCNPs). Functional SCNPs can be formed by direct polymerization of functional monomers, followed by crosslinking (a). Alternatively, functionalization can be introduced post-polymerization, either before crosslinking (b, top pathway) or after crosslinking (b, bottom pathway).

By employing post-polymerization modification (PPM), a well-developed concept from the field of polymer chemistry, the library of functional handles that can be incorporated onto SCNPs is greatly expanded.³⁵⁻³⁹ PPM is based on the (co-) polymerization of monomers bearing reactive moieties, which can be used for subsequent conjugation of functional ligands after polymerization. This allows for the introduction of chemical moieties, which are otherwise incompatible with the polymerization method or interfere with the required crosslinking reaction. As an example, poly(acrylic acid) polymers were equipped photo-crosslinkable units through post-polymerization esterification and subsequently folded into SCNPs (schematically depicted in Scheme 1.1b, bottom pathway).⁴⁰ Kröger et al. showed how water-solubility could be introduced into SCNPs through hydrolyzing functional monomers, either pre- or post-intramolecular chain collapse, with no distinct differences between the final SCNPs prepared via the two pathways.⁴¹ This approach circumvents the requirement of a specific solvent for nanoparticle fabrication. A different elegant methodology for the synthesis of well-defined SCNPs was developed by Palmans and Meijer and coworkers. By introducing a hydrogen-bonding motif into a reactive pre-polymer, the polymers self-assemble into SCNPs. Systematically introducing different functional moieties, beside the crosslinking-agent, yielded a large variety of functional SCNPs which were used in a biomedical setting.^{28, 42-44} A similar approach was used by the group of Zimmerman. Hydrophobic collapse of the polymer backbone in water was induced by equipping a polymer with positively charged alkyl-ammonium pendants through post-polymerization modification, followed by subsequent covalent intramolecular crosslinking to form SCNPs. These SCNPs were used as synthetic enzymes to perform catalysis, as well as transport proteins into a cells.^{27, 30, 45-46}

However, by starting with the functionalization of the pre-polymer, the subsequent crosslinking chemistry still needs to be compatible with the introduced ligands, limiting the modularity. More importantly, this approach may alter the conformation of the polymer and therefore influence crosslinking behavior and eventually also the SCNPs' colloidal properties. For example, a range of co-polymers was created through PPM with a hydrogen-bonding motif for the supramolecular folding into SCNPs. Upon changing the ratio of hydrophobic and hydrophilic pendants while keeping the degree of polymerization and crosslinker-density constant, a change in the folding behavior of the supramolecular SCNPs was observed.⁴⁷ Therefore, post-formation modification of SCNPs, analogous to post-polymerization modification of polymers, has emerged as a strategy to rapidly and easily prepare functional SCNPs. Introduction of functional groups after intramolecular chain collapse ensures that the initial 3D-structure of the SCNPs remains largely unaltered, decoupling particle formation from the functionalization step (schematically depicted in Scheme 1.1b, top pathway). Furthermore, the scope of functional group incorporation is widened, since it no longer requires compatibility

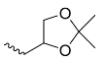
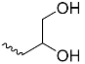

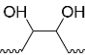
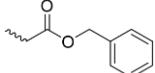
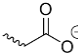
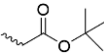
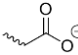
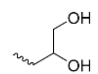
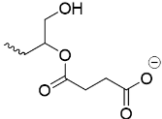
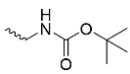
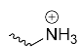
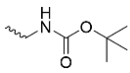
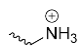
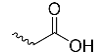
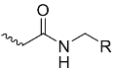

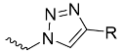
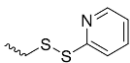
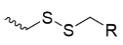
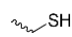
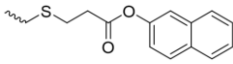
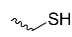
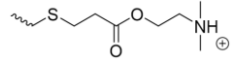
with the crosslinking methodology. Post-formation modification may therefore facilitate systematic investigations into the structure-property relationships of SCNPs.⁴⁸

Over the years, a number of different chemistries has been explored to tailor the SCNP surface post-formation, as summarized in Table 1.1. For example, Loinaz and co-workers functionalized SCNPs surface-terminated with carboxylic acids, with peptides through amidation for targeting pancreatic tumors,⁴⁹ whereas SCNPs with pendant benzyl esters were rendered water-soluble by reduction through hydrogenation.⁵⁰

An outstanding issue during the post-formation functionalization of SCNPs is the lack of control over the amount of ligands that are incorporated on the particle surface. Since most of the reactions mentioned in Table 1.1 have limited efficiency and selectivity, functional ligands or reagents are typically added in large excess to ensure full conversion of all reactive handles. Only in the case of the succinic anhydride ring-opening, the functionalization grade is gradually increased to create a range of functional SCNPs.⁵¹⁻⁵² Still, the quantification of incorporation is impeded, since routine techniques, such as UV-Vis, FT-IR and ¹H NMR spectroscopy, often lack the specificity to discern between signals from the backbone and the functional ligand. This becomes particularly problematic when trying to create libraries of SCNPs with incremental introduction of surface moieties. Such ranges are required to find the optimal density for effective cellular interactions, because of the complex interplay between ligand and receptors.⁹ For example, self-assembled micellar NPs with increasing pendant glucose-moieties showed an optimum glucose-density for efficient brain uptake, with total coverage of the surface with glucose leading to decreased efficacy.⁶⁴⁻⁶⁵ Furthermore, this glucose-optimum turned out to be dependent on the type of construct, indicating the lack of generic design rules and thus the need for facile post-modification methods to attain well-defined and uniform sets of functional NPs.

Chapter 1

Table 1.1. Overview of covalent post-formation modifications on SCNPs.

Pre-functionalization	Post-functionalization	Method	Goal	Refs
		Acidic conditions	Water-solubility	12, 16, 51-54
		K_2OsO_4	Water-solubility	12, 54
		H_2 , Pd/C	Water-solubility	50
		TFA	Water-solubility	55
		Succinic anhydride ring-opening	Anionic charge range	51-52
		HCl in dioxane	Intermediate for subsequent amidation	56
		TFA	Anti-microbial activity	57
		Amide coupling	Peptide coupling	49, 58-59
		Cu(I) catalyzed alkyne azide click-conditions	Zwitterionic or labelling	60-61
		Disulfide-exchange	Protein and peptide coupling	56, 62
		Thiol-Michael addition	Labelling	63
		Thiol-Michael addition	Positive charge	63

As a result of the aforementioned functionalization problems, systematic investigations into the influence of surface chemistry of SCNPs on biomedical applications are still in their infancy. An effective method to tackle the functionalization problem is the use of active pentafluorophenyl (PFP) esters. Introduced in 2005 in the field of polymer chemistry,⁶⁶ PFP-esters are readily substituted with functional primary amines, a process which can be conveniently followed by background-free ¹⁹F NMR spectroscopy. Equipping SCNPs with pendant PFP-esters would therefore allow to effectively modify the SCNP surface in a stepwise fashion, with generic chemical structures to alter physicochemical properties, such as surface charge or hydrophilicity, as well as the introduction of targeting ligands. This approach can provide the means to elucidate structure-activity relationships of SCNPs to identify the optimal conditions for efficient cellular interactions and develop new nanomedicine-based therapies.

1.3 Aim and outline of this thesis

The aim of this thesis is to develop a modular single-chain polymer nanoparticle platform, which can be used to systematically study the influence of surface functionalization on cellular interactions.

In **Chapter 2**, we synthesize PFP-SCNPs from a co-polymer precursor containing pendant PFP-groups and protected thiols. After deprotection, the PFP-SCNPs are formed through intramolecular crosslinking with a di-acrylate crosslinker by a thiol-Michael addition. After formation, we study the influence of tertiary amines on the intracellular delivery of SCNPs. The number of protonatable groups on the SCNP surface is systematically increased and the set of SCNPs is evaluated for cellular uptake and intracellular location in endothelial cells.

In **Chapter 3**, we explore the influence of tertiary amines on the passage of SCNPs through the blood-brain barrier (BBB). A set of SCNPs with increasing surface protonatable groups is evaluated on a filter-free BBB model, in which transcytosis and the endosomal release after cellular uptake are studied.

In **Chapter 4**, SCNPs are used for controlled drug delivery of atovaquone, a common anti-malarial drug, currently being repurposed as an anti-cancer drug. Atovaquone is conjugated to the PFP-SCNPs and the influence of surface charge, as well as protonatability of the SCNPs to intracellularly deliver the drug and improve its efficacy to induce apoptosis is studied.

In **Chapter 5**, PFP-chemistry is combined with copper(I)-catalyzed azide alkyne cycloaddition (CuAAC) click chemistry to further expand the modularity of the PFP-SCNP system. SCNPs are ligated with increasing amounts of amino-alkyne moieties and subsequently reacted with azido-propylglucose through two different

conjugation positions to arrive at a set of glyco-SCNPs. The influence of the glucose conjugation position and ligand density on cellular uptake is studied in HeLa cells.

In **Chapter 6**, we describe a possible method for scaling up SCNPs synthesis and techniques to attain more elaborate libraries of functional SCNPs for structure-activity studies. Furthermore, a first biodistribution study in mice is performed.

1.4 References

1. Mitchell, M. J.; Billingsley, M. M.; Haley, R. M.; Wechsler, M. E.; Peppas, N. A.; Langer, R., Engineering precision nanoparticles for drug delivery. *Nat Rev Drug Discov* **2021**, *20* (2), 101-124.
2. Mout, R.; Moyano, D. F.; Rana, S.; Rotello, V. M., Surface functionalization of nanoparticles for nanomedicine. *Chem Soc Rev* **2012**, *41* (7), 2539-44.
3. Zielinska, A.; Carreiro, F.; Oliveira, A. M.; Neves, A.; Pires, B.; Venkatesh, D. N.; Durazzo, A.; Lucarini, M.; Eder, P.; Silva, A. M.; Santini, A.; Souto, E. B., Polymeric Nanoparticles: Production, Characterization, Toxicology and Ecotoxicology. *Molecules* **2020**, *25* (16).
4. Chen, X.; Hussain, S.; Abbas, A.; Hao, Y.; Malik, A. H.; Tian, X.; Song, H.; Gao, R., Conjugated polymer nanoparticles and their nanohybrids as smart photoluminescent and photoresponsive material for biosensing, imaging, and theranostics. *Mikrochim Acta* **2022**, *189* (3), 83.
5. Paisley, N. R.; Tonge, C. M.; Hudson, Z. M., Stimuli-Responsive Thermally Activated Delayed Fluorescence in Polymer Nanoparticles and Thin Films: Applications in Chemical Sensing and Imaging. *Front Chem* **2020**, *8*, 229.
6. Kakkar, A.; Traverso, G.; Farokhzad, O. C.; Weissleder, R.; Langer, R., Evolution of macromolecular complexity in drug delivery systems. *Nat Rev Chem* **2017**, *1* (8).
7. Ramos, J.; Forcada, J.; Hidalgo-Alvarez, R., Cationic polymer nanoparticles and nanogels: from synthesis to biotechnological applications. *Chem Rev* **2014**, *114* (1), 367-428.
8. Sanna, V.; Sechi, M., Therapeutic Potential of Targeted Nanoparticles and Perspective on Nanotherapies. *ACS Med Chem Lett* **2020**, *11* (6), 1069-1073.
9. Tjandra, K. C.; Thordarson, P., Multivalency in Drug Delivery-When Is It Too Much of a Good Thing? *Bioconjug Chem* **2019**, *30* (3), 503-514.
10. Martinez-Veracoechea, F. J.; Frenkel, D., Designing super selectivity in multivalent nanoparticle binding. *Proc Natl Acad Sci U S A* **2011**, *108* (27), 10963-8.
11. Zhu, M.; Nie, G.; Meng, H.; Xia, T.; Nel, A.; Zhao, Y., Physicochemical Properties Determine Nanomaterial Cellular Uptake, Transport, and Fate. *Accounts of Chemical Research* **2013**, *46* (3), 622-631.
12. Bai, Y.; Hang, X.; Wu, P.; Feng, X.; Hwang, K.; Lee, J. M.; Phang, X. Y.; Lu, Y.; Zimmerman, S. C., Chemical Control over Cellular Uptake of Organic Nanoparticles by Fine Tuning Surface Functional Groups. *ACS Nano* **2015**, *9* (10), 10.
13. Woythe, L.; Tito, N. B.; Albertazzi, L., A quantitative view on multivalent nanomedicine targeting. *Adv Drug Deliv Rev* **2021**, *169*, 1-21.
14. Alqarni, M. A. M.; Waldron, C.; Yilmaz, G.; Becer, C. R., Synthetic Routes to Single Chain Polymer Nanoparticles (SCNPs): Current Status and Perspectives. *Macromol Rapid Commun* **2021**, e2100035.
15. Hamelmann, N. M.; Paulusse, J. M. J., Single-chain polymer nanoparticles in biomedical applications. *J Control Release* **2023**.
16. Kroger, A. P. P.; Hamelmann, N. M.; Juan, A.; Lindhoud, S.; Paulusse, J. M. J., Biocompatible Single-Chain Polymer Nanoparticles for Drug Delivery - a Dual Approach. *ACS applied Materials & Interfaces* **2018**, *20*, 6.
17. Braunecker, W. A.; Matyjaszewski, K., Controlled/living radical polymerization: Features, developments, and perspectives. *Progress in Polymer Science* **2007**, *32* (1), 93-146.

18. Corrigan, N.; Jung, K.; Moad, G.; Hawker, C. J.; Matyjaszewski, K.; Boyer, C., Reversible-deactivation radical polymerization (Controlled/living radical polymerization): From discovery to materials design and applications. *Progress in Polymer Science* **2020**, *111*.
19. Beck, J. B.; Killops, K. L.; Kang, T.; Sivanandan, K.; Bayles, A.; Mackay, M. E.; Wooley, K. L.; Hawker, C. J., Facile Preparation of Nanoparticles by Intramolecular Crosslinking of Isocyanate Functionalized Copolymers. *Macromolecules* **2009**, *42* (15), 5629-5635.
20. Kuhn, W.; Balmer, G., Crosslinking of single linear macromolecules. *Journal of Polymer Science* **1962**, *57* (165), 311-319.
21. Harth, E.; Horn, B. V.; Lee, V. Y.; Germack, D. S.; Gonzales, C. P.; Miller, R. D.; Hawker, C. J., A Facile Approach to Architecturally Defined Nanoparticles via Intramolecular Chain Collapse. *Journal of the American Chemical Society* **2002**, *124* (29), 8653-8660.
22. De-La-Cuesta, J.; Gonzalez, E.; Pomposo, J. A., Advances in Fluorescent Single-Chain Nanoparticles. *Molecules* **2017**, *22* (11).
23. Rubio-Cervilla, J.; Gonzalez, E.; Pomposo, J. A., Advances in Single-Chain Nanoparticles for Catalysis Applications. *Nanomaterials (Basel)* **2017**, *7* (10).
24. Chen, J.; Garcia, E. S.; Zimmerman, S. C., Intramolecularly Cross-Linked Polymers: From Structure to Function with Applications as Artificial Antibodies and Artificial Enzymes. *Acc Chem Res* **2020**, *53* (6), 1244-1256.
25. Altintas, O.; Barner-Kowollik, C., Single-Chain Folding of Synthetic Polymers: A Critical Update. *Macromol Rapid Commun* **2016**, *37* (1), 29-46.
26. Hamelmann, N. M.; Paats, J. D.; Paulusse, J. M. J., Cytosolic Delivery of Single-Chain Polymer Nanoparticles. *ACS Macro Lett* **2021**, *10* (11), 1443-1449.
27. Chen, J.; Li, K.; Shon, J. S. L.; Zimmerman, S. C., Single-Chain Nanoparticle Delivers a Partner Enzyme for Concurrent and Tandem Catalysis in Cells. *J Am Chem Soc* **2020**, *142* (10), 4565-4569.
28. Liu, Y.; Pujals, S.; Stals, P. J. M.; Paulohrl, T.; Presolski, S. I.; Meijer, E. W.; Albertazzi, L.; Palmans, A. R. A., Catalytically Active Single-Chain Polymeric Nanoparticles: Exploring Their Functions in Complex Biological Media. *J Am Chem Soc* **2018**, *140* (9), 3423-3433.
29. Zeng, R.; Chen, L.; Yan, Q., CO₂-Folded Single-Chain Nanoparticles as Recyclable, Improved Carboxylase Mimics. *Angew Chem Int Ed Engl* **2020**.
30. Chen, J.; Li, K.; Bonson, S. E.; Zimmerman, S. C., A Bioorthogonal Small Molecule Selective Polymeric "Clickase". *J Am Chem Soc* **2020**, *142* (32), 13966-13973.
31. Huo, M.; Wang, N.; Fang, T.; Sun, M.; Wei, Y.; Yuan, J., Single-chain polymer nanoparticles: Mimic the proteins. *Polymer* **2015**, *66*, A11-A21.
32. Falciani, C.; Zevolini, F.; Brunetti, J.; Riolo, G.; Gracia, R.; Marradi, M.; Loinaz, I.; Ziemann, C.; Cossío, U.; Llop, J.; Bracci, L.; Pini, A., Antimicrobial Peptide-Loaded Nanoparticles as Inhalation Therapy for *Pseudomonas aeruginosa* Infections. *International Journal of Nanomedicine* **2020**, *Volume 15*, 1117-1128.
33. Nguyen, T. K.; Lam, S. J.; Ho, K. K.; Kumar, N.; Qiao, G. G.; Egan, S.; Boyer, C.; Wong, E. H., Rational Design of Single-Chain Polymeric Nanoparticles That Kill Planktonic and Biofilm Bacteria. *ACS Infect Dis* **2017**, *3* (3), 237-248.
34. Kroger, A. P. P.; Komil, M. I.; Hamelmann, N. M.; Juan, A.; Stenzel, M. H.; Paulusse, J. M. J., Glucose Single-Chain Polymer Nanoparticles for Cellular Targeting. *ACS Macro Lett* **2019**, *8* (1), 95-101.
35. Chen, X.; Michinobu, T., Postpolymerization Modification: A Powerful Tool for the Synthesis and Function Tuning of Stimuli-Responsive Polymers. *Macromolecular Chemistry and Physics* **2022**, *223* (1), 2100370.
36. Rimmele, M.; Glockhofer, F.; Heeney, M., Post-polymerisation approaches for the rapid modification of conjugated polymer properties. *Mater Horiz* **2022**, *9* (11), 2678-2697.

37. Soares, F. A.; Steinbüchel, A., Enzymatic and Chemical Approaches for Post-Polymerization Modifications of Diene Rubbers: Current state and Perspectives. *Macromolecular Bioscience* **2021**, *21* (12).
38. Shahrokhinia, A.; Biswas, P.; Reuther, J. F., Orthogonal synthesis and modification of polymer materials. *Journal of Polymer Science* **2021**, *59* (16), 1748-1786.
39. Blasco, E.; Sims, M. B.; Goldmann, A. S.; Sumerlin, B. S.; Barner-Kowollik, C., 50th Anniversary Perspective: Polymer Functionalization. *Macromolecules* **2017**, *50* (14), 5215-5252.
40. Heiler, C.; Offenloch, J. T.; Blasco, E.; Barner-Kowollik, C., Photochemically Induced Folding of Single Chain Polymer Nanoparticles in Water. *ACS Macro Lett* **2017**, *6* (1), 56-61.
41. Kroger, A. P. P.; Hamelmann, N. M.; Juan, A.; Lindhoud, S.; Paulusse, J. M. J., Biocompatible Single-Chain Polymer Nanoparticles for Drug Delivery-A Dual Approach. *ACS Appl Mater Interfaces* **2018**, *10* (37), 30946-30951.
42. Deng, L.; Albertazzi, L.; Palmans, A. R. A., Elucidating the Stability of Single-Chain Polymeric Nanoparticles in Biological Media and Living Cells. *Biomacromolecules* **2022**, *23* (1), 326-338.
43. Liu, Y.; Pauloehr, T.; Presolski, S. I.; Albertazzi, L.; Palmans, A. R.; Meijer, E. W., Modular Synthetic Platform for the Construction of Functional Single-Chain Polymeric Nanoparticles: From Aqueous Catalysis to Photosensitization. *J Am Chem Soc* **2015**, *137* (40), 13096-105.
44. Morgese, G.; de Waal, B. F. M.; Varela-Aramburu, S.; Palmans, A. R. A.; Albertazzi, L.; Meijer, E. W., Anchoring Supramolecular Polymers to Human Red Blood Cells by Combining Dynamic Covalent and Non-Covalent Chemistries. *Angew Chem Int Ed Engl* **2020**.
45. Chen, J.; Wang, J.; Li, K.; Wang, Y.; Gruebele, M.; Ferguson, A. L.; Zimmerman, S. C., Polymeric "Clickase" Accelerates the Copper Click Reaction of Small Molecules, Proteins, and Cells. *J Am Chem Soc* **2019**, *141* (24), 9693-9700.
46. Xiong, T. M.; Garcia, E. S.; Chen, J.; Zhu, L.; Alzona, A. J.; Zimmerman, S. C., Enzyme-like catalysis by single chain nanoparticles that use transition metal cofactors. *Chem Commun (Camb)* **2022**, *58* (7), 985-988.
47. Ter Huurne, G. M.; de Windt, L. N. J.; Liu, Y.; Meijer, E. W.; Voets, I. K.; Palmans, A. R. A., Improving the Folding of Supramolecular Copolymers by Controlling the Assembly Pathway Complexity. *Macromolecules* **2017**, *50* (21), 8562-8569.
48. Gruber, A.; Navarro, L.; Klinger, D., Reactive Precursor Particles as Synthetic Platform for the Generation of Functional Nanoparticles, Nanogels, and Microgels. *Advanced Materials Interfaces* **2019**, *7* (5).
49. Benito, A. B.; Aiertza, M. K.; Marradi, M.; Gil-Iceta, L.; Shekhter Zahavi, T.; Szczupak, B.; Jimenez-Gonzalez, M.; Reese, T.; Scanziani, E.; Passoni, L.; Matteoli, M.; De Maglie, M.; Orenstein, A.; Oron-Herman, M.; Kostenich, G.; Buzhansky, L.; Gazit, E.; Grande, H. J.; Gomez-Vallejo, V.; Llop, J.; Loinaz, I., Functional Single-Chain Polymer Nanoparticles: Targeting and Imaging Pancreatic Tumors in Vivo. *Biomacromolecules* **2016**, *17* (10), 3213-3221.
50. Qian, G.; Zhu, B.; Wang, Y.; Deng, S.; Hu, A., Size-tunable polymeric nanoreactors for one-pot synthesis and encapsulation of quantum dots. *Macromol Rapid Commun* **2012**, *33* (16), 1393-8.
51. Hamelmann, N. M.; Paats, J. D.; Avalos-Padilla, Y.; Lantero, E.; Spanos, L.; Siden-Kiamos, I.; Fernandez-Busquets, X.; Paulusse, J. M. J., Single-Chain Polymer Nanoparticles Targeting the Ookinete Stage of Malaria Parasites. *ACS Infect Dis* **2023**, *9* (1), 56-64.
52. Arias-Alpizar, G.; Koch, B.; Hamelmann, N. M.; Neustrup, M. A.; Paulusse, J. M. J.; Jiskoot, W.; Kros, A.; Bussmann, J., Stabilin-1 is required for the endothelial clearance of small anionic nanoparticles. *Nanomedicine* **2021**, *34*, 102395.
53. Li, Y.; Bai, Y.; Zheng, N.; Liu, Y.; Vincil, G. A.; Pedretti, B. J.; Cheng, J.; Zimmerman, S. C., Crosslinked dendronized polyols as a general approach to brighter and more stable fluorophores. *Chem Commun (Camb)* **2016**, *52* (19), 3781-4.
54. Bai, Y.; Xing, H.; Vincil, G. A.; Lee, J.; Henderson, E. J.; Lu, Y.; Lemcoff, N. G.; Zimmerman, S. C., Practical synthesis of water-soluble organic nanoparticles with a single reactive group and a functional carrier scaffold. *Chem. Sci.* **2014**, *5* (7), 2862-2868.

-
55. Perez-Baena, I.; Loinaz, I.; Padro, D.; García, I.; Grande, H. J.; Odriozola, I., Single-chain polyacrylic nanoparticles with multiple Gd(III) centres as potential MRI contrast agents. *Journal of Materials Chemistry* **2010**, *20* (33).
56. Hamilton, S. K.; Harth, E., Molecular Dendritic Transporter Nanoparticle Vectors Provide Efficient Intracellular Delivery of Peptides. *ACS Nano* **2009**, *3* (2), 402-410.
57. Tian, X.; Xue, R.; Yang, F.; Yin, L.; Luan, S.; Tang, H., Single-Chain Nanoparticle-Based Coatings with Improved Bactericidal Activity and Antifouling Properties. *Biomacromolecules* **2021**, *22* (10), 4306-4315.
58. Gracia, R.; Marradi, M.; Salerno, G.; Pérez-Nicado, R.; Pérez-San Vicente, A.; Dupin, D.; Rodríguez, J.; Loinaz, I.; Chiodo, F.; Nativi, C., Biocompatible single-chain polymer nanoparticles loaded with an antigen mimetic as potential anticancer vaccine. *ACS Macro Letters* **2018**, *7* (2), 196-200.
59. Gracia, R.; Marradi, M.; Cossío, U.; Benito, A.; Pérez-San Vicente, A.; Gómez-Vallejo, V.; Grande, H. J.; Llop, J.; Loinaz, I., Synthesis and functionalization of dextran-based single-chain nanoparticles in aqueous media. *Journal of Materials Chemistry B* **2017**, *5* (6), 1143-1147.
60. Hoffmann, J. F.; Roos, A. H.; Schmitt, F. J.; Hinderberger, D.; Binder, W. H., Fluorescent and Water Dispersible Single-Chain Nanoparticles: Core-Shell Structured Compartmentation. *Angew Chem Int Ed Engl* **2021**, *60* (14), 7820-7827.
61. de Luzuriaga, A. R.; Ormategui, N.; Grande, H. J.; Odriozola, I.; Pomposo, J. A.; Loinaz, I., Intramolecular Click Cycloaddition: An Efficient Room-Temperature Route towards Bioconjugable Polymeric Nanoparticles. *Macromolecular Rapid Communications* **2008**, *29* (12-13), 1156-1160.
62. Koda, Y.; Terashima, T.; Sawamoto, M.; Maynard, H. D., Amphiphilic/fluorous random copolymers as a new class of non-cytotoxic polymeric materials for protein conjugation. *Polymer Chemistry* **2015**, *6* (2), 240-247.
63. Kröger, A. P. P.; Boonen, R. J. E. A.; Paulusse, J. M. J., Well-defined single-chain polymer nanoparticles via thiol-Michael addition. *Polymer* **2017**, *120*, 119-128.
64. Min, H. S.; Kim, H. J.; Naito, M.; Ogura, S.; Toh, K.; Hayashi, K.; Kim, B. S.; Fukushima, S.; Anraku, Y.; Miyata, K.; Kataoka, K., Systemic Brain Delivery of Antisense Oligonucleotides across the Blood-Brain Barrier with a Glucose-Coated Polymeric Nanocarrier. *Angew Chem Int Ed Engl* **2020**, *59* (21), 8173-8180.
65. Xie, J.; Gonzalez-Carter, D.; Tockary, T. A.; Nakamura, N.; Xue, Y.; Nakakido, M.; Akiba, H.; Dirisala, A.; Liu, X.; Toh, K.; Yang, T.; Wang, Z.; Fukushima, S.; Li, J.; Quader, S.; Tsumoto, K.; Yokota, T.; Anraku, Y.; Kataoka, K., Dual-Sensitive Nanomicelles Enhancing Systemic Delivery of Therapeutically Active Antibodies Specifically into the Brain. *ACS Nano* **2020**, *14* (6), 6729-6742.
66. Eberhardt, M.; Mruk, R.; Zentel, R.; Théato, P., Synthesis of pentafluorophenyl(meth)acrylate polymers: New precursor polymers for the synthesis of multifunctional materials. *European Polymer Journal* **2005**, *41* (7), 1569-1575.

Chapter 2

Pentafluorophenyl-based single-chain polymer nanoparticles as a modular platform for controlling cellular uptake

Single-chain polymer nanoparticles (SCNPs) are well-defined soft objects, formed by intramolecularly crosslinked linear polymers, which resemble the size and approximate the structure of proteins. By introducing reactive groups into the precursor backbone, SCNPs may be used post-formation as a modular platform to systematically study the influence of ligands and ligand density on *in vitro* behavior.

In this study, we present the formation of SCNPs with activated pentafluorophenyl (PFP) esters. A co-polymer containing PFP-methacrylate and xanthate moieties is efficiently deprotected to yield free thiols, which are subsequently used for intramolecular crosslinking via a thiol-Michael addition to obtain pentafluorophenyl-based single-chain polymer nanoparticles (PFP-SCNPs). Intramolecular crosslinking is confirmed by size exclusion chromatography, dynamic light scattering and ¹H DOSY NMR. The PFP-SCNPs are subsequently functionalized with increasing amounts of tertiary amines, leading to a range of SCNPs with increasing zeta-potential. Cellular uptake of the SCNPs is investigated in bEND.3 cells, indicating different uptake behavior, based on the particles' surface charge. Confocal microscopy revealed cytosolic delivery of the SCNPs with the highest zeta potential. These results indicate the importance of surface charge on cellular fate and provide an easy method for tailoring NPs towards specific biomedical applications.

This chapter is a selection from: A. P. P. Kröger‡, J.-W. D. Paats‡, R. J. E. A. Boonen, N. M. Hamelmann, J. M. J. Paulusse, *Polymer Chemistry* **2020**, *11* (37), 6056-6065 and N. M. Hamelmann, J.-W. D. Paats, J. M. J. Paulusse, *ACS Macro Lett* **2021**, *10* (11), 1443-1449.

‡ These authors contributed equally.

2.1 Introduction

Over the past decades, polymeric nanoparticles have been extensively employed as biocompatible materials, due to their large structural flexibility and tunable, high biocompatibility.¹⁻² Ever increasing progress in synthetic methodologies has led to a wide range of polymeric materials currently being available, enabling a variety of applications, ranging from imaging³⁻⁴ and sensing⁵⁻⁶ to drug delivery.⁷⁻⁹ Of all materials properties, particularly size plays an important role in the performance and behavior of nanoparticles (NPs) for biomedical applications.¹⁰ Intravenously injected 200 nm gold particles were mainly found in the liver, whereas 15 nm and 50 nm NPs were found in a variety of organs, including the brain.¹¹⁻¹² For enhanced cellular uptake, especially of interest are NPs in the size range of proteins.¹³⁻¹⁴ Bai et al. showed an increase in internalization of organic NPs in HeLa Cells with decreasing particle size, with a factor 3 difference between 40 nm and 7 nm particles.¹⁵ This stresses the need for sub-20 nm nanoparticles. However, access to this size regime remains a synthetic challenge. One way to overcome this hurdle, is the use of single-chain polymer nanoparticles (SCNPs).

SCNPs are prepared through exclusive intramolecular crosslinking of individual polymer chains.¹⁶⁻²⁶ Size and dispersity of SCNPs are directly related to the size and size distribution of the polymers from which they are prepared, and these properties can therefore be controlled very accurately, yielding nanoparticles in the 5-20 nm size range, resembling the size and structure of proteins.²⁷⁻²⁹ The structure of SCNPs is in between a flexible polymer and a rigid nanoparticle.³⁰ This combines the ability for multivalent target-ligand interactions,³¹ with the increased cellular uptake observed for rigid particles.³²⁻³³ In 1962, the first covalently crosslinked SCNPs were synthesized under very dilute conditions (10^{-6} - 10^{-5} M).³⁴ However, intermolecular reactions were still apparent, resulting in ill-defined nanostructures. Furthermore, these conditions precluded multigram synthesis and therefore, hampered its usefulness towards further applications. In 2002, the group of Hawker introduced the formation of SCNPs under continuous addition, where a benzocyclobutene-functional polymer was slowly added to a high temperature solution, which subsequently induced the intramolecular crosslinking.³⁵ This improved approach allowed for much higher concentrations of reactants (up to a factor 10^4). However, the harsh reaction conditions (200 °C) limit the applicability of such systems. Utilizing much milder reactions, a large variety of crosslinking methods to synthesize SCNPs has been developed since.³⁶⁻³⁸ As previously demonstrated by our group, one particularly efficient reaction for intramolecular crosslinking is using a thiol-Michael addition.³⁹ The reaction can be initiated by a phosphine,⁴⁰⁻⁴¹ which simultaneously provides a reductive environment, preventing the formation of disulfide bonds. However, the lability of free thiols impedes incorporation into linear growing polymer chains, requiring the use of a protective group, which is stable and tolerant towards

controlled radical polymerization.⁴² For this purpose, Nicolaÿ designed a protective xanthate moiety (xanthate methacrylate, XMA) that may be employed.⁴³ Post-polymerization aminolysis of the xanthate group yields free reactive thiols on the polymer, which can be subsequently used for efficient intramolecular crosslinking and the formation of SCNPs.

In order to render SCNPs suitable for biomedical applications, the exterior of the NPs needs to be readily modified for the introduction of active ligands and systematic investigations into cell-materials interactions. Post-formation functionalization enables modification of polymers,⁴⁴ nanoparticles⁴⁵⁻⁴⁶ and nanogels⁴⁷⁻⁴⁸ without markedly altering their size and structure. Exploiting post-formation functionalization of SCNPs would allow careful tuning of the exterior properties, while maintaining the SCNP's backbone structure intact. Pentafluorophenyl (PFP) esters have found widespread application in bioconjugation chemistry.⁴⁹ These activated esters are soluble in a range of organic solvents and less susceptible to hydrolysis than NHS esters.⁵⁰ PFP-functional polymers have been successfully used in post-polymerization functionalization reactions with both primary and secondary amines.⁵¹ Conjugation of antibodies to PFP-acrylate polymer brushes was achieved by Son et al., enabling capture and purification of target proteins.⁵² In the stepwise compaction of *N*-substituted maleimide copolymers, the PFP-moiety was used as intramolecular crosslinking reaction to prepare SCNPs.⁵³⁻⁵⁴ Furthermore, Palmans and co-workers used poly(PFP-acrylate) to prepare polymer precursors for intramolecular self-assembly of SCNPs.⁵⁵⁻⁵⁷ Recently, PFP-polymers were also modified with quaternary ammonium groups and catalytic centers to form SCNPs with increased catalytic activity, even working inside HeLa cells.⁵⁸⁻⁵⁹

For many biomedical applications, NPs need to reach a specific organelle within the cell to be effective, such as the nucleus⁶⁰ or the mitochondria.⁶¹ Therefore, efficient internalization of NPs and subsequent release from endosomal structures into the cytosol is required for optimal activity. To facilitate cellular uptake of SCNPs, tertiary amines can be employed, which have for example already found widespread application in the field of gene delivery.⁶²⁻⁶⁴ Tertiary amines are partially protonated at neutral pH,⁶⁵⁻⁶⁶ leading to increased interactions with negatively charged cell membranes and subsequent NP endocytosis. The decreased pH within the endosome leads to an influx of protons and chloride counterions, resulting in osmotic swelling and, combined with the increased charged repulsion of the protonated NPs, rupturing of the endosome and release of its contents into the cytosol. This whole process is referred to as the proton sponge effect, although the exact mechanism is currently under heavy debate.⁶⁷⁻⁶⁸ However, positively charged particles can also induce cytotoxic effects, indicating the delicate balance between cellular uptake and cell death.⁶⁹⁻⁷¹ Therefore, the charge density of the particles' surface needs to be carefully controlled and optimized for efficient cellular uptake.

In this work, we report the preparation and characterization of PFP-functional SCNPs via thiol-Michael addition crosslinking, and their use as a flexible platform to easily modify and functionalize the surface of SCNPs, while maintaining the backbone structure unaltered. We use this platform to systematically study the influence of the surface density of protonatable amines and subsequent surface charge on the particles' subcellular location, by creating a range of SCNPs with increasing amounts of protonatable tertiary amines. The SCNPs are evaluated for cytotoxic effects on brain endothelial cells (bEND.3) and cellular uptake is studied by flow cytometry and confocal microscopy.

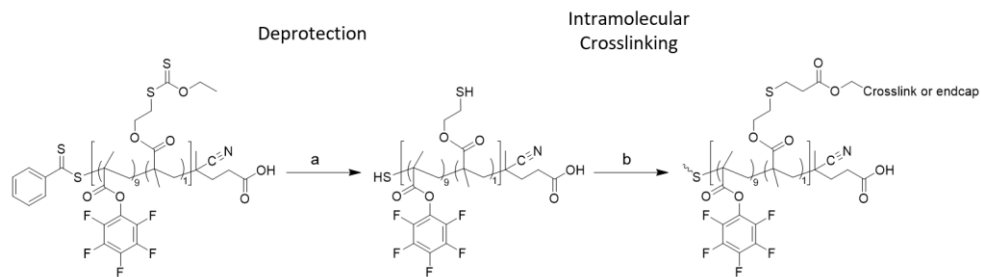
2.2 Results and Discussion

Synthesis and characterization of PFP-SCNPs

Both monomers xanthate methacrylate (crosslinkable group, XMA) and PFPMA (modifiable group) were synthesized according to a modified literature procedures with comparable yields.^{43, 51} RAFT Co-polymerizations of the two monomers (in a 9 to 1 ratio of PFPMA to XMA) were carried out and stopped after reaching approximately 70% conversion, since higher conversions resulted in deviations from first-order kinetics, to yield copolymers with PDI ~ 1.4 and a degree of polymerization of ~230. Both monomers were consumed according to the feed ratio (Figure S2.1).

To yield the free reactive thiol, XMA was deprotected using ethanolamine (Scheme 2.1). Since XMA deprotection and the post-polymerization functionalization are not fully orthogonal reactions, a certain amount of PFP conversion has to be accepted. Therefore, preferably the deprotection agent is chosen in line with the subsequent functionalization. Furthermore, the deprotected polymer needs to be isolated after deprotection to halt further PFP-substitution before proceeding with the crosslinking reaction. Full deprotection of the XMA moiety was achieved after 150 minutes, determined by the disappearance of the ¹H NMR C(=S)OCH₂-CH₃ signal at $\delta = 4.6$ ppm and the appearance of a -OCH₂-CH₂SH signal at $\delta = 4.1$ ppm (see Figure S2.2), with only 6% conversion of PFP moieties (*data not shown*). Intramolecular crosslinking to form SCNPs was performed under continuous addition, where deprotected polymer was slowly added to a solution of di-acrylate crosslinker and phosphine initiator over 2 h (Scheme 2.1). After complete addition, the solution was stirred during 2 h to ensure maximum degree of crosslinking. Particles were

subsequently end-capped with methyl acrylate to quench residual thiols and prevent intermolecular crosslinking in later stages.



Scheme 2.1. Deprotection of p(PFPMA-XMA) co-polymer, followed by intramolecular chain collapse into pentafluorophenyl single-chain polymer nanoparticles (**PFP-SCNPs**). Reagents and conditions: (a) ethanolamine, THF, N₂, r.t.; (b) 1) PBU₃, 1,4-butanediol diacrylate, DCM, THF, N₂, r.t.; 2) methyl acrylate, overnight, r.t.

Successful thiol-Michael addition is observed in the ¹H NMR spectrum by the appearance of signals at $\delta = 4.18$ and $\delta = 3.29$ ppm (see Figure 2.1a) corresponding to the newly formed thioether linkage. Successful end-capping is confirmed by the appearance of a methoxy-signal at 3.62 ppm and the absence of alkene groups. The ¹⁹F NMR spectrum shows the presence of pendant PFP groups in the ratio 2:1:2 (ortho : para : meta), confirming that no significant para-fluoro-substitution has taken place (Figure S2.3a).⁷²⁻⁷⁴ The signal corresponding to the ortho-fluoro atoms displays a broadening upon crosslinking, which is not observed as strongly for the meta- and para-fluoro peaks. (Figure S2.3b). This peak broadening might be a result of increased crowding around the pentafluorophenyl rings upon chain compaction,

leading to decreased T_2 relaxation times and subsequent line broadening. However, these results do not discriminate between inter- and intramolecular binding.

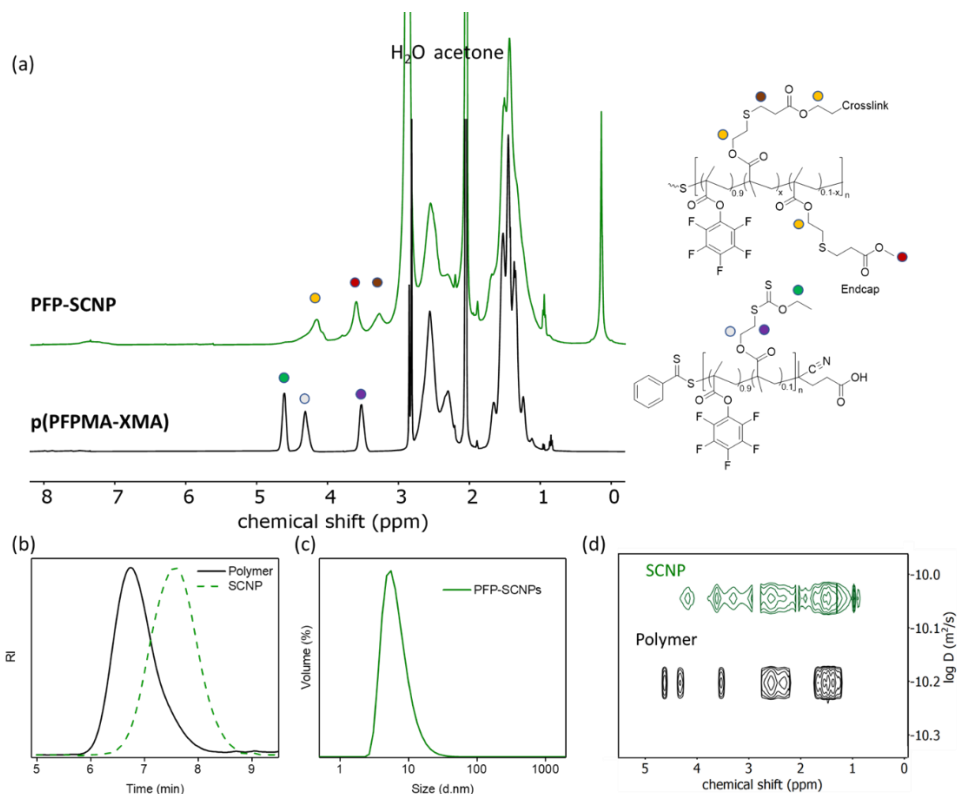


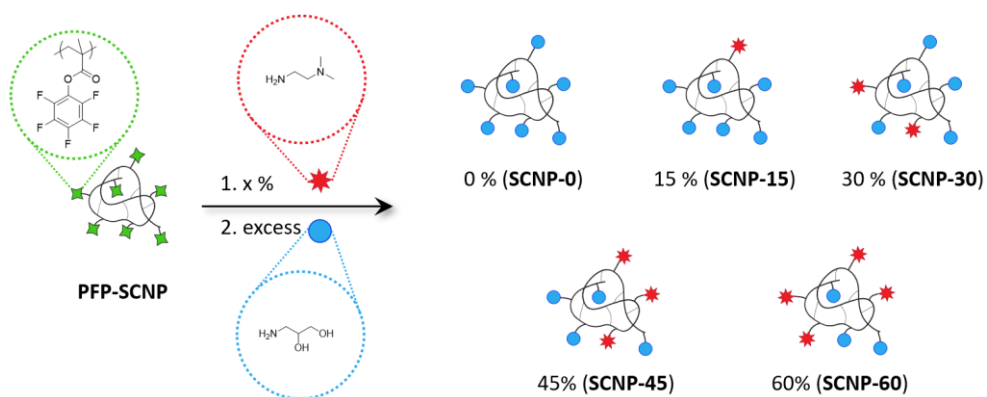
Figure 2.1. Characterization of **PFP-SCNPs**. (a) ^1H NMR spectra of p(PFPMA-XMA) and **PFP-SCNP** in d-acetone; (b) SEC trace of precursor polymer and subsequent **PFP-SCNP**; (c) DLS spectrum in CHCl_3 ; (d) ^1H DOSY NMR spectrum in d-acetone comparing precursor polymer with collapsed **PFP-SCNPs**.

Size exclusion chromatography revealed a shift towards longer retention times upon chain compaction, indicating a decrease in hydrodynamic radius, with an apparent molecular weight decrease of 60% (Figure 2.1b). To account for possible size decrease by partial substitution of the pentafluorophenyl side groups, a 7% ethanolamine functionalized PFPMA homo-polymer was analyzed by SEC (Figure S2.4), showing only a 12% decrease in apparent molecular weight, confirming the significance of the measured size reduction upon collapse. DLS analysis showed a single population of particles with a hydrodynamic radius of around 10 nm (based on volume %) and without discernible multi-chain aggregates. Furthermore, ^1H DOSY

NMR spectroscopy revealed a decrease in hydrodynamic radius from 10.5 nm to 7.4 nm upon chain collapse (Figure 2.1c-d, Figure S2.5), together confirming successful intramolecular chain collapse to form **PFP-SCNPs**.

Functionalization of PFP-SCNPs

Previously, we have shown that the **PFP-SCNPs** can be equipped with a wide variety of different pendants, such as peptides and targeting moieties, ranging from hydrophobic to hydrophilic.⁷⁵ Here, a range of functional SCNPs was synthesized by conjugating the **PFP-SCNPs** with different ratios of the protonatable tertiary amine *N,N*-dimethylethylenediamine (DMEN) and 1-aminoglycerol to yield **SCNP-0** to **SCNP-60**, as depicted in Scheme 2.2.



Scheme 2.2. Schematic representation of the functionalization of **PFP-SCNPs** with increasing amounts of protonatable tertiary amine, followed by end-capping of remaining PFP-esters with 1-aminoglycerol.

The conjugation was conveniently followed by ¹⁹F NMR spectroscopy, indicating full conversion for all samples within 24 h (Figure S2.6). Remaining PFP groups were end-capped with 1-aminoglycerol to render the SCNPs water-soluble. Incorporation of the functional groups was further evidenced by ¹H NMR spectroscopy, where signals at $\delta = 2.2$ ppm, corresponding to the two methyl groups attached to the tertiary amine and the adjacent methylene group increased at increasing incorporation ratio, while the signals at $\delta = 2.9$, $\delta = 3.5$ and $\delta = 4.5$ -5.0 ppm, corresponding to the incorporation of 1-aminoglycerol diminished (see Figure 2.2). The absence of signals in the ¹⁹F NMR spectra (*data not shown*) further indicates successful functionalization of SCNPs with increasing amounts of tertiary amine groups, while no reactive PFP groups remained.

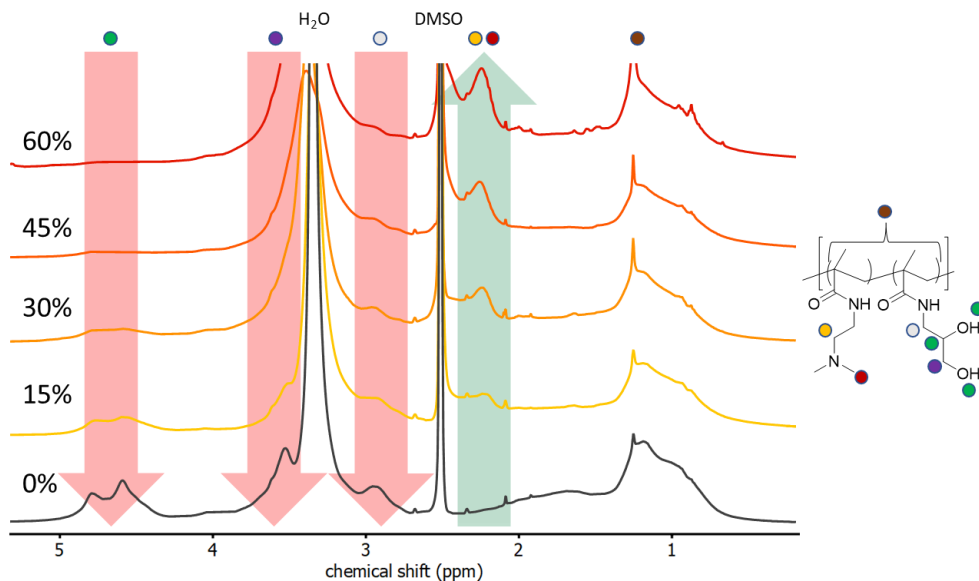


Figure 2.2. Overlaid ^1H NMR spectra of tertiary amine functionalized SCNPs, indicating the increase (green) and decrease (red) of respective functional groups at increasing tertiary amine incorporation.

The functionalized SCNPs were analyzed by SEC as shown in Figure 2.3a. The elution profiles of **SCNP-0** to **SCNP-60** show a small shift towards lower molecular mass upon higher degrees of substitution, indicating only a minor influence of the substituents on the hydrodynamic volume of the particles (see also Table 2.1). Additionally, DLS measurements show particles with comparable hydrodynamic diameters of approximately 10 nm (based on volume %) (Figure 2.3b, Figure S2.7). Surface charge of the particles was evaluated in HEPES buffer at pH 7.0 (Figure 2.3c). For 0% incorporation of tertiary amines, the alcohol-groups render the particles negatively charged, but upon increasing the content of tertiary amines, the SCNP surface becomes positively charged with an apparent plateau of +27 mV for **SCNP-60**. TEM imaging on **SCNP-0** confirmed SCNPs with an approximate (dry) size of ~10 nm, with no large clustering present (Figure 2.3d). ^1H NMR DOSY experiments conducted in D_2O reveal a hydrodynamic radius between 5-6 nm (Table 2.1).

For subsequent *in vitro* cell studies, the functionalized SCNPs were labelled with 5-(4,6-dichlorotriazinyl) aminofluorescein (DTAF), which was confirmed by SEC analysis, showing no significant residual free label present (Figure S2.8).

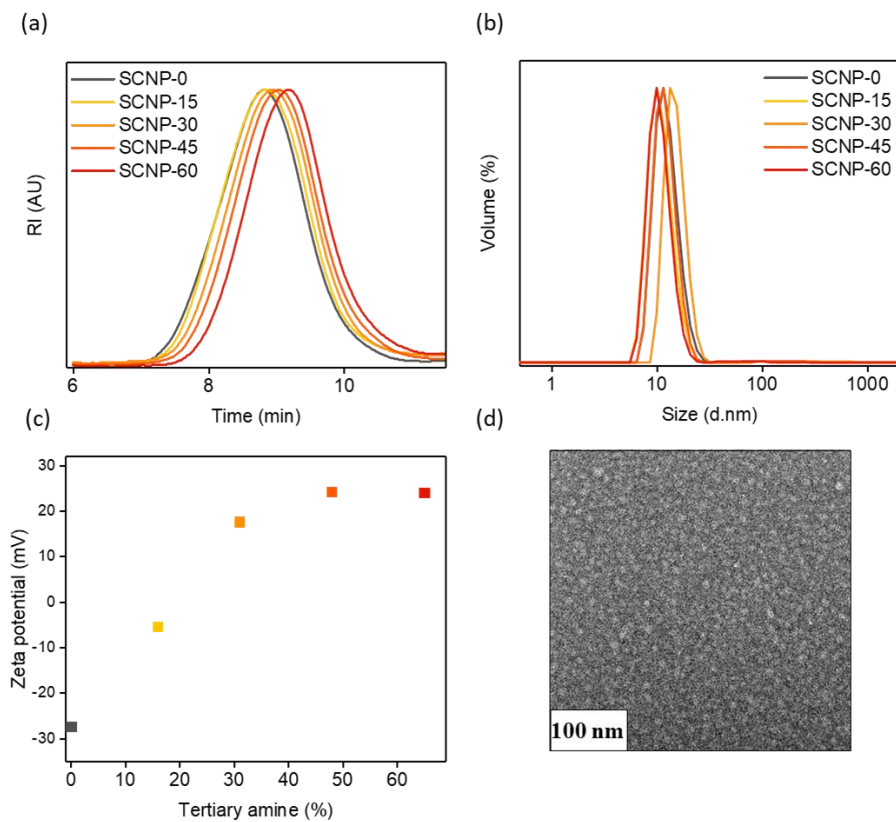


Figure 2.3. Characterization of functionalized SCNPs. (a) overlaid GPC-traces in DMF; (b) overlaid DLS-spectra in 5 wt% NaCl-solution; (c) zeta-potential measurements in 10 mM HEPES buffer pH 7.0; (d) TEM-image of **SCNP-0** with negative staining.

Table 2.1. Overview of charge range of SCNPs: theoretical molecular weight, hydrodynamic radii at different pH values and elution maximum.

	$M_{n, \text{theo}}^{\text{a}}$ (kDa)	$R_{\text{h, DOSY}}^{\text{b}}$ (nm)	Elution peak GPC (min)
SCNP-0	39.8	5.8	8.82
SCNP-15	39.7	5.0	8.85
SCNP-30	39.5	5.0	8.95
SCNP-45	39.5	5.3	9.04
SCNP-60	39.4	5.3	9.18

(a) Determined by ^1H NMR spectroscopy on the linear precursor for the **PFP-SCNPs**, followed by molecular weight calculations based on ligand substitution as determined by ^{19}F NMR spectroscopy; (b) determined by ^1H DOSY NMR in D_2O .

Intracellular location of SCNPs

After successful functionalization of **PFP-SCNP**, thereby eliminating batch-to-batch differences as the nanoparticle core remains unaltered, the effect of nanoparticle surface charge on their subcellular fate can be systematically investigated. As a start, possible cytotoxicity was studied, since cationic charges are known to induce cytotoxic effects.⁶⁹⁻⁷¹ Brain endothelial b.End3 cells were incubated with **SCNP-0** to **SCNP-60** over a wide concentration range. The results in Figure S2.9a show that **SCNP-0** to **SCNP-30** do not exert significant cytotoxicity. However, upon increasing ligand density as well as nanoparticle concentration, cell viabilities decrease. **SCNP-45** only induces cytotoxic effects at a maximum tested concentration of 500 $\mu\text{g}/\text{mL}$, whereas **SCNP-60** already decreased cell viability from 200 $\mu\text{g}/\text{mL}$ onwards. At low concentrations however, the entire range of SCNPs is non-cytotoxic after 24 h of incubation and can thus be used for studying the particles' intracellular fate. To this end, b.End3 cells were incubated with **SCNP-0**, **SCNP-15** and **SCNP-30** at 50 $\mu\text{g}/\text{mL}$ for 6 h and the cells were subsequently stained with membrane and nuclei stainings. In Figure 2.4, a gradual decrease of green fluorescent signal from **SCNP-0** to **SCNP-30** can be observed, confirming higher uptake of negatively charged **SCNP-0** as compared to **SCNP-30**, as also confirmed by flow cytometry (FACS) data (Figure S2.9b). Furthermore, the fluorescent signal of the SCNPs is observed as vesicular structures inside the cells. These results resemble the uptake behavior of glycerol-SCNPs shown in previous work, indicating endosomal uptake.⁷⁶

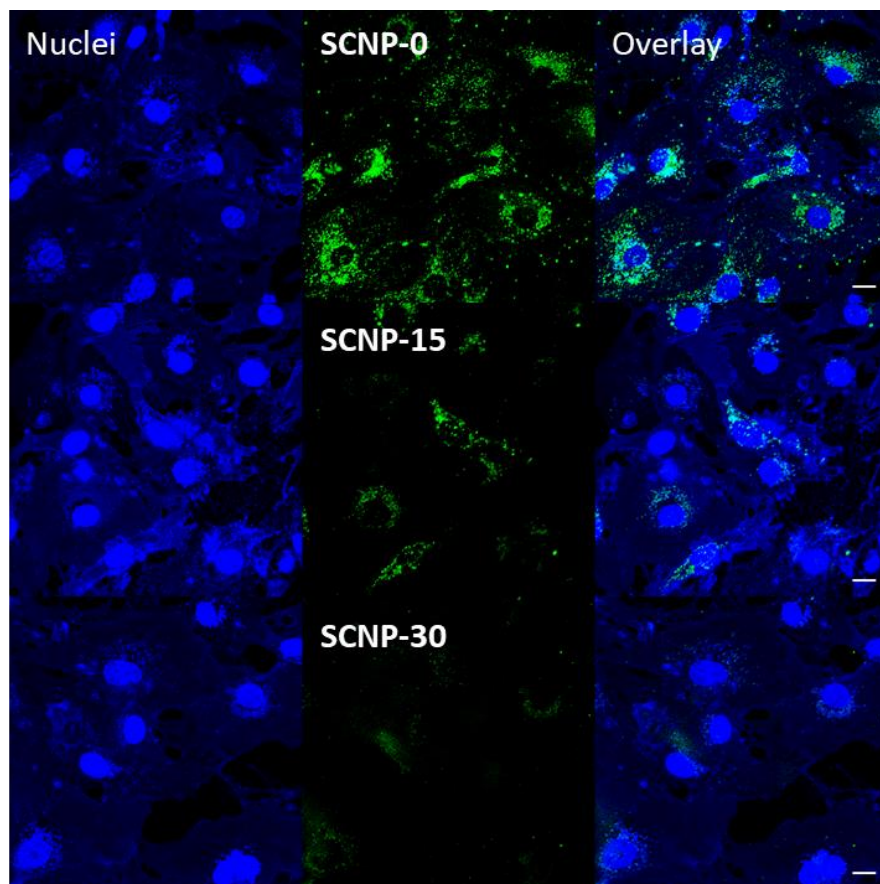


Figure 2.4. CLSM images of **SCNP-0**, **SCNP-15** and **SCNP-30** uptake in bEND.3 cells after 6 h incubation at 50 $\mu\text{g}/\text{mL}$. Nuclei and membranes were stained blue, while a green fluorescent label was used on the SCNPs, scale bars 10 μm .

Because of the high uptake rates for **SCNP-45** and **SCNP-60** (measured by FACS, see Figure S2.9b), these particles were incubated for only 1 h at 50 $\mu\text{g}/\text{mL}$ with bEND.3 cells for confocal laser scanning microscopy (CLSM) purposes. Subsequently, the cells were stained with membrane and nuclei stainings. In contrast to **SCNP-0** to **SCNP-30**, lower amounts of SCNPs are present in vesicle-like structures in the case of **SCNP-45**. Instead, the signal of the SCNPs is observed throughout the cell cytosol as shown in Figure 2.5. In gene⁷⁷⁻⁷⁸ and protein⁷⁹⁻⁸⁰ delivery, polymers with tertiary amines are utilized to form complexes with negatively charged cargoes, to deliver the cargo in the cytosol of cells by exploiting the proton sponge effect. In line with these studies, amine moieties on the SCNPs become protonated at the relatively low endosomal/lysosomal pH increasing the internal osmotic pressure after internalization. With increasing surface functionality of the

SCNPs, the pressure increases, leading to lysing of the endosomes and endosomal escape of **SCNP-45**. For **SCNP-60**, this cytosolic delivery is also observed, but additional signals corresponding to aggregated SCNPs are also observed.

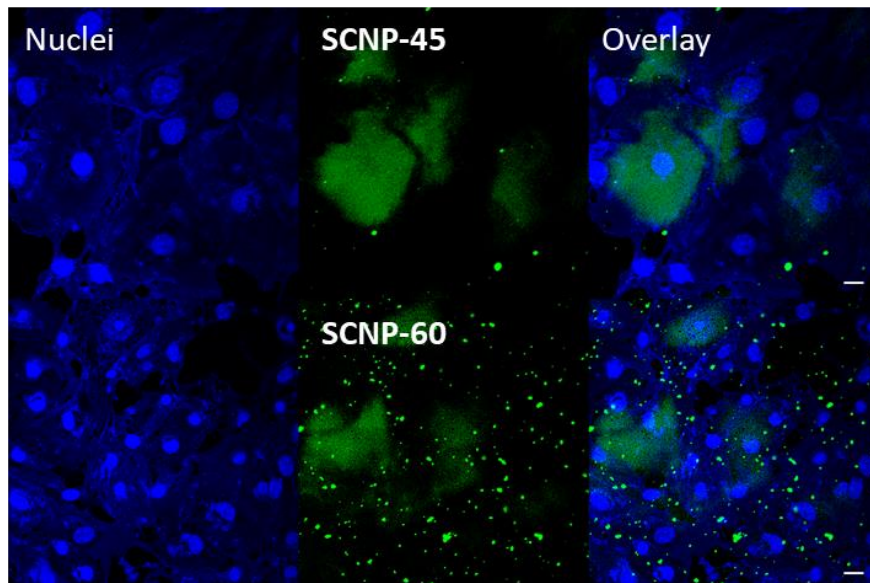


Figure 2.5. CLSM images of **SCNP-45** and **SCNP-60** uptake in bEND.3 cells after 1 h incubation at 50 $\mu\text{g/mL}$. Nuclei and membranes were stained blue, while a green fluorescent label was used on the SCNPs, scale bar 10 μm .

2.3 Conclusion

In this work, we demonstrate the development of pentafluorophenyl-based single-chain polymer nanoparticles (**PFP-SCNPs**), based on covalent intramolecular chain collapse and the subsequent modification of the surface of these nanoparticles yielding highly modular functional SCNPs. The SCNPs were subsequently equipped with a range of protonatable tertiary amines, from 0 to 60%. Significant differences in uptake behavior were observed for **SCNP-0** to **30** and **SCNP-45** and **60**. Confocal microscopy and FACS-measurements revealed that **SCNP-0** displays high cellular uptake, but show localized fluorescence, indicating endosomal uptake. Increasing the particles' surface charge leads to decreased cellular uptake up to **SCNP-30**. However, successful cytosolic delivery of **SCNP-45** and **SCNP-60** was observed. The higher amounts of tertiary amines in **SCNPs-45** and **SCNP-60** were sufficient to increase the ionic strength inside the endosome and rupture the membrane, promoting endosomal escape. These versatile SCNPs provide a promising platform for various drug delivery applications as the surface modification enables directing the delivery to different subcellular targets, importantly including the cytosol.

Being able to direct the SCNPs to reach the cytosol is crucial for many biomedical applications, since that is where the majority of (protein-based) targets resides.⁸¹ However, for crossing biological barriers, nanoparticles need to be endocytosed, followed by intracellular trafficking and subsequently undergo exocytosis upon reaching the other side of the cell.⁸²⁻⁸³ Premature escape from endosomes into the cytosol clearly impedes this process and demonstrates the need for tailored surfaces, depending on the application in mind. Therefore, the current charge range can be further exploited to study the optimum surface potential for efficient transcytosis, such as is needed for crossing the blood brain barrier. Furthermore, the control and ease of functionalization contributes to the ability to rapidly adapt SCNPs for therapeutic translation, since the platform allows for the consecutive addition of different ligands. This will allow tailoring SCNPs towards specific needs, by combining different functional ligands with controlled ligand density.

2.4 Materials and Methods

Potassium ethyl xanthogenate (96%), 2-bromoethanol (95%), methacryloyl chloride (98%), methyl acrylate (99%), pentafluorophenol (99%), 1,4-butanediol diacrylate (>90%), tri-*n*-butylphosphine (99%), triethylamine (TEA, 99%), ethanolamine (>98%), 3-amino-1,2-propanediol (1-aminoglycerol, 97%), 4-cyano-4-(phenylcarbonothioylthio)pentanoic acid (CPADB, >99%), *N,N*-dimethylethylenediamine (DMEN, 95%), 1,4-dioxane (anhydrous, >99.8%), DMSO (anhydrous, 99.9%), chloroform-*d* (99.8% atom % D) and DMSO-*d*₆ (99.9 atom % D) and Dulbecco modified Eagles medium (DMEM), fetal bovine serum (FBS), penicillin-streptomycin (containing 10.000 units penicillin, 10 mg streptomycin mL⁻¹), resazurin sodium salt (BioReagent), phosphate buffered saline (PBS, pH 7.4), Hanks' balanced salt solution (HBSS), Trypsin-EDTA solution (sterile filtered, BioReagent) and 4,6-diamidino-2-phenylindole dihydrochloride (DAPI, 98%) were purchased from Sigma-Aldrich. Propidium iodide (PI), fluorescent label 5-(4,6-Dichlorotriazinyl) aminofluorescein (DTAF), and Lyso Tracker™ Deep Red and SnakeSkin™ dialysis tubing (10K MWCO) were purchased from ThermoFisher Scientific. CF® 405M Wheat Germ Agglutinin (WGA) was purchased from Biotium. Cell culture bEND.3 cells were purchased from ATCC. Tetrahydrofuran (THF, >99%), dichloromethane (DCM, >99%) and methanol (>99%) were purchased from LPS B.V. *N,N*-dimethylformamide (DMF, >99.8%) was purchased from VWR. Chloroform (>99.8%) was purchased from Merck. Monomers 2-(Ethyl xanthate) ethyl methacrylate (XMA) and pentafluorophenyl methacrylate (PFPMA) were synthesized according to modified literature procedures.^{43, 51} Disposable PD-10 desalting columns were purchased from GE healthcare All chemicals were used without further purification unless stated otherwise. When stated as dry, solvents were treated with molecular sieves (3 Å) 24 h before usage and stored under nitrogen.

^1H -NMR (400 MHz) and ^{19}F -NMR (376 MHz) spectra were recorded on a Bruker 400 spectrometer. Size exclusion chromatography (SEC) analysis was performed on a Waters e2695 Separations Module equipped with an Agilent PLgel 5 μm MIXED-D 300x7.5 mm column and Waters photodiode array detector (PDA 2998), fluorescence detector (FLR 2475) and refractive index detector (RI 2414). Chloroform and DMF with 50 mM LiCl were employed as eluent with molecular weights calibrated against linear polystyrene and PEO/PEG, respectively. Dynamic light scattering (DLS) and zeta potential measurements were performed on a Malvern Instruments Zetasizer ZS in chloroform, 5 wt% NaCl solution in milliQ or 10 mM Hepes Buffer pH 7.0. Samples for SEC and DLS were filtered using a GE Healthcare Whatman SPARTAN 13/0.2 RC 0.2 μm syringe filter prior to measurements. Transmission Electron Microscopy (TEM) was performed on a Philips CM300ST-FEG Transmission Electron Microscope 300 kV equipped with GATAN Ultrascan1000 (2kx2k CCD camera) and GATAN Tridiem energy filter (2Kx2K CCD camera). For the sample preparation, 5 μL of a 0.5 mg/mL solution in milliQ was casted on copper grids and incubated for 30 seconds. Excess solution was removed by filter paper. Subsequently, the sample was stained by adding 5 μL of a 1% (w/v) uranyl acetate solution for 30 seconds, followed by removal of the excess solution by filter paper.

p(PFPMA-XMA) co-polymer

Prior to polymerization, PFPMA and XMA was filtered over neutral alumina to remove inhibitor. PFPMA and XMA were copolymerized in molar ratios of 9:1. In a typical polymerization experiment, PFPMA (13.2 g, 52.2 mmol, 300 eq.), XMA (1.36 g, 5.8 mmol, 33.3 eq.), RAFT agent CPADB (48.6 mg, 0.17 mmol, 1 eq) and AIBN (5.7 mg, 0.035 mmol, 0.2 eq.) were combined with 1,4-dioxane (14 mL) in a polymerization flask fitted with a rubber septum. After purging for 30 minutes with nitrogen, the flask was placed in a preheated oil bath at 80 $^{\circ}\text{C}$. After reaching 70% conversion, the flask was submerged in an ice bath and diluted with dichloromethane (2 mL), followed by repeated precipitations in cold heptane to yield a pink powder (8.5 g, 83% yield).

^1H NMR (acetone- d_6) δ_{H} : 4.71–4.50 (br), 4.41–4.19 (br), 3.65–3.37 (br), 2.78–2.18 (br), 1.77–1.06 (br). ^{19}F NMR (acetone- d_6) δ_{F} : -152.1 (br), -159.6 (br), -164.5 (br).

PFP-SCNP formation

p(PFPMA-XMA) co-polymer (600 mg, 0.24 mmol XMA-units) was dissolved in THF (12 mL) and purged with nitrogen for 15 minutes, followed by addition of ethanolamine (87.0 μL , 1.92 mmol, 6 eq.), resulting in immediate loss of pink color. The solution was stirred for 150 minutes, and full deprotection followed by precipitation in cold methanol. After centrifugation (10 minutes \times 10000 rpm), the

deprotected polymer was redissolved in 11 mL of THF. The deprotected polymer was filtered and under vigorous stirring slowly dropped into a nitrogen purged dichloromethane solution (132 mL), containing 1,4-butanediol diacrylate (50.0 μ L, 0.24 mmol, 1 eq) and tributylphosphine (11.8 μ L, 0.05 mmol, 0.2 eq.). The solution was stirred for another 120 minutes, after which methyl acrylate (1 mL, 11 mmol, 46 eq.) was added. The solution was stirred overnight and concentrated under reduced pressure. **PFP-SCNPs** were isolated by precipitation twice into cold methanol as a white solid (310 mg, 55% yield).

^1H NMR (acetone- d_6) δ_{H} : 7.66–7.04 (br), 4.53–3.99 (br), 3.75–3.48 (br), 3.45–3.15 (br), 2.70–2.25 (br), 1.79–1.00 (br). ^{19}F NMR (acetone- d_6) δ_{F} : -152.2 (br), -159.5 (br), -164.4 (br).

p(PFPMA) homopolymer

Prior to polymerization, PFPMA was filtered over neutral alumina to remove inhibitor. PFPMA (2.16, 8.6 mmol, 300 eq.), RAFT agent CPADB (8.0 mg, 0.03 mmol, 1 eq.) and AIBN (0.47 mg, 0.003 mmol, 0.1 eq) were combined with 1,4-dioxane (2 mL) in a polymerization flask fitted with a rubber septum. After purging for 30 minutes with nitrogen, the flask was placed in a preheated oil bath at 80 °C. After reaching 70% conversion, the flask was submerged in an ice bath and diluted with dichloromethane followed by repeated precipitations in cold heptane to yield a pink powder (1.1 g, 83% yield). The polymer was dissolved in 1,4-dioxane (11 mL) and AIBN (86 mg, 0.5 mmol, 28 eq.) was added. After purging for 30 minutes with nitrogen, the flask was placed in a preheated oil bath at 80° C and stirred overnight. The 1,4-dioxane was subsequently removed under reduced pressure and the polymer was redissolved in DCM and purified by repeated precipitations in cold heptane to yield a white powder (0.9 g, 82% yield).

^1H NMR (acetone- d_6) δ_{H} : 2.62–2.25 (br), 2.20–1.99 (br), 3.65–3.37 (br), 1.75–1.51 (br), 1.51–1.23 (br). ^{19}F NMR (acetone- d_6) δ_{F} : -150.5 (br), -151.5 -157.0 (br), -162.1 (br).

Pentafluorophenyl functionalized SCNPs

The range of differently positively charged was made from the same batch **PFP-SCNPs**. As an example, for the 15% substituted SCNPs (**SCNP-15**), 50 mg of **PFP-SCNPs** (0.17 mmol PFP, 1 eq.) was dissolved in 3 mL dry THF under nitrogen atmosphere. Triethylamine was added (96 μ L, 0.69 mmol, 4 eq.), followed by *N,N*-dimethylethylenediamine (DMEN) (2.3 mg, 0.026 mmol, 0.15 eq, from a 5.0 wt% stock solution in dry THF) and the solution was stirred for 24h at 45° C. Full conversion was confirmed by ^{19}F NMR analysis, followed by the addition of 3-amino-1,2,-propanediol (314 mg, 3.4 mmol, 20 eq., 10 wt% solution in DMF) to endcap the remaining reactive PFP-groups. After stirring overnight at room temperature, the

mixture was dialysed against 1 wt% NaCl for 24 hours, followed by another 48 hours against demineralized water. The clear solutions were lyophilized to yield a white powder (25 mg, 79% yield).

Fluorescent labelling

Functionalized SCNPs (10 mg) were dissolved in 2 mL of 0.1 M carbonate-bicarbonate buffer (pH 9.7). 5-DTAF (0.02 eq. to alcohol groups, 10 mg/mL stock solution in dry DMSO) was added and the solutions were stirred under ambient conditions overnight, after which they were purified by elution with water from a PD-10 column and subsequently lyophilized to yield yellow powders (9 mg, 90% yield).

Cell Culture

bEND.3 cells (p.25-30) were cultured in DMEM medium with 10% FBS, L-glutamine and Pen/Strep.

Cytotoxicity

bEND.3 cells were seeded at 10×10^3 cells per well in 100 μ L DMEM medium in 96 well plates and incubated overnight at 37 °C in humidified 5% CO₂-containing atmosphere. From a stock solution of 1 mg/mL **SCNPs-0-60** sample solutions of 50, 100, 200 and 500 μ g/mL were prepared. The medium was aspirated from the wells and 50 μ L of the sample solution was added per well in triplicates. In the reference wells 50 μ L DMEM was added. The SCNPs were incubated for 24 h with the cells, before the medium was aspirated and the cells were washed with PBS. A resazurin assay was utilized to analyze the viability of the cells, 100 μ L of the resazurin solution was added per well and incubated with the cells for 4 h. Afterwards, the fluorescence intensity was measured by an EnSpire plate reader at excitation and emission wavelengths of 560/590 nm.

Cellular uptake by FACS

In 48 well plates bEND.3 cells were seeded at 30×10^3 cells per well in 300 μ L medium and incubated overnight. Sample solutions of each particle at 100 μ g/mL were prepared. The particles were incubated with the cells for 1, 3 and 6 h. Then, the cells were washed with PBS and harvested using trypsin. Subsequently, the samples were centrifuges at 1.5 g for 4 min and the supernatant was removed. The cell pellet was resuspended in 300 μ L PBS. During the flow cytometry the samples were additionally incubated with a PI staining to analyze the cell viability. The FACS analysis was performed using BD Bioscience FACS Aria II with excitation and emission filter of 488-530/30 and 630-660/30 nm.

Confocal laser scanning microscopy

bEND.3 cells were incubated at 10×10^3 cells per well in 100 μ L medium on a 96 senso plate overnight. Cells were incubated with sample solutions of SCNPs at 50 μ g/mL for 1h (**SCNP-45** and **SCNP-60**) or 6h (**SCNP-0**, **15** and **30**). Afterwards, the cells were fixated using a 4% PFA solution. CF@405 M WGA staining was used at 5 μ g/mL for 15 min at 37 °C and a DAPI counter staining was added for 3 min at room temperature. Subsequently, the cells were washed and stored in HANKS buffer. The cells were examined using a Nikon confocal microscope A1, equipped with the following laser wavelengths: 375, 488 and 561 nm.

2.5 Supplementary information

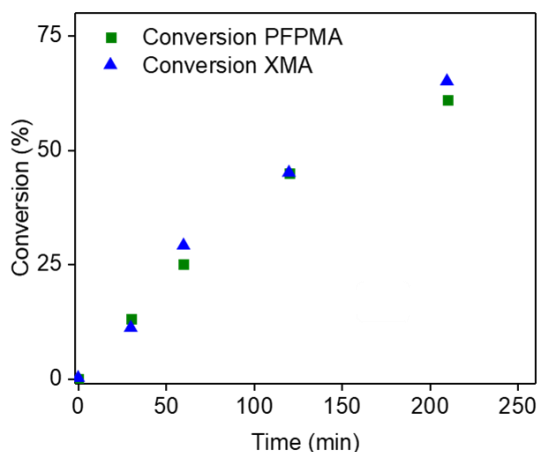


Figure S2.1. Conversion plot of monomers units during p(PFPMA-XMA) polymerization.

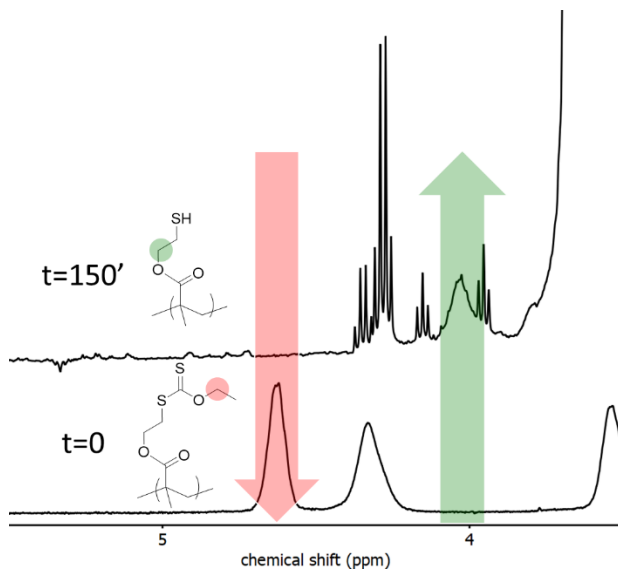


Figure S2.2. Deprotection of p(PFPMA-XMA) by ethanolamine. After 150', deprotection is complete, indicated by the disappearance of the peak at $\delta = 4.6$ ppm and the appearance of a new peak at $\delta = 4.1$ ppm.

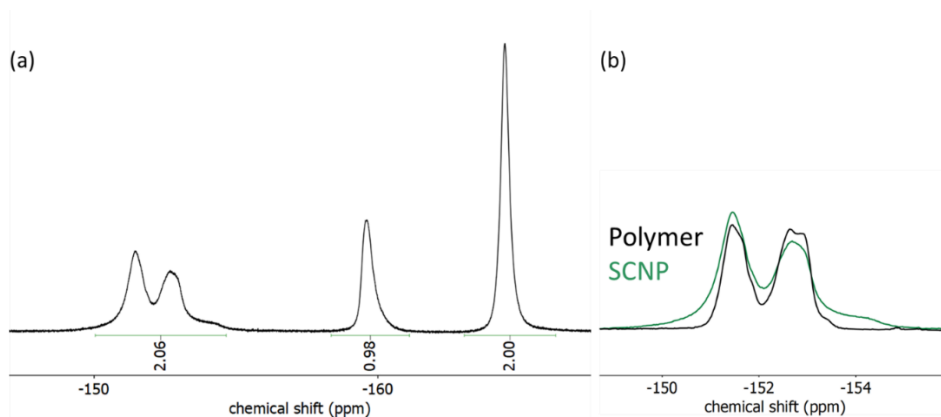


Figure S2.3. ^{19}F NMR spectra of (a) PFP-SCNP and (b) zoom-in on ortho position, indicating line broadening for PFP-SCNPs compared to precursor.

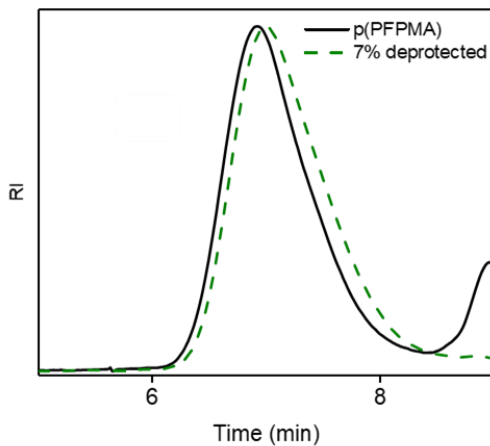


Figure S2.4. Overlaid GPC-traces of p(PFPMA) and partially deprotected p(PFPMA)

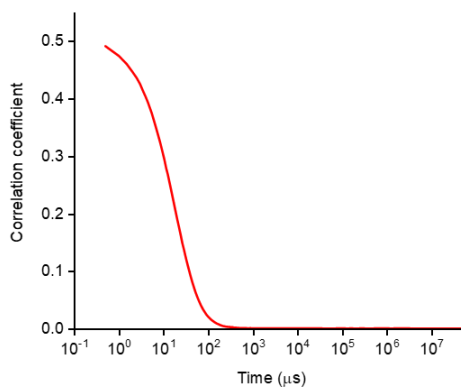


Figure S2.5. Correlation curve of DLS-measurement of the precursor PFP-SCNP.

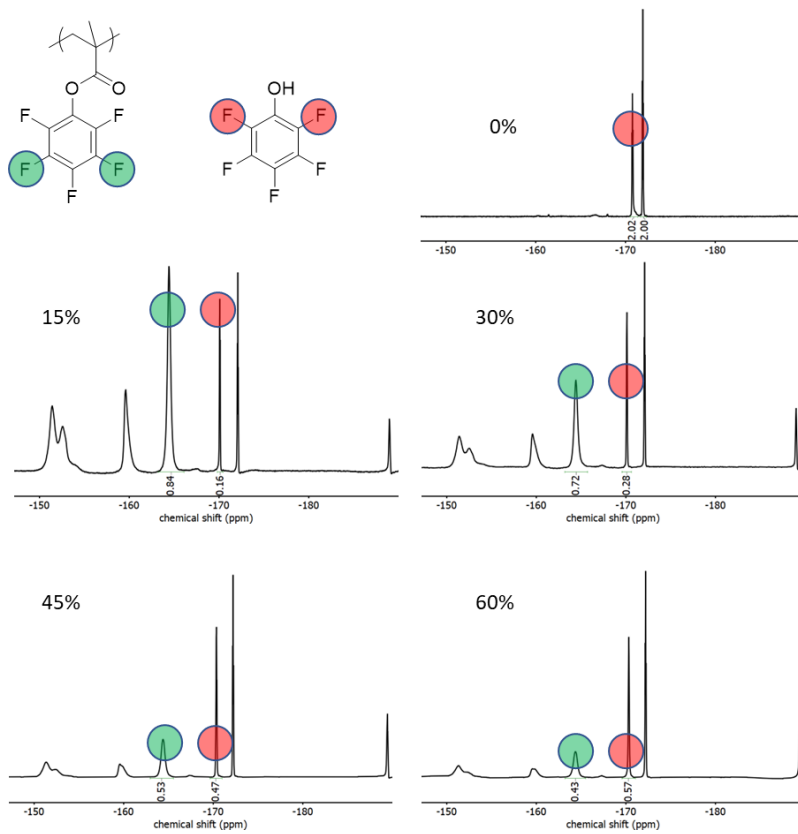


Figure S2.6. Conversion of active PFP-esters quantified by ^{19}F NMR-spectroscopy.

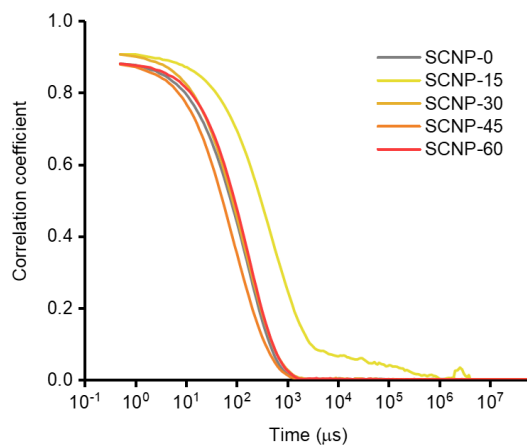


Figure S2.7. Correlation curve of the DLS-measurements of the range of functionalization SCNPs.

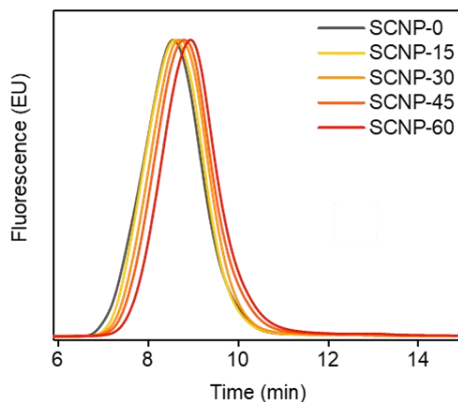


Figure S2.8. Fluorescent GPC-traces of functionalized SCNPs (excitation wavelength 492 nm, emission wavelength 516 nm)

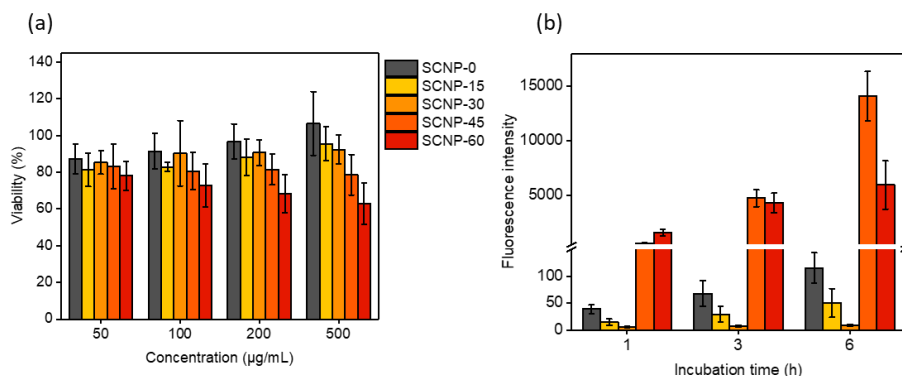


Figure S2.9. a) Cell viability of bEND.3 cells after incubation with SCNPs after 24 h; b) Fluorescence intensity of SCNPs in bEND.3 cells after 1, 3 and 6 h incubation measured by FACS.

2.6 References

- Hawker, C. J.; Wooley, K. L., The Convergence of Synthetic Organic and Polymer Chemistries. *Science* **2005**, 309 (5738), 1200-1205.
- Karabasz, A.; Bzowska, M.; Szczepanowicz, K., Biomedical Applications of Multifunctional Polymeric Nanocarriers: A Review of Current Literature. *Int J Nanomedicine* **2020**, 15, 8673-8696.
- Algar, W. R.; Massey, M.; Rees, K.; Higgins, R.; Krause, K. D.; Darwish, G. H.; Peveler, W. J.; Xiao, Z.; Tsai, H.-Y.; Gupta, R.; Lix, K.; Tran, M. V.; Kim, H., Photoluminescent Nanoparticles for Chemical and Biological Analysis and Imaging. *Chemical Reviews* **2021**, 121 (15), 9243-9358.
- Zhang, L.; Jin, D.; Stenzel, M. H., Polymer-Functionalized Upconversion Nanoparticles for Light/Imaging-Guided Drug Delivery. *Biomacromolecules* **2021**, 22 (8), 3168-3201.

5. Chen, X.; Hussain, S.; Abbas, A.; Hao, Y.; Malik, A. H.; Tian, X.; Song, H.; Gao, R., Conjugated polymer nanoparticles and their nanohybrids as smart photoluminescent and photoresponsive material for biosensing, imaging, and theranostics. *Mikrochim Acta* **2022**, *189* (3), 83.
6. Paisley, N. R.; Tonge, C. M.; Hudson, Z. M., Stimuli-Responsive Thermally Activated Delayed Fluorescence in Polymer Nanoparticles and Thin Films: Applications in Chemical Sensing and Imaging. *Front Chem* **2020**, *8*, 229.
7. Mitchell, M. J.; Billingsley, M. M.; Haley, R. M.; Wechsler, M. E.; Peppas, N. A.; Langer, R., Engineering precision nanoparticles for drug delivery. *Nat Rev Drug Discov* **2021**, *20* (2), 101-124.
8. Kakkar, A.; Traverso, G.; Farokhzad, O. C.; Weissleder, R.; Langer, R., Evolution of macromolecular complexity in drug delivery systems. *Nat Rev Chem* **2017**, *1* (8).
9. Calzoni, E.; Cesaretti, A.; Polchi, A.; Di Michele, A.; Tancini, B.; Emiliani, C., Biocompatible Polymer Nanoparticles for Drug Delivery Applications in Cancer and Neurodegenerative Disorder Therapies. *J Funct Biomater* **2019**, *10* (1).
10. Dolai, J.; Mandal, K.; Jana, N. R., Nanoparticle Size Effects in Biomedical Applications. *ACS Applied Nano Materials* **2021**, *4* (7), 6471-6496.
11. Sonavane, G.; Tomoda, K.; Makino, K., Biodistribution of colloidal gold nanoparticles after intravenous administration: effect of particle size. *Colloids Surf B Biointerfaces* **2008**, *66* (2), 274-80.
12. De Jong, W. H.; Hagens, W. I.; Krystek, P.; Burger, M. C.; Sips, A. J.; Geertsma, R. E., Particle size-dependent organ distribution of gold nanoparticles after intravenous administration. *Biomaterials* **2008**, *29* (12), 1912-9.
13. Hoshyar, N.; Gray, S.; Han, H.; Bao, G., The effect of nanoparticle size on in vivo pharmacokinetics and cellular interaction. *Nanomedicine* **2016**, *11* (6), 673-692.
14. Shang, L.; Nienhaus, K.; Nienhaus, G. U., Engineered nanoparticles interacting with cells: Size matters. *Journal of Nanobiotechnology* **2014**, *12* (1).
15. Bai, Y.; Hang, X.; Wu, P.; Feng, X.; Hwang, K.; Lee, J. M.; Phang, X. Y.; Lu, Y.; Zimmerman, S. C., Chemical Control over Cellular Uptake of Organic Nanoparticles by Fine Tuning Surface Functional Groups. *ACS Nano* **2015**, *9* (10), 10.
16. Beck, J. B.; Killops, K. L.; Kang, T.; Sivanandan, K.; Bayles, A.; Mackay, M. E.; Wooley, K. L.; Hawker, C. J., Facile Preparation of Nanoparticles by Intramolecular Crosslinking of Isocyanate Functionalized Copolymers. *Macromolecules* **2009**, *42* (15), 5629-5635.
17. Lo Verso, F.; Pomposo, J. A.; Colmenero, J.; Moreno, A. J., Multi-orthogonal folding of single polymer chains into soft nanoparticles. *Soft Matter* **2014**, *10* (27), 4813-21.
18. Perez-Baena, I.; Asenjo-Sanz, I.; Arbe, A.; Moreno, A. J.; Lo Verso, F.; Colmenero, J.; Pomposo, J. A., Efficient Route to Compact Single-Chain Nanoparticles: Photoactivated Synthesis via Thiol-Yne Coupling Reaction. *Macromolecules* **2014**, *47* (23), 8270-8280.
19. Prasher, A.; Loynd, C. M.; Tuten, B. T.; Frank, P. G.; Chao, D.; Berda, E. B., Efficient fabrication of polymer nanoparticles via sonogashira cross-linking of linear polymers in dilute solution. *Journal of Polymer Science Part A: Polymer Chemistry* **2016**, *54* (1), 209-217.
20. Hanlon, A. M.; Chen, R.; Rodriguez, K. J.; Willis, C.; Dickinson, J. G.; Cashman, M.; Berda, E. B., Scalable Synthesis of Single-Chain Nanoparticles under Mild Conditions. *Macromolecules* **2017**, *50* (7), 2996-3003.
21. Frisch, H.; Bloesser, F. R.; Barner-Kowollik, C., Controlling Chain Coupling and Single-Chain Ligation by Two Colours of Visible Light. *Angew Chem Int Ed Engl* **2019**, *58* (11), 3604-3609.
22. Rubio-Cervilla, J.; Frisch, H.; Barner-Kowollik, C.; Pomposo, J. A., Synthesis of Single-Ring Nanoparticles Mimicking Natural Cyclotides by a Stepwise Folding-Activation-Collapse Process. *Macromol Rapid Commun* **2019**, *40* (1), e1800491.
23. Zhou, Y.; Qu, Y.; Yu, Q.; Chen, H.; Zhang, Z.; Zhu, X., Controlled synthesis of diverse single-chain polymeric nanoparticles using polymers bearing furan-protected maleimide moieties. *Polymer Chemistry* **2018**, *9* (23), 3238-3247.
24. Song, C.; Li, L.; Dai, L.; Thayumanavan, S., Responsive single-chain polymer nanoparticles with host-guest features. *Polymer Chemistry* **2015**, *6* (26), 4828-4834.

25. Artar, M.; Souren, E. R. J.; Terashima, T.; Meijer, E. W.; Palmans, A. R. A., Single Chain Polymeric Nanoparticles as Selective Hydrophobic Reaction Spaces in Water. *ACS Macro Letters* **2015**, *4* (10), 1099-1103.
26. Seo, M.; Beck, B. J.; Paulusse, J. M. J.; Hawker, C. J.; Kim, S. Y., Polymeric Nanoparticles via Noncovalent Cross-Linking of Linear Chains. *Macromolecules* **2008**, *41* (17), 6413-6418.
27. Lyon, C. K.; Prasher, A.; Hanlon, A. M.; Tuten, B. T.; Tooley, C. A.; Frank, P. G.; Berda, E. B., A brief user's guide to single-chain nanoparticles. *Polymer Chemistry* **2015**, *6* (2), 181-197.
28. Huo, M.; Wang, N.; Fang, T.; Sun, M.; Wei, Y.; Yuan, J., Single-chain polymer nanoparticles: Mimic the proteins. *Polymer* **2015**, *66*, A11-A21.
29. Blasco, E.; Tuten, B. T.; Frisch, H.; Lederer, A.; Barner-Kowollik, C., Characterizing single chain nanoparticles (SCNPs): a critical survey. *Polymer Chemistry* **2017**, *8* (38), 5845-5851.
30. Pomposo, J. A.; Perez-Baena, I.; Lo Verso, F.; Moreno, A. J.; Arbe, A.; Colmenero, J., How Far Are Single-Chain Polymer Nanoparticles in Solution from the Globular State? *ACS Macro Lett.* **2014**, *3* (8), 767-772.
31. Woythe, L.; Tito, N. B.; Albertazzi, L., A quantitative view on multivalent nanomedicine targeting. *Adv Drug Deliv Rev* **2021**, *169*, 1-21.
32. Sun, J.; Zhang, L.; Wang, J.; Feng, Q.; Liu, D.; Yin, Q.; Xu, D.; Wei, Y.; Ding, B.; Shi, X.; Jiang, X., Tunable Rigidity of (Polymeric Core)–(Lipid Shell) Nanoparticles for Regulated Cellular Uptake. *Adv. Mater.* **2015**, *27* (8), 1402-1407.
33. Wang, S.; Guo, H.; Li, Y.; Li, X., Penetration of nanoparticles across a lipid bilayer: effects of particle stiffness and surface hydrophobicity. *Nanoscale* **2019**, *11* (9), 4025-4034.
34. Kuhn, W.; Balmer, G., Crosslinking of single linear macromolecules. *Journal of Polymer Science* **1962**, *57* (165), 311-319.
35. Harth, E.; Horn, B. V.; Lee, V. Y.; Germack, D. S.; Gonzales, C. P.; Miller, R. D.; Hawker, C. J., A Facile Approach to Architecturally Defined Nanoparticles via Intramolecular Chain Collapse. *Journal of the American Chemical Society* **2002**, *124* (29), 8653-8660.
36. Kroger, A. P. P.; Paulusse, J. M. J., Single-chain polymer nanoparticles in controlled drug delivery and targeted imaging. *J Control Release* **2018**, *286*, 326-347.
37. Mavila, S.; Eivgi, O.; Berkovich, I.; Lemcoff, N. G., Intramolecular Cross-Linking Methodologies for the Synthesis of Polymer Nanoparticles. *Chem Rev* **2016**, *116* (3), 878-961.
38. Alqarni, M. A. M.; Waldron, C.; Yilmaz, G.; Becer, C. R., Synthetic Routes to Single Chain Polymer Nanoparticles (SCNPs): Current Status and Perspectives. *Macromol Rapid Commun* **2021**, e2100035.
39. Kröger, A. P. P.; Boonen, R. J. E. A.; Paulusse, J. M. J., Well-defined single-chain polymer nanoparticles via thiol-Michael addition. *Polymer* **2017**, *120*, 119-128.
40. Chan, J. W.; Hoyle, C. E.; Lowe, A. B.; Bowman, M., Nucleophile-Initiated Thiol-Michael Reactions: Effect of Organocatalyst, Thiol, and Ene. *Macromolecules* **2010**, *43* (15), 6381-6388.
41. Desmet, G. B.; Sabbe, M. K.; D'Hooge, D. R.; Espeel, P.; Celasun, S.; Marin, G. B.; Du Prez, F. E.; Reyniers, M.-F., Thiol-Michael addition in polar aprotic solvents: nucleophilic initiation or base catalysis? *Polymer Chemistry* **2017**, *8* (8), 1341-1352.
42. Braunecker, W. A.; Matyjaszewski, K., Controlled/living radical polymerization: Features, developments, and perspectives. *Progress in Polymer Science* **2007**, *32* (1), 93-146.
43. Nicolaÿ, R., Synthesis of Well-Defined Polythiol Copolymers by RAFT Polymerization. *Macromolecules* **2011**, *45* (2), 821-827.
44. Campos, L. M.; Killops, K. L.; Sakai, R.; Paulusse, J. M. J.; Dameron, D.; Drockenmuller, E.; Messmore, B. W.; Hawker, C. J., Development of Thermal and Photochemical Strategies for Thiol–Ene Click Polymer Functionalization. *Macromolecules* **2008**, *41* (19), 7063-7070.
45. Gruber, A.; Navarro, L.; Klinger, D., Reactive Precursor Particles as Synthetic Platform for the Generation of Functional Nanoparticles, Nanogels, and Microgels. *Advanced Materials Interfaces* **2020**, *7* (5), 1901676.

46. Lee, Y.; Pyun, J.; Lim, J.; Char, K., Modular synthesis of functional polymer nanoparticles from a versatile platform based on poly(pentafluorophenylmethacrylate). *Journal of Polymer Science Part A: Polymer Chemistry* **2016**, *54* (13), 1895-1901.
47. Gruber, A.; Işık, D.; Fontanezi, B. B.; Böttcher, C.; Schäfer-Korting, M.; Klinger, D., A versatile synthetic platform for amphiphilic nanogels with tunable hydrophobicity. *Polymer Chemistry* **2018**, *9* (47), 5572-5584.
48. Han, K.; Tiwari, R.; Heuser, T.; Walther, A., Simple Platform Method for the Synthesis of Densely Functionalized Microgels by Modification of Active Ester Latex Particles. *Macromolecular Rapid Communications* **2016**, *37* (16), 1323-1330.
49. Kakuchi, R.; Theato, P., Post-Polymerization Modifications via Active Esters. In *Functional Polymers by Post-Polymerization Modification*, 2012; pp 45-64.
50. Das, A.; Theato, P., Activated Ester Containing Polymers: Opportunities and Challenges for the Design of Functional Macromolecules. *Chem Rev* **2016**, *116* (3), 1434-95.
51. Eberhardt, M.; Mruk, R.; Zentel, R.; Théato, P., Synthesis of pentafluorophenyl(meth)acrylate polymers: New precursor polymers for the synthesis of multifunctional materials. *European Polymer Journal* **2005**, *41* (7), 1569-1575.
52. Son, H.; Ku, J.; Kim, Y.; Li, S.; Char, K., Amine-Reactive Poly(pentafluorophenyl acrylate) Brush Platforms for Cleaner Protein Purification. *Biomacromolecules* **2018**, *19* (3), 951-961.
53. Zamfir, M.; Theato, P.; Lutz, J.-F., Controlled folding of polystyrene single chains: design of asymmetric covalent bridges. *Polym. Chem.* **2012**, *3* (7), 1796-1802.
54. Roy, R. K.; Lutz, J. F., Compartmentalization of single polymer chains by stepwise intramolecular cross-linking of sequence-controlled macromolecules. *J Am Chem Soc* **2014**, *136* (37), 12888-91.
55. Liu, Y.; Pauloehrl, T.; Presolski, S. I.; Albertazzi, L.; Palmans, A. R.; Meijer, E. W., Modular Synthetic Platform for the Construction of Functional Single-Chain Polymeric Nanoparticles: From Aqueous Catalysis to Photosensitization. *J Am Chem Soc* **2015**, *137* (40), 13096-105.
56. Deng, L.; Albertazzi, L.; Palmans, A. R. A., Elucidating the Stability of Single-Chain Polymeric Nanoparticles in Biological Media and Living Cells. *Biomacromolecules* **2022**, *23* (1), 326-338.
57. Liu, Y.; Pujals, S.; Stals, P. J. M.; Pauloehrl, T.; Presolski, S. I.; Meijer, E. W.; Albertazzi, L.; Palmans, A. R. A., Catalytically Active Single-Chain Polymeric Nanoparticles: Exploring Their Functions in Complex Biological Media. *J Am Chem Soc* **2018**, *140* (9), 3423-3433.
58. Chen, J.; Li, K.; Shon, J. S. L.; Zimmerman, S. C., Single-Chain Nanoparticle Delivers a Partner Enzyme for Concurrent and Tandem Catalysis in Cells. *J Am Chem Soc* **2020**, *142* (10), 4565-4569.
59. Chen, J.; Wang, J.; Li, K.; Wang, Y.; Gruebele, M.; Ferguson, A. L.; Zimmerman, S. C., Polymeric "Clickase" Accelerates the Copper Click Reaction of Small Molecules, Proteins, and Cells. *J Am Chem Soc* **2019**, *141* (24), 9693-9700.
60. Pan, L.; Liu, J.; Shi, J., Cancer cell nucleus-targeting nanocomposites for advanced tumor therapeutics. *Chem Soc Rev* **2018**, *47* (18), 6930-6946.
61. Shi, Y.; Luo, Z.; You, J., Subcellular delivery of lipid nanoparticles to endoplasmic reticulum and mitochondria. *Wiley Interdiscip Rev Nanomed Nanobiotechnol* **2022**, *14* (5), e1803.
62. Elzes, M. R.; Mertens, I.; Sedlacek, O.; Verbraeken, B.; Doensen, A. C. A.; Mees, M. A.; Glassner, M.; Jana, S.; Paulusse, J. M. J.; Hoogenboom, R., Linear Poly(ethylenimine-propylenimine) Random Copolymers for Gene Delivery: From Polymer Synthesis to Efficient Transfection with High Serum Tolerance. *Biomacromolecules* **2022**, *23* (6), 2459-2470.
63. Li, L.; Wei, Y.; Gong, C., Polymeric Nanocarriers for Non-Viral Gene Delivery. *J Biomed Nanotechnol* **2015**, *11* (5), 739-70.
64. Agarwal, S.; Zhang, Y.; Maji, S.; Greiner, A., PDMAEMA based gene delivery materials. *Materials Today* **2012**, *15* (9), 388-393.
65. Lee, H.; Son, S. H.; Sharma, R.; Won, Y. Y., A discussion of the pH-dependent protonation behaviors of poly(2-(dimethylamino)ethyl methacrylate) (PDMAEMA) and poly(ethylenimine-ran-2-ethyl-2-oxazoline) (P(EI-r-EOz)). *J Phys Chem B* **2011**, *115* (5), 844-60.

66. Koper, G. J. M.; Borkovec, M., Proton binding by linear, branched, and hyperbranched polyelectrolytes. *Polymer* **2010**, *51* (24), 5649-5662.
67. Bus, T.; Traeger, A.; Schubert, U. S., The great escape: how cationic polyplexes overcome the endosomal barrier. *J Mater Chem B* **2018**, *6* (43), 6904-6918.
68. Rennick, J. J.; Nowell, C. J.; Pouton, C. W.; Johnston, A. P. R., Resolving subcellular pH with a quantitative fluorescent lifetime biosensor. *Nat Commun* **2022**, *13* (1), 6023.
69. Frohlich, E., The role of surface charge in cellular uptake and cytotoxicity of medical nanoparticles. *Int J Nanomedicine* **2012**, *7*, 5577-91.
70. Romoren, K.; Thu, B. J.; Bols, N. C.; Evensen, O., Transfection efficiency and cytotoxicity of cationic liposomes in salmonid cell lines of hepatocyte and macrophage origin. *Biochim Biophys Acta* **2004**, *1663* (1-2), 127-34.
71. Manzanares-Guevara, L. A.; Licea-Claverie, A.; Oroz-Parra, I.; Licea-Navarro, A. F., On the cytotoxicity of a cationic tertiary amine PEGylated nanogel as nanocarrier for anticancer therapies. *MRS Communications* **2018**, *8* (3), 1204-1210.
72. Maiti, B.; Haldar, U.; Rajasekhar, T.; De, P., Functional-Polymer Library through Post-Polymerization Modification of Copolymers Having Oleate and Pentafluorophenyl Pendants. *Chemistry* **2017**, *23* (60), 15156-15165.
73. Varadharajan, D.; Delaittre, G., Accessing libraries of bifunctional block copolymers using two distinct pentafluorophenyl moieties. *Polymer Chemistry* **2016**, *7* (48), 7488-7499.
74. Cakir, N.; Tunca, U.; Hizal, G.; Durmaz, H., Heterofunctionalized Multiarm Star Polymers via Sequential Thiol-para-Fluoro and Thiol-Ene Double "Click" Reactions. *Macromolecular Chemistry and Physics* **2016**, *217* (5), 636-645.
75. Kröger, A. P. P.; Paats, J. D.; Boonen, R. J. E. A.; Hamelmann, N. M.; Paulusse, J. M. J., Pentafluorophenyl-based single-chain polymer nanoparticles as a versatile platform towards protein mimicry. *Polymer Chemistry* **2020**, *11* (37), 6056-6065.
76. Kroger, A. P. P.; Hamelmann, N. M.; Juan, A.; Lindhoud, S.; Paulusse, J. M. J., Biocompatible Single-Chain Polymer Nanoparticles for Drug Delivery - a Dual Approach. *ACS applied Materials & Interfaces* **2018**, *20*, 6.
77. Pack, D. W.; Hoffman, A. S.; Pun, S.; Stayton, P. S., Design and development of polymers for gene delivery. *Nat. Rev. Drug. Discov.* **2005**, *4* (7), 581-593.
78. Sprouse, D.; Reineke, T. M., Investigating the Effects of Block versus Statistical Glycopolycations Containing Primary and Tertiary Amines for Plasmid DNA Delivery. *Biomacromolecules* **2014**, *15* (7), 2616-2628.
79. Goswami, R.; Jeon, T.; Nagaraj, H.; Zhai, S.; Rotello, V. M., Accessing Intracellular Targets through Nanocarrier-Mediated Cytosolic Protein Delivery. *Trends Pharmacol. Sci.* **2020**, *41* (10), 743-754.
80. Vasir, J. K.; Labhasetwar, V., Biodegradable nanoparticles for cytosolic delivery of therapeutics. *Adv. Drug Deliv. Rev.* **2007**, *59* (8), 718-728.
81. Postupalenko, V.; Desplancq, D.; Orlov, I.; Arntz, Y.; Spehner, D.; Mely, Y.; Klaholz, B. P.; Schultz, P.; Weiss, E.; Zuber, G., Protein Delivery System Containing a Nickel-Immobilized Polymer for Multimerization of Affinity-Purified His-Tagged Proteins Enhances Cytosolic Transfer. *Angew. Chem. Int. Ed. Engl.* **2015**, *54* (36), 10583-6.
82. Pulgar, V. M., Transcytosis to Cross the Blood Brain Barrier, New Advancements and Challenges. *Front Neurosci* **2018**, *12*, 1019.
83. Ayloo, S.; Gu, C., Transcytosis at the blood-brain barrier. *Curr Opin Neurobiol* **2019**, *57*, 32-38.

Chapter 3

Transport of single-chain polymer nanoparticles across the blood-brain barrier

The surface charge on nanoparticles has been shown to dramatically affect cellular uptake behavior and intracellular pathways. In this work, we study the effect of surface charge on the transcytosis of single-chain polymer nanoparticles (SCNPs) across the blood-brain barrier (BBB). SCNPs are well-defined soft objects, formed by exclusive intramolecular crosslinking of linear polymers, to form small nanoparticles in a size range similar to that of proteins. The SCNPs are equipped with increasing amounts of protonatable tertiary amines and their transcytosis is studied on an *in vitro* BBB model. The set of SCNPs shows high transport rates through the barrier (up to 30% after 18 h), with higher surface charge density leading to higher cellular association, and subsequent lower transcytosis rates. Confocal microscopy revealed endosomal escape for SCNPs with the highest number of tertiary amines. This study highlights the importance of selecting the right surface charge with the prospected application in mind.

Manuscript in preparation: J-W.D Paats, L. Ribovski, S. Michel-Souzy, J. M. J. Paulusse*

* Corresponding author

3.1 Introduction

Neurological disorders are currently recognized as one of the major causes of functional impairments and mortality.¹ In 2016, 276 million people worldwide suffered from neurological disabilities, with 9 million deaths occurring each year. With the increased aging of the population worldwide, these numbers are only expected to grow in the coming years. Many of the neurological disorders, such as Alzheimer's disease and epilepsy are associated with the central nervous system (CNS), which is tightly protected from the surroundings by several different barriers.² One of these is the blood-brain barrier (BBB), a specialized and highly selective set of microvascular endothelial vessels, responsible for supplying nutrients to and preventing harmful substances and pathogens from entering the brain, thereby allowing precise control over the homeostasis of this part of the central nervous system.³⁻⁴ However, the tightly regulated entry is also a major drawback for the delivery of therapeutics and diagnostics into the brain. Only small (<500 Da), lipophilic molecules are able to passively pass the barrier paracellularly, whereas the vast majority of other substances (e.g. glucose, amino acids and macromolecules) require transport proteins, receptors or vesicle formation to enter the brain.⁵ To circumvent the limitations imposed by the BBB, several strategies have emerged to aid in transporting pharmaceuticals into the brain. Invasive techniques have been developed, such as the use of intracerebral implants⁶⁻⁷ or convection-enhanced infusing⁸⁻⁹ for direct delivery to the target site. Using focused ultrasound, nowadays the BBB can even be temporarily disrupted in a non-invasive manner, to allow for increased brain delivery of therapeutics.¹⁰ However, the widespread application of these methods is hampered by the limited availability and the high costs. Alternatively, pharmaceuticals can be chemically converted into prodrugs by attaching lipids to increase paracellular transport¹¹ or equipped with recognition groups to make use of specific transporters and receptors.¹²⁻¹³ The downside is the requirement of new conjugation and optimization strategies for every single drug, severely complicating the synthetic feasibility. This stresses the urgent need for new BBB-targeting strategies.¹⁴⁻¹⁵ To this end, nanoparticle (NP)-based delivery systems have emerged as a promising tool to enhance targeted brain delivery.¹⁶⁻²⁰ NPs allow careful control over size, while simultaneously allowing for incorporation of additional functionality, higher drug loading, improved pharmacokinetics and biocompatibility. Over the years, a plethora of different NPs have been investigated as potential nanocarriers for crossing the BBB, ranging from small organic macrostructures such as dendrimers, to larger-sized lipid-based vesicles and inorganic nanostructures.²¹⁻²⁴ However, despite promising preclinical results, only very scarce examples of NPs exist that have been approved for clinical brain targeting (namely liposomes), with no active clinical trials currently running.²⁵⁻²⁶

Several NP properties have been proven to be critical for effective brain entry, such as zeta potential, shape, surface functionalization and especially size.^{23, 27} Decreasing the NP size has been reported to result in superior transport efficiency across *in vitro* BBB models and in *in vivo* mouse studies.²⁸⁻²⁹ Tuning down the size of polymeric micelles from 120 nm to 60 nm showed an increase in brain uptake, as was shown by Meng et al.³⁰ A similar trend was also observed for hard polystyrene NPs of 100 nm and 50 nm in size.³¹ Furthermore, when studying a broad size range of gold NPs, Sonavane et al. found 50 and 15 nm gold nanoparticles accumulating in the brain (among other organs), whereas 200 nm NPs only showed minute presence.³² Considering the large increase in surface to volume ratio, even smaller size NPs are likely to display further enhanced brain transport. However, soft NPs in the size range of proteins have so far not been studied for their ability to cross the BBB, due to the still limited access to NPs in this size range.³³

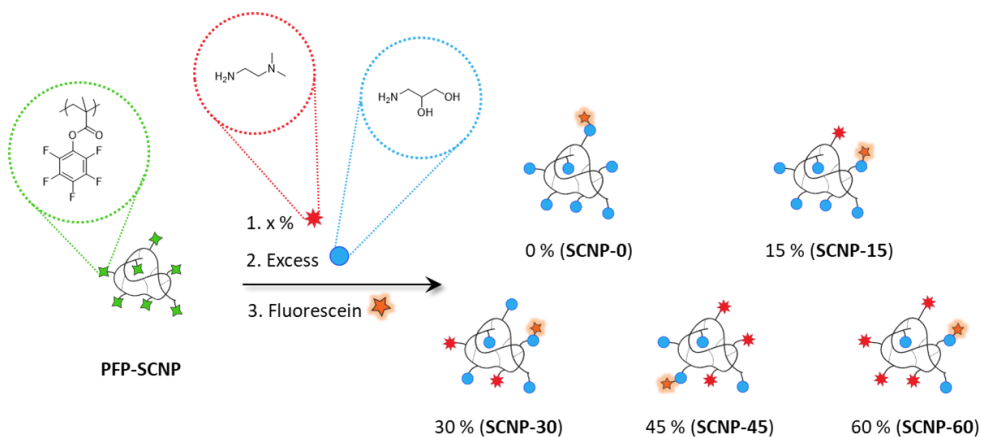
Another crucial surface property of NPs for brain entry is surface charge. Electrostatic interactions between positively charged NPs and the negatively charged endothelial cell membrane can lead to increased adsorptive interactions and possible endocytosis. Vesicles containing NPs can subsequently follow several intracellular pathways, such as recycling back to the apical membrane, fusing with endosomes for degradation or transcytosis to the basolateral side for release into the brain.³⁴⁻³⁵ This adsorption mediated transcytosis pathway has been explored as a means to improve BBB transcytosis.³⁶⁻³⁹ However, while cationic charges are known to promote cellular uptake (or only mere adherence to the cell membrane), this uptake is not necessarily followed by exocytosis to the basolateral side of the barrier. Furthermore, NPs bearing cationic charges are generally associated with cellular toxicity.⁴⁰⁻⁴¹ In contrast to neutral or anionic NPs, cationic NPs have also been reported to alter the integrity of the BBB.⁴² Consequently, finding the optimum balance between cellular uptake and transcytosis, while avoiding toxicity, requires careful alteration of the NP's surface composition.

To create small (10 nm) and synthetically flexible NPs, one method is the intramolecular crosslinking of individual polymer chains, resulting in so called single-chain polymer nanoparticles (SCNPs). SCNPs are soft and semi-flexible nanomaterials that have become of interest to a wide range of applications.⁴³⁻⁴⁵ Furthermore, equipping the SCNPs with active pentafluorophenyl (PFP) esters allows for careful tuning of surface properties (as described in Chapter 2)⁴⁶ and introduction of binding ligands for optimizing BBB transport. In this work, we evaluate the influence of surface charge, introduced in the form of tertiary amines, on the transport of SCNPs across the BBB. Pentafluorophenyl-ester-functional SCNPs were conjugated with tertiary amine groups to yield a set of five differently charged SCNPs, ranging from moderately negatively to strongly positively charged. The transport characteristics of this set of SCNPs was evaluated on a filter-free *in vitro*

BBB model based on hCMEC/D3 human brain endothelial cells and the association of SCNPs with the apical, cellular, and basolateral compartments was quantified. Confocal microscopy was used to further elucidate the distinct intracellular trafficking pathways of the different SCNPs.

3.2 Results and discussion

PFP-SCNPs were synthesized and conjugated with the desired amounts of *N,N*-dimethylamino-ethylamine (DMEN) to introduce tertiary amines, after which remaining active esters were conjugated with 1-aminoglycerol, to yield a set of SCNPs with increasing surface potential, as also previously described in Chapter 2 (see Scheme 3.1 and Table 3.1).⁴⁶⁻⁴⁷ Since 1-aminoglycerol and DMEN have nearly the same molecular weight, the range of SCNPs has very similar masses, close to 40 kDa. However, a shift towards smaller hydrodynamic volume is observed by size exclusion chromatography (SEC) upon increased DMEN content. At 0% incorporation of tertiary amines, the alcohol groups render the particle's surface negatively charged, while a plateau value of +24 mV is reached at the highest incorporation ratio of DMEN. It is important to note that zeta potential is pH and ionic strength dependent, however, the trend of increasing zeta potential is expected to remain comparable under biological conditions (e.g. in medium).



Scheme 3.1. Schematic representation of the functionalization of **PFP-SCNPs** with increasing amounts of protonatable tertiary amines, followed by conjugation of remaining PFP-esters with 1-aminoglycerol and subsequent fluorescent labelling with fluorescein (DTAF).

Table 3.1. Selected data for the charge range of SCNPs: theoretical molecular weight, number of tertiary amine groups per particle, surface charge and elution time in SEC.

	$M_{n, \text{theo}}^a$ (kDa)	# tertiary amine groups	Zeta potential ^b (mV)	Elution peak SEC (min)
SCNP-0	39.8	0	-27	8.82
SCNP-15	39.7	29	-5	8.85
SCNP-30	39.5	58	18	8.95
SCNP-45	39.5	87	24	9.04
SCNP-60	39.4	116	24	9.18

(a) Determined by ¹H NMR spectroscopy on the linear precursor for the **PFP-SCNPs**, followed by molecular weight calculations based on ligand substitution as determined by ¹⁹F NMR spectroscopy; (b) measured in 10 mM HEPES buffer, pH 7.0.

SCNPs transcytosis in a BBB model

To elucidate the effect of surface charge on the transport of SCNPs across the BBB, the range of SCNPs with increasing tertiary amine density was evaluated on a filter-free *in vitro* BBB model (Figure 3.1a-b).⁴⁸ Because positively charged NPs are reported to induce damage to cells,⁴⁹ as a start, the integrity of the barrier was investigated. A monolayer of hCMEC/D3 cells was exposed to the set of SCNPs and release of lactate dehydrogenase (LDH) was compared to untreated samples. No significant increase in the percentage of LDH release was detected, indicating that there is no evident damage to the plasma membrane of the cells that compose the monolayer (Figure S3.1). This supports that the transport of the SCNPs across the BBB is not altered due to damage to the BBB. Further validation of the integrity of the BBB model was performed by comparing the permeability of short 4 kDa and long 2000 kDa fluorescently-labelled dextran (Figure S3.2). The decreased permeability for 2000 kDa dextran shows the size-dependency of the transport through the barrier. Subsequently, **SCNP-0** to **SCNP-60** were incubated for 3, 6 and 18 h at the apical compartment, and afterwards the SCNP levels associated with the apical, cellular and basolateral compartments were compared. The transport of the whole set of SCNPs increased with incubation time, up to 32% after 18 h of incubation, which is significantly higher than other NPs evaluated earlier on the same model (i.e. 5-18% after 24 h).⁵⁰⁻⁵¹ Furthermore, a clear relation between the SCNP's association with the endothelial cells and transportation across the BBB can be observed for all incubation times (Figure 3.1c-e) and correlates with the increase in zeta potential. An increase in surface charge leads to higher cellular association, at the cost of transport to the basolateral compartment. **SCNP-60** accumulated in the

cells to a greater extent than any of the other SCNPs, which is most apparent after 18 h (Figure 3.1e).

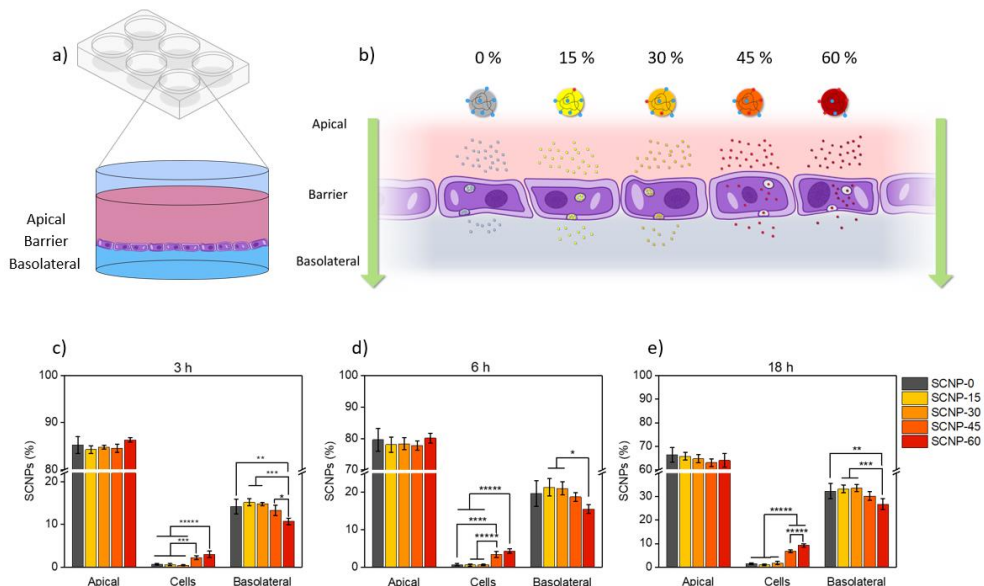


Figure 3.1. Impact of tertiary amine density on the transport properties of SCNPs across an *in vitro* BBB model. (a) Schematic of BBB-model in wells-plate (b) Schematic representation of SCNP accumulation in the BBB cells and transport across the BBB for (c) 3 h, (d) 6 h and (e) 18 h with monolayers of hCMEC/D3. Fluorescence was measured for the apical, cell and basolateral fractions by fluorescence spectroscopy. Significances are indicated by * $p < 0.05$, ** $p < 0.01$, *** $p < 0.001$, **** $p < 0.0001$, ***** $p < 0.00001$.

To further validate the BBB model, the monolayer exposed to SCNPs for 18 h was also tested for its apparent permeability (P_{app}) employing FITC-labelled dextran 4 kDa (Figure S3.3). No change in permeability was identified, demonstrating the integrity of the barrier. Lastly, western blot analysis did reveal an upregulation of ZO-1 when the model was exposed to SCNPs with the highest charges (**SCNP-45** and **SCNP-60**, Figure S3.4). Although no permeability changes were detected (as already seen from the apparent permeability in Figure S3.3), the increase in ZO-1 expression may be associated with a cellular response to attenuate mild damage and remains to be further investigated.⁵²⁻⁵³

Intracellular location of SCNPs

The transport study indicated that an increase in positive charge (**SCNP-45** and **SCNP-60**) leads to stronger cell association and decreased transport across the BBB. Previous work on the interaction of SCNPs with mouse brain endothelial (bEnd.3) cells revealed that **SCNP-45** and **SCNP-60** are able to escape the

endosome and accumulate in the cytosol,⁴⁷ which would likely hamper exocytosis on the basolateral side.³⁴ Therefore, we studied the intracellular location of the SCNP-range in a BBB-monolayer. Confocal microscopy revealed a diffuse signal throughout the cell for the samples incubated with **SCNP-45** and **SCNP-60**, confirming cytosolic entry (Figure 3.2). Concurrently, **SCNP-0** to **SCNP-30** display punctuated patterns, which point towards entrapment of the nanoparticles within endosomal structures.

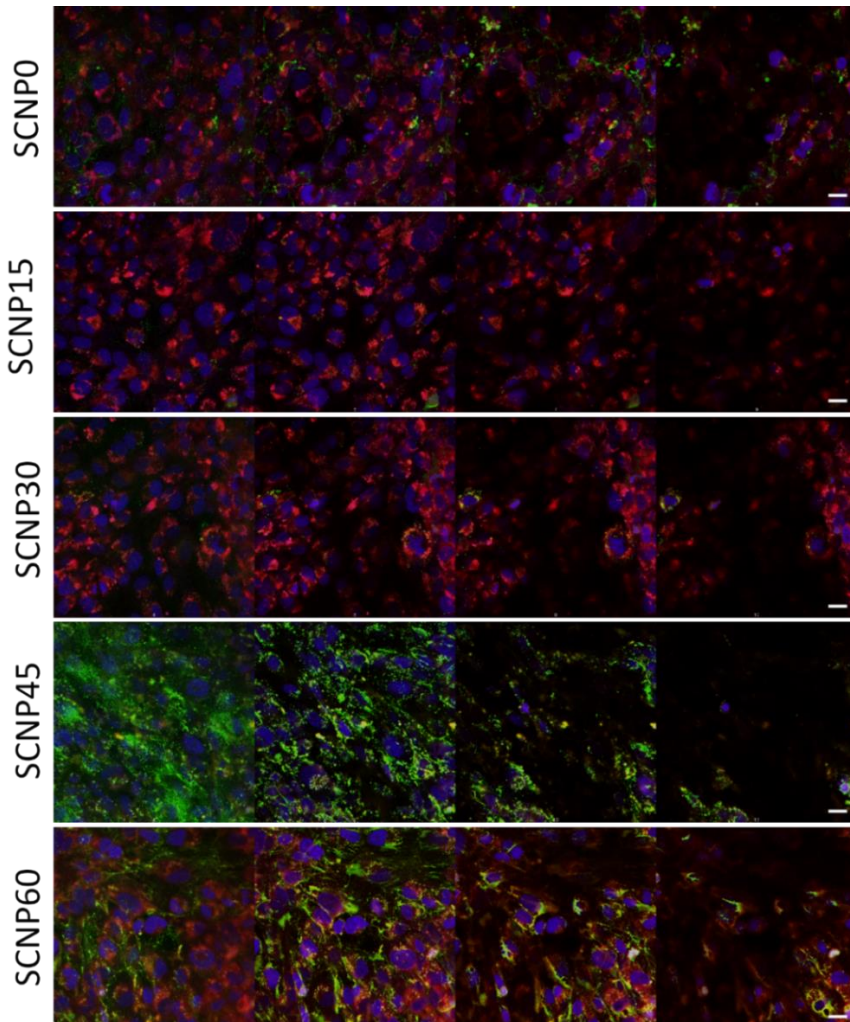


Figure 3.2. Representative confocal stacks of **SCNP-0**, **SCNP-15**, **SCNP-30**, **SCNP-45** and **SCNP-60** distribution in a hCMEC/D3 monolayer. Nuclei were stained blue, lyso/endosomes were stained red, while a green fluorescent label was used on the SCNPs. Scale bar: 20 μm .

A proposed mechanism for endosomal escape and subsequent cytosolic delivery is the 'proton sponge effect'.⁵⁴⁻⁵⁵ After reaching the endosome, the protonatable groups on the SCNPs buffer the protons pumped by ATPases, resulting in an increased influx of chloride counterions, thereby increasing the endosomal osmotic pressure. As a result, the osmotic imbalance is counteracted by an influx of water, leading to an increased endosomal membrane tension and subsequent burst release of the content. Additional swelling of the endosome is induced by the volumetric expansion of the SCNPs upon protonation, caused by the electrostatic repulsion of neighboring charged groups (as measured by ¹H DOSY NMR, Table 3.2). This 'umbrella effect' additionally contributes to the swelling of the endosome.⁵⁶ The effect is more pronounced upon higher tertiary amine content, though still showing the same plateau-behavior as observed earlier for the surface charge measurements (as shown in Table 3.1). This plateau could be caused by the SCNP's crosslinking, which physically imposes a maximum swelling that can be attained.

Table 3.2. Hydrodynamic radii (R_h) determined by ¹H DOSY NMR in D₂O at pH 7 and pH 4 and the increase in R_h and volume after acidification.

	R_h , DOSY, pH 7 (nm)	R_h , DOSY, pH 4 (nm)	ΔR_h	Δ Volume
SCNP-0	5.8	5.6	-5 %	-10%
SCNP-15	5.0	8.0	+60 %	+300%
SCNP-30	5.0	10.5	+110 %	+800%
SCNP-45	5.3	11.2	+110 %	+800%
SCNP-60	5.3	12.0	+125 %	+1000%

To shed more light on the effect of the endosomal pH on cytosolic delivery and potentially lowering of transcytosis, we employed a bafilomycin A1 (BafA1) assay. BafA1 is a V-ATPase inhibitor, preventing acidification of endosomes during maturation and thus preventing the influx of protons and counter-ions.⁵⁷⁻⁵⁸ **SCNP-45** was used as a model particle to analyze the effect of pH on the intracellular trafficking of the SCNPs that displayed endosomal escape. After pre-incubation with BafA1, the intracellular location of **SCNP-45** was studied by confocal microscopy. With BafA1 incubation, the green fluorescent pattern in the cells is more punctuated and less diffuse, compared to non-incubated cells (Figure 3.3). This suggests that neutralization of the pH of the endosomes reduces endosomal escape of **SCNP-45**. However, although the diffuse pattern is considerably diminished in the +BafA1

samples, it is not absent, suggesting that endosomal escape might occur through multiple mechanisms.

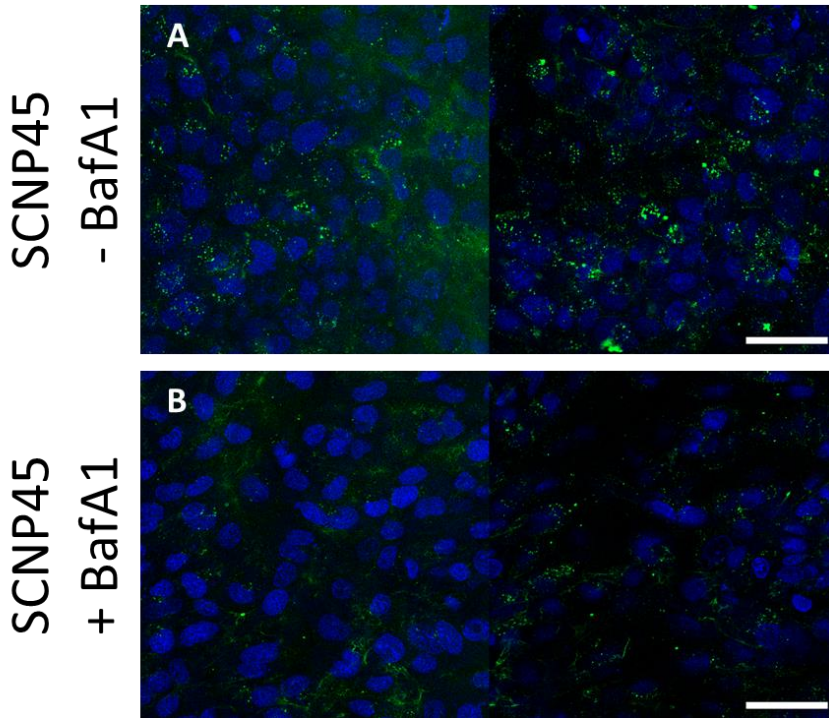


Figure 3.3. BafA1 analysis. Representative confocal stacks/images of hCMEC/D3 cells layer exposed to **SCNP-45** for 1 h in the (a) presence and (b) absence of BafA1. The distance between the stacked images is 2 μm . Nuclei were stained blue, while a green fluorescent label was used on the SCNPs. Scale bar: 50 μm .

In addition to the proton sponge effect, another possible mechanism for release of NPs from the endo/lysosomes into the cytoplasm is damage or disruption of the membrane triggered by the electrostatic interaction of the particle's positive surface charge and the anionic lipidic bilayer.⁵⁹⁻⁶⁰ The interaction would destabilize and/or induce endosomal pore formation, allowing NPs to escape.⁶¹⁻⁶² Majzoub et al. showed for DNA-containing liposomes that the membrane charge density impacts the particle's intracellular pathways and endosomal escape.⁶³ Liposomes with low positive membrane charge favored Rab11-mediated recycling pathways, whereas high positive membrane charge lead to increased endosomal escape (as evidenced by increased transfection efficiency). A similar trend is observed in the transport studies on our set of SCNPs (see Figure 3.1c-e). **SCNP-0**, **SCNP-15** and **SCNP-30** show lower retention in the endothelial cells as compared to **SCNP-45** and **SCNP-60**, but higher rates of transcytosis. Since Rab11-positive endosomes are associated

with the recycling of intracellular content which can be transported to apical or basolateral membranes to be released, this would explain the observed trend: Endosomal trapping leads to higher transcytosis rates and high surface charge leads to intracellular endosomal release, preventing the use of recycling pathways and thus transcytosis.⁶⁴⁻⁶⁷ However, the exact mechanism of endosomal escape and the role of positive surface charge on intracellular pathways and trafficking remains to be further investigated.

3.3 Conclusion

In this study, we evaluated the transport properties of a set of SCNPs with increasing tertiary amine content on an *in vitro* BBB model. Transcytosis rates up to 32 % after 18 h were observed, which is significantly higher than previously measured NPs on the same BBB model. Increasing the amount of tertiary amines on the SCNPs results in decreased transcytosis rates and increased endosomal escape into the cytosol. However, it cannot be excluded that the current model is not capable of properly discriminating between the different surface functionalities and that the small size is the predominant factor in determining the transcytosis results. Studying a 10-200 nm size range of homogenous NPs would help to discern between the influence of the NP's colloidal properties and surface functionalization on BBB transport. Alternatively, transport can be studied in more advanced *in vitro* co-culture models or *in vivo* to shed more light on the transport characteristics. Upon inhibiting acidification of the endosomes, only partial reduction of cytosolic delivery is observed. This shows that endosomal escape is not only governed by endosomal swelling and bursting induced by the proton sponge effect, but a more complex interplay between the particle's surface charge and the endosomes is at hand. Overall, these results indicate that the SCNPs' surface charge is an important factor to consider for brain delivery, since the intracellular trafficking pathways and subsequent transcytosis are influenced by the amount of protonatable amines on the surface.

3.4 Materials and Methods

Fluorescently labelled dextrans and bafilomycin A1 (BafA1, >90%) were purchased from Sigma-Aldrich. All chemicals were used without further purification unless stated otherwise. Zeta potential measurements were performed on a Malvern Instruments Zetasizer ZS in HEPES buffer (10 mM, no added NaCl, pH 7.0). ¹H NMR DOSY experiments were performed as described in chapter 3. Size exclusion chromatography (SEC) analysis was performed on a Waters e2695 Separations Module equipped with an Agilent PLgel 5 µm MIXED-D 300x7.5 mm column and Waters photodiode array detector (PDA 2998), fluorescence detector (FLR 2475)

and refractive index detector (RI 2414). DMF with 50 mM LiCl was employed as eluent.

For cell experiments, endothelial basal medium 2 (#190860, EBM-2) was purchased from Lonza. The supplements fetal bovine serum (FBS), penicillin–streptomycin, HEPES (Gibco #15630106), chemically defined lipid concentrate (Gibco, #11905-031) and recombinant basic fibroblast growth factor (bFGF, #100-18B) from Peprotech. Ascorbic acid (#A4544) and hydrocortisone (#H0888) were obtained from Sigma. Collagen type-I from rat tail (#ALX-522-435, LOT 01031910 or LOT 04272115) was purchased from Enzo Life Sciences for preparing the collagen gels for the filter free BBB model or coating cell culture flasks and plates. Collagen type-I from rat tail from Sigma (#C3867, Batch Number SLCK5464) was employed exclusively for coating cell culture flasks. 10x PBS (#70011044), NucRed™ Live 647 (#R37106), ZO-1 (#617300), LysoTracker Red DND-99 (#L12492) and CyQUANT™ LDH Cytotoxicity Assay (#662892) were obtained from ThermoFisher. Bafilomycin A1 (#BML-CM110-0100) was also obtained from Enzo Life Sciences. 24-well Sensoplates (#662892) were purchased from Greiner-Bio.

Synthesis of SCNPs with charge range

Fluorescent **SCNP-0** to **SCNP-60** were synthesized as previously described in Chapter 2.

Cell culture

Human cerebral microvascular endothelial cell line (hCMEC/D3) were used between passages 32 and 38. Endothelial basal medium 2 was supplemented with 5 % (v/v) FBS, 1 % (v/v) penicillin–streptomycin, 10 mM HEPES, 1 ng/mL bFGF, 5 µg/ml ascorbic acid, 1.4 µM hydrocortisone and 1:100 chemically defined lipid concentrate (Gibco, #11905-031, LOT). Flasks were precoated with 150 µg/ml collagen type-I from rat tail (Enzo Life Sciences, #ALX-522-435, LOT 01031910 or LOT 04272115, or Sigma #C3867, Batch Number SLCK5464). Cells were subcultured every 3 days and grown at 37 °C, 5% CO₂ in humidified atmosphere.

LDH assay

LDH release in hCMEC/D3 cells incubated with 100 µl of 100 µg/ml of non-fluorescent SCNPs with different tertiary amine densities for 24 h at 37 °C, 5% CO₂.

Transcytosis assay

The transport of SCNPs was evaluated using an *in vitro* filter free BBB model.^{48, 68} Collagen gels are prepared using rat tail collagen type-I in 0.02 N acetic acid solution (Enzo Life Sciences, #ALX-522-435, LOT 01031910 or LOT 04272115) mixed with 1 M NaOH, ddH₂O and 10x PBS. Collagen solution final concentration is 2 mg ml⁻¹

in 1xPBS at neutral conditions. Solution was kept on ice to slow down polymerization. 450 μl of solution were added per well on 24-well plates and incubated at 37 °C, 5% CO₂ for 1 h to allow polymerization. Gels were washed with 1xHBSS before use. Cells are seeded on top of the gel at initial cell seeding density is 1x10⁵ cells per cm². Media is changed every second and fourth day after seeding, besides, on day 2, wells are washed with 1xHBSS before fresh medium is added. On the 5th day, apical medium is removed and hCMEC/D3 monolayer is washed once with 1xHBSS. After wash, 500 μl of prewarmed 100 $\mu\text{g ml}^{-1}$ SCNPs in complete EBM-2 medium were incubated with hCMEC/D3 monolayers at the apical compartment for 3, 6 and 18 h. 1 μl of 1 mg ml⁻¹ TexasRed-labelled dextran of 10 kDa was added per well one-hour prior finishing incubation to track major variations in permeability. For 18 h incubation, additional experiments with TexasRed-labelled dextran of 10 kDa at final concentration of 370 $\mu\text{g ml}^{-1}$ were performed to evaluate apparent permeability variations, however, those results were not considered for quantification of percentage of transcytosis. Fluorescence was corrected in reference to controls without treatment.

$$SCNPs (\%) = \frac{SCNPs \text{ fluorescence compartment}}{SCNPs \text{ total fluorescence}} \times 100$$

Western-blot

hCMEC/D3 were seeded on collagen-coated 24-well plates (150 $\mu\text{g/mL}$) at initial density of 1 x 10⁵ cells per cm² and grown for 5 days. On the 5th day, cells were exposed to 500 μl of 100 $\mu\text{g/mL}$ **SCNP-0**, **SCNP-15**, **SCNP-30**, **SCNP-45** and **SCNP-60** in EBM-2 complete medium. Samples without treatment were used as control. After 18 h, particles' suspension was removed, cells were washed once with ice-cold HBSS and 100 μl of Laemmli Buffer was added per well. Samples were collected and stored at -20 °C until use. Samples were heated at 98° C for 10 min and 10 μl of each lysate was loaded on SDS/PAGE with 15% acrylamide. Gels were transferred to a nitrocellulose membrane (Biorad) and were incubated with the primary antibodies ZO-1 polyclonal antibody (1:1000, ThermoFisher, #61-7300) in PBS-Tween 0.1%-BSA 3% or monoclonal β -actin (1:2000, Sigma-Aldrich, #A5441) for 1 h in PBS-Tween 0.1%-BSA 3%. The membranes were washed with PBS-Tween 0.1% and incubated in PBS-Tween 0.1%-BSA 3% with horseradish peroxidase (HRP)-conjugated secondary anti-rabbit antibody anti-rabbit (1:2000, CellSignalling, #7074S) or anti-mouse antibody (1:2000, Sigma) respectively. The blots were revealed via a homemade enhanced chemiluminescence reagent and scanned using FluorChem M machine (Proteinsimple).

SCNPs endosomal escape and colocalization studies

Confocal microscopy was employed to analyze the intracellular trafficking of the SCNPs, more specifically the colocalization between SCNPs and LysoTracker Red DND-99 (#L12492, ThermoFisher) an endo-lysosomal staining. As previously described, hCMEC/D3 cells were seeded in precoated 24-well Sensoplates at initial seeding density of 1×10^5 cells per cm^2 and grown for 4-5 days. 500 μl of 100 $\mu\text{g}/\text{ml}$ DTAF-labelled SCNPs were incubated with the cell monolayer for 4 h. 100 nM LysoTracker Red DND-99 was co-incubated for 1 h as well as 1 drop NucRed™ Live 647 ReadyProbes™ Reagent (ThermoFisher, #R37106) per well for 30 min. After 4 h, the SCNPs and dyes were removed, cells were washed twice with 1xHBSS followed by incubation with 4% paraformaldehyde (PFA) for 5 min. PFA was removed, cells were washed three times with 1xHBSS and PBS:Glycerol (50:50) was added as mounting medium.

To evaluate the effect of pH on the endosomal escape, cell monolayers grown on precoated Sensoplates were pre-exposed to 200 nM Bafilomycin A1 (BafA1), a V-ATPase inhibitor, for 30 min, followed by co-incubation with **SCNP-45** for 1 h. After 1 h, cells were washed, fixed with 4% PFA and stained with Hoechst.

Assessment of apparent permeability (P_{app}) of *in vitro* BBB model exposed to SCNPs and FITC-dextran

BBB model was exposed to the labelled-SCNPs (**SCNP-0**, **SCNP-15**, **SCNP-30**, **SCNP-45** and **SCNP-60**) on its basolateral side for 18 h at 37° C. After 17 h incubation, 10 kDa Dextran labelled with TexasRed was co-incubated with the SCNPs for 1 h and P_{app} calculated as described previously.⁴⁸

Apparent permeability (P_{app}) of the *in vitro* BBB model employing dextran 4 kDa and dextran 2000 kDa labelled with FITC

P_{app} was evaluated at the 5th day by incubating 500 μl of 1 mg/ml of fluorescent-labelled dextran for 1 h.

3.5 Supplementary information

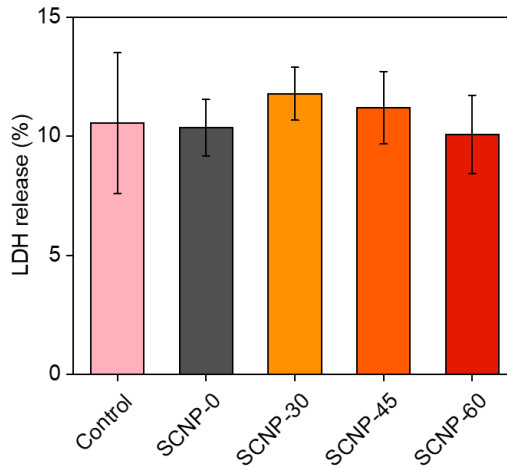


Figure S3.1. Percentage of LDH release in hCMEC/D3 cells incubated SCNP-0 to SCNP-60 and a control.

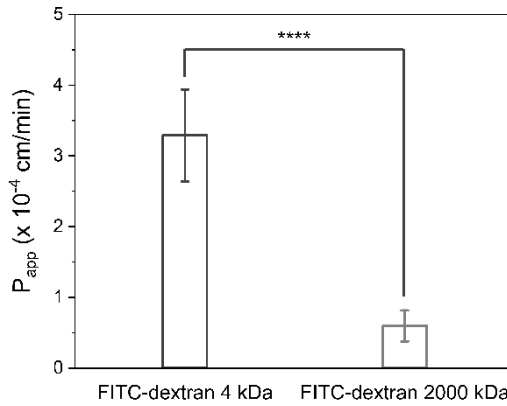


Figure S3.2. Apparent permeability (P_{app}) of the in vitro BBB model employing dextran 4 kDa and dextran 2000 kDa labelled with FITC (fluorescein). **** $p < 0.001$

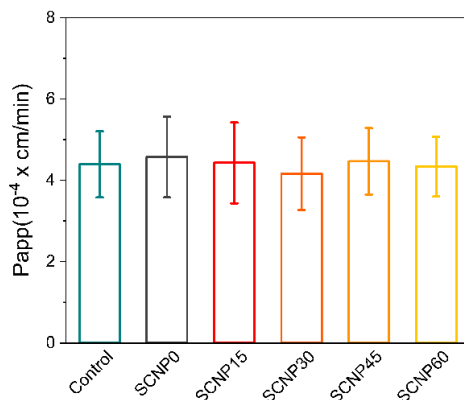


Figure S3.3. Evaluation of SCNPs influence on apparent permeability (P_{app}) of the in vitro BBB model.

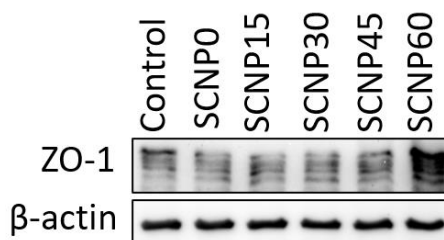


Figure S3.4. Effect of SCNPs with different densities of tertiary amines on the expression of ZO-1.

3.6 References

1. GBD 2015 Neurological Disorders Collaborator Group, Global, regional, and national burden of neurological disorders during 1990-2015: a systematic analysis for the Global Burden of Disease Study 2015. *The Lancet Neurology* **2017**, *16* (11), 877-897.
2. Reinhold, A. K.; Rittner, H. L., Barrier function in the peripheral and central nervous system-a review. *Pflugers Arch* **2017**, *469* (1), 123-134.
3. Abbott, N. J.; Patabendige, A. A.; Dolman, D. E.; Yusof, S. R.; Begley, D. J., Structure and function of the blood-brain barrier. *Neurobiol Dis* **2010**, *37* (1), 13-25.
4. Kadry, H.; Noorani, B.; Cucullo, L., A blood-brain barrier overview on structure, function, impairment, and biomarkers of integrity. *Fluids Barriers CNS* **2020**, *17* (1), 69.
5. Chen, Y.; Liu, L., Modern methods for delivery of drugs across the blood-brain barrier. *Adv Drug Deliv Rev* **2012**, *64* (7), 640-65.
6. Vukelja, S. J.; Anthony, S. P.; Arseneau, J. C.; Berman, B. S.; Casey Cunningham, C.; Nemunaitis, J. J.; Samlowski, W. E.; Fowers, K. D., Phase 1 study of escalating-dose OncoGel® (ReGel®/paclitaxel) depot injection, a controlled-release formulation of paclitaxel, for local management of superficial solid tumor lesions. *Anti-Cancer Drugs* **2007**, *18* (3).

7. Rousseau, J.; Barth, R. F.; Moeschberger, M. L.; Elleaume, H., Efficacy of Intracerebral Delivery of Carboplatin in Combination With Photon Irradiation for Treatment of F98 Glioma-Bearing Rats. *Int. J. Radiat. Oncol. Biol. Phys.* **2009**, *73* (2), 530-536.
8. Mehta, A. M.; Sonabend, A. M.; Bruce, J. N., Convection-Enhanced Delivery. *Neurotherapeutics : the journal of the American Society for Experimental NeuroTherapeutics* **2017**, *14* (2), 358-371.
9. Stine, C. A.; Munson, J. M., Convection-Enhanced Delivery: Connection to and Impact of Interstitial Fluid Flow. *Front Oncol* **2019**, *9*, 966.
10. Meng, Y.; Hynynen, K.; Lipsman, N., Applications of focused ultrasound in the brain: from thermoablation to drug delivery. *Nat Rev Neurol* **2021**, *17* (1), 7-22.
11. Pignatello, R.; Maltese, A.; Maugeri, F.; Bucolo, C., Enhancement of availability of cloricromene at brain level by a lipophilic prodrug. *J Pharm Pharmacol* **2006**, *58* (7), 1001-5.
12. Montaser, A. B.; Jarvinen, J.; Loffler, S.; Huttunen, J.; Auriola, S.; Lehtonen, M.; Jalkanen, A.; Huttunen, K. M., L-Type Amino Acid Transporter 1 Enables the Efficient Brain Delivery of Small-Sized Prodrug across the Blood-Brain Barrier and into Human and Mouse Brain Parenchymal Cells. *ACS Chem Neurosci* **2020**, *11* (24), 4301-4315.
13. Regina, A.; Demeule, M.; Che, C.; Lavallee, I.; Poirier, J.; Gabathuler, R.; Beliveau, R.; Castaigne, J. P., Antitumour activity of ANG1005, a conjugate between paclitaxel and the new brain delivery vector Angiopep-2. *Br J Pharmacol* **2008**, *155* (2), 185-97.
14. Pardridge, W. M., The blood-brain barrier: bottleneck in brain drug development. *NeuroRx* **2005**, *2* (1), 3-14.
15. Pardridge, W. M., Blood-brain barrier delivery. *Drug Discov Today* **2007**, *12* (1-2), 54-61.
16. Khan, A. R.; Yang, X.; Fu, M.; Zhai, G., Recent progress of drug nanoformulations targeting to brain. *J Control Release* **2018**, *291*, 37-64.
17. Pulgar, V. M., Transcytosis to Cross the Blood Brain Barrier, New Advancements and Challenges. *Front Neurosci* **2018**, *12*, 1019.
18. Tsou, Y. H.; Zhang, X. Q.; Zhu, H.; Syed, S.; Xu, X., Drug Delivery to the Brain across the Blood-Brain Barrier Using Nanomaterials. *Small* **2017**, *13* (43).
19. Wang, L.; Shi, Y.; Jiang, J.; Li, C.; Zhang, H.; Zhang, X.; Jiang, T.; Wang, L.; Wang, Y.; Feng, L., Micro-Nanocarriers Based Drug Delivery Technology for Blood-Brain Barrier Crossing and Brain Tumor Targeting Therapy. *Small* **2022**, *18* (45), e2203678.
20. Ding, S.; Khan, A. I.; Cai, X.; Song, Y.; Lyu, Z.; Du, D.; Dutta, P.; Lin, Y., Overcoming blood-brain barrier transport: Advances in nanoparticle-based drug delivery strategies. *Mater Today* **2020**, *37*, 112-125.
21. Reddy, S.; Tatiparti, K.; Sau, S.; Iyer, A. K., Recent advances in nano delivery systems for blood-brain barrier (BBB) penetration and targeting of brain tumors. *Drug Discov Today* **2021**, *26* (8), 1944-1952.
22. Zhang, W.; Mehta, A.; Tong, Z.; Esser, L.; Voelcker, N. H., Development of Polymeric Nanoparticles for Blood-Brain Barrier Transfer-Strategies and Challenges. *Adv Sci* **2021**, *8* (10), 2003937.
23. Hersh, A. M.; Alomari, S.; Tyler, B. M., Crossing the Blood-Brain Barrier: Advances in Nanoparticle Technology for Drug Delivery in Neuro-Oncology. *Int J Mol Sci* **2022**, *23* (8).
24. Ahlawat, J.; Guillama Barroso, G.; Masoudi Asil, S.; Alvarado, M.; Armendariz, I.; Bernal, J.; Carabaza, X.; Chavez, S.; Cruz, P.; Escalante, V.; Estorga, S.; Fernandez, D.; Lozano, C.; Marrufo, M.; Ahmad, N.; Negrete, S.; Olvera, K.; Parada, X.; Portillo, B.; Ramirez, A.; Ramos, R.; Rodriguez, V.; Rojas, P.; Romero, J.; Suarez, D.; Urueta, G.; Viel, S.; Narayan, M., Nanocarriers as Potential Drug Delivery Candidates for Overcoming the Blood-Brain Barrier: Challenges and Possibilities. *ACS Omega* **2020**, *5* (22), 12583-12595.
25. Teixeira, M. I.; Lopes, C. M.; Amaral, M. H.; Costa, P. C., Surface-modified lipid nanocarriers for crossing the blood-brain barrier (BBB): A current overview of active targeting in brain diseases. *Colloids Surf B Biointerfaces* **2023**, *221*, 112999.

26. Hua, S.; de Matos, M. B. C.; Metselaar, J. M.; Storm, G., Current Trends and Challenges in the Clinical Translation of Nanoparticulate Nanomedicines: Pathways for Translational Development and Commercialization. *Front Pharmacol* **2018**, *9*, 790.
27. Lombardo, S. M.; Schneider, M.; Tureli, A. E.; Gunday Tureli, N., Key for crossing the BBB with nanoparticles: the rational design. *Beilstein J Nanotechnol* **2020**, *11*, 866-883.
28. Cruz, L. J.; Stammes, M. A.; Que, I.; van Beek, E. R.; Knol-Blankevoort, V. T.; Snoeks, T. J. A.; Chan, A.; Kaijzel, E. L.; Löwik, C. W. G. M., Effect of PLGA NP size on efficiency to target traumatic brain injury. *Journal of Controlled Release* **2016**, *223*, 31-41.
29. Hanada, S.; Fujioka, K.; Inoue, Y.; Kanaya, F.; Manome, Y.; Yamamoto, K., Cell-based in vitro blood-brain barrier model can rapidly evaluate nanoparticles' brain permeability in association with particle size and surface modification. *Int J Mol Sci* **2014**, *15* (2), 1812-25.
30. Meng, Q.; Meng, H.; Pan, Y.; Liu, J.; Li, J.; Qi, Y.; Huang, Y., Influence of nanoparticle size on blood-brain barrier penetration and the accumulation of anti-seizure medicines in the brain. *Journal of Materials Chemistry B* **2022**, *10* (2), 271-281.
31. Brown, T. D.; Habibi, N.; Wu, D.; Lahann, J.; Mitragotri, S., Effect of Nanoparticle Composition, Size, Shape, and Stiffness on Penetration Across the Blood-Brain Barrier. *ACS Biomaterials Science & Engineering* **2020**, *6* (9), 4916-4928.
32. Sonavane, G.; Tomoda, K.; Makino, K., Biodistribution of colloidal gold nanoparticles after intravenous administration: effect of particle size. *Colloids Surf B Biointerfaces* **2008**, *66* (2), 274-80.
33. Kiessling, F.; Mertens, M. E.; Grimm, J.; Lammers, T., Nanoparticles for Imaging: Top or Flop? *Radiology* **2014**, *273* (1), 10-28.
34. Herve, F.; Ghinea, N.; Scherrmann, J. M., CNS delivery via adsorptive transcytosis. *AAPS J* **2008**, *10* (3), 455-72.
35. Ayloo, S.; Gu, C., Transcytosis at the blood-brain barrier. *Curr Opin Neurobiol* **2019**, *57*, 32-38.
36. Jallouli, Y.; Paillard, A.; Chang, J.; Sevin, E.; Betbeder, D., Influence of surface charge and inner composition of porous nanoparticles to cross blood-brain barrier in vitro. *Int J Pharm* **2007**, *344* (1-2), 103-9.
37. Parikh, T.; Bommana, M. M.; Squillante, E., 3rd, Efficacy of surface charge in targeting pegylated nanoparticles of sulpiride to the brain. *Eur J Pharm Biopharm* **2010**, *74* (3), 442-50.
38. Chen, Y. P.; Chou, C. M.; Chang, T. Y.; Ting, H.; Dembele, J.; Chu, Y. T.; Liu, T. P.; Changou, C. A.; Liu, C. W.; Chen, C. T., Bridging Size and Charge Effects of Mesoporous Silica Nanoparticles for Crossing the Blood-Brain Barrier. *Front Chem* **2022**, *10*, 931584.
39. Fenart, L.; Casanova, A.; Dehouck, B.; Duhem, C.; Slupek, S.; Cecchelli, R.; Betbeder, D., Evaluation of effect of charge and lipid coating on ability of 60-nm nanoparticles to cross an in vitro model of the blood-brain barrier. *J Pharmacol Exp Ther* **1999**, *291* (3), 1017-22.
40. Knudsen, K. B.; Northeved, H.; Kumar, P. E.; Permin, A.; Gjetting, T.; Andresen, T. L.; Larsen, S.; Wegener, K. M.; Lykkesfeldt, J.; Jantzen, K.; Loft, S.; Moller, P.; Roursgaard, M., In vivo toxicity of cationic micelles and liposomes. *Nanomedicine* **2015**, *11* (2), 467-77.
41. Han, G.; Ghosh, P.; Rotello, V. M., Functionalized gold nanoparticles for drug delivery. *Nanomedicine (London, England)* **2007**, *2* (1), 113-23.
42. Lockman, P. R.; Koziara, J. M.; Mumper, R. J.; Allen, D. D., Nanoparticle surface charges alter blood-brain barrier integrity and permeability. *J Drug Target* **2004**, *12* (9-10), 635-41.
43. Hamelmann, N. M.; Paulusse, J. M. J., Single-chain polymer nanoparticles in biomedical applications. *J Control Release* **2023**.
44. Alqarni, M. A. M.; Waldron, C.; Yilmaz, G.; Becer, C. R., Synthetic Routes to Single Chain Polymer Nanoparticles (SCNPs): Current Status and Perspectives. *Macromol Rapid Commun* **2021**, e2100035.
45. Kroger, A. P. P.; Paulusse, J. M. J., Single-chain polymer nanoparticles in controlled drug delivery and targeted imaging. *J Control Release* **2018**, *286*, 326-347.

46. Kröger, A. P. P.; Paats, J. D.; Boonen, R. J. E. A.; Hamelmann, N. M.; Paulusse, J. M. J., Pentafluorophenyl-based single-chain polymer nanoparticles as a versatile platform towards protein mimicry. *Polymer Chemistry* **2020**, *11* (37), 6056-6065.
47. Hamelmann, N. M.; Paats, J. D.; Paulusse, J. M. J., Cytosolic Delivery of Single-Chain Polymer Nanoparticles. *ACS Macro Lett* **2021**, *10* (11), 1443-1449.
48. De Jong, E.; Williams, D. S.; Abdelmohsen, L. K. E. A.; Van Hest, J. C. M.; Zuhorn, I. S., A filter-free blood-brain barrier model to quantitatively study transendothelial delivery of nanoparticles by fluorescence spectroscopy. *Journal of Controlled Release* **2018**, *289*, 14-22.
49. Goodman, C. M.; McCusker, C. D.; Yilmaz, T.; Rotello, V. M., Toxicity of Gold Nanoparticles Functionalized with Cationic and Anionic Side Chains. *Bioconjugate Chemistry* **2004**, *15* (4), 897-900.
50. Ribovski, L.; de Jong, E.; Mergel, O.; Zu, G.; Keskin, D.; van Rijn, P.; Zuhorn, I. S., Low nanogel stiffness favors nanogel transcytosis across an in vitro blood-brain barrier. *Nanomedicine* **2021**, *34*, 102377.
51. Zhang, H.; van Os, W. L.; Tian, X.; Zu, G.; Ribovski, L.; Bron, R.; Bussmann, J.; Kros, A.; Liu, Y.; Zuhorn, I. S., Development of curcumin-loaded zein nanoparticles for transport across the blood-brain barrier and inhibition of glioblastoma cell growth. *Biomater Sci* **2021**, *9* (21), 7092-7103.
52. Hue, C. D.; Cho, F. S.; Cao, S.; Bass, C. R. D.; Meaney, D. F.; Morrison, B., Dexamethasone Potentiates In Vitro Blood-Brain Barrier Recovery after Primary Blast Injury by Glucocorticoid Receptor-Mediated Upregulation of ZO-1 Tight Junction Protein. *Journal of Cerebral Blood Flow & Metabolism* **2015**, *35* (7), 1191-1198.
53. Ko, J.-A.; Yanai, R.; Nishida, T., Up-regulation of ZO-1 expression and barrier function in cultured human corneal epithelial cells by substance P. *FEBS Letters* **2009**, *583* (12), 2148-2153.
54. Bus, T.; Traeger, A.; Schubert, U. S., The great escape: how cationic polyplexes overcome the endosomal barrier. *J Mater Chem B* **2018**, *6* (43), 6904-6918.
55. Martens, T. F.; Remaut, K.; Demeester, J.; De Smedt, S. C.; Braeckmans, K., Intracellular delivery of nanomaterials: How to catch endosomal escape in the act. *Nano Today* **2014**, *9* (3), 344-364.
56. Nguyen, J.; Szoka, F. C., Nucleic Acid Delivery: The Missing Pieces of the Puzzle? *Accounts of Chemical Research* **2012**, *45* (7), 1153-1162.
57. van Weert, A. W.; Dunn, K. W.; Geuze, H. J.; Maxfield, F. R.; Stoorvogel, W., Transport from late endosomes to lysosomes, but not sorting of integral membrane proteins in endosomes, depends on the vacuolar proton pump. *The Journal of cell biology* **1995**, *130* (4), 821-34.
58. Bowman, E. J.; Siebers, A.; Altendorf, K., Bafilomycins: a class of inhibitors of membrane ATPases from microorganisms, animal cells, and plant cells. *Proc Natl Acad Sci U S A* **1988**, *85* (21), 7972-6.
59. Smith, S. A.; Selby, L. I.; Johnston, A. P. R.; Such, G. K., The Endosomal Escape of Nanoparticles: Toward More Efficient Cellular Delivery. *Bioconjugate Chemistry* **2019**, *30* (2), 263-272.
60. Rehman, Z. u.; Hoekstra, D.; Zuhorn, I. S., Mechanism of Polyplex- and Lipoplex-Mediated Delivery of Nucleic Acids: Real-Time Visualization of Transient Membrane Destabilization without Endosomal Lysis. *ACS Nano* **2013**, *7* (5), 3767-3777.
61. Vaidyanathan, S.; Orr, B. G.; Banaszak Holl, M. M., Role of Cell Membrane-Vector Interactions in Successful Gene Delivery. *Acc Chem Res* **2016**, *49* (8), 1486-93.
62. Yue, Y.; Jin, F.; Deng, R.; Cai, J.; Dai, Z.; Lin, M. C.; Kung, H. F.; Matthebjerg, M. A.; Andresen, T. L.; Wu, C., Revisit complexation between DNA and polyethylenimine—effect of length of free polycationic chains on gene transfection. *J Control Release* **2011**, *152* (1), 143-51.
63. Majzoub, R. N.; Wonder, E.; Ewert, K. K.; Kotamraju, V. R.; Teesalu, T.; Safinya, C. R., Rab11 and LysoTracker Markers Reveal Correlation between Endosomal Pathways and Transfection Efficiency of Surface-Functionalized Cationic Liposome–DNA Nanoparticles. *The Journal of Physical Chemistry B* **2016**, *120* (26), 6439-6453.
64. Takahashi, S.; Kubo, K.; Waguri, S.; Yabashi, A.; Shin, H.-W.; Katoh, Y.; Nakayama, K., Rab11 regulates exocytosis of recycling vesicles at the plasma membrane. *Journal of Cell Science* **2012**, *125* (17), 4049-4057.

65. Weisz, O. A.; Rodriguez-Boulan, E., Apical trafficking in epithelial cells: signals, clusters and motors. *Journal of Cell Science* **2009**, *122* (23), 4253-4266.
66. Morad, G.; Carman, C. V.; Hagedorn, E. J.; Perlin, J. R.; Zon, L. I.; Mustafaoglu, N.; Park, T.-E.; Ingber, D. E.; Daisy, C. C.; Moses, M. A., Tumor-Derived Extracellular Vesicles Breach the Intact Blood–Brain Barrier via Transcytosis. *ACS Nano* **2019**, *13* (12), 13853-13865.
67. Villaseñor, R.; Schilling, M.; Sundaresan, J.; Lutz, Y.; Collin, L., Sorting Tubules Regulate Blood-Brain Barrier Transcytosis. *Cell Reports* **2017**, *21* (11), 3256-3270.
68. Ribovski, L.; de Jong, E.; Mergel, O.; Zu, G.; Keskin, D.; van Rijn, P.; Zuhorn, I. S., Low nanogel stiffness favors nanogel transcytosis across an in vitro blood–brain barrier. *Nanomedicine: Nanotechnology, Biology and Medicine* **2021**, *34*, 102377.

Chapter 4

Controlled drug delivery by subcellular targeting with single-chain polymer nanoparticles

The intracellular location of therapeutics is key for optimal efficacy. Single-chain polymer nanoparticles (SCNPs) are a promising class of nanocarriers to systematically investigate the influence of surface groups on the subcellular location of NPs. In this Chapter, a series of functional SCNPs, equipped with the anticancer prodrug of atovaquone, is used to study how subcellular location affects the drug's efficiency. SCNPs were prepared with different quantities of protonatable tertiary amines (i.e. 15% and 40%) on the surface, as well as SCNPs with 40% of quaternized ammonium groups with a permanent positive charge. The nanocarriers were evaluated on HeLa cells and SCNPs were observed in lysosomes, the cytosol or the extracellular cell membrane, depending on the type and extent of surface functionalization on the SCNPs. The results show a strong decrease in cell viability solely in the case of cytosolic delivery of atovaquone to the cancer cells, underlining the advantages controlled subcellular delivery of therapeutics can offer.

Manuscript submitted: N.M. Hamelmann‡, J-W.D Paats‡, J. M. J. Paulusse

‡ These authors contributed equally.

4.1 Introduction

The vast majority of drug targets resides within the cell, and being able to reach the cell cytosol is therefore critical to achieve optimal efficacy in controlled drug delivery. Nanoparticles (NPs) are commonly employed to improve delivery, since they can provide suitable pharmacokinetics, increased drug loading and specific targeting.¹⁻³ However, directing the intracellular location of NPs is still frequently neglected. Earlier work has shown that the intracellular fate of NPs can be controlled by introducing protonatable surface groups. Using polymers with guanidium pendant groups, proteins were encapsulated and successfully delivered into the cytosol.⁴⁻⁵ Guanidium-functionalized dendrimers were used to deliver peptides intracellularly,⁶ whereas enzymes were successfully transported intracellularly by NPs with high amounts of permanently charged ammonium side-groups.⁷ However, permanent charges are associated with cellular toxicity⁸ and furthermore, the enzymes remained trapped in the endosomes.

One excellent candidate NP system for subcellular delivery of a therapeutic cargo are single-chain polymer nanoparticles (SCNPs). SCNPs possess a unique size range from 5-20 nm with low dispersity, combined with scalability and exquisite control over their functionalization.⁹⁻¹² Their small size, in the range of proteins and small viruses, has been shown to promote cellular uptake,¹³ while equipping the SCNPs with active pentafluorophenyl (PFP) esters provides the possibility of facile introduction of functional moieties.¹⁴ This allows for systematic evaluation of specific parameters, such as intracellular location, while keeping the core nanoparticle structure unaltered. In Chapter 2 we showed that carefully controlling the amounts of tertiary amines can promote cytosolic delivery of NPs.¹⁵ The key advantages of using this approach are avoidance of external methods for delivery (e.g. electroporation¹⁶), improved biocompatibility and the ease of incorporation of generic targeting groups.

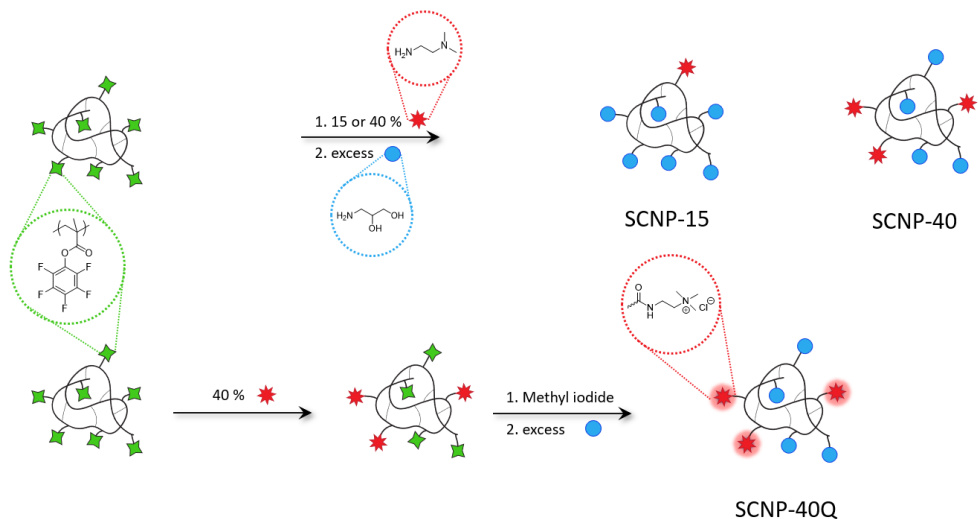
Atovaquone is a first line anti-malarial drug, often in combination with anti-malarial agent proguanil.¹⁷⁻¹⁸ Recently, atovaquone was found to be also effective in cancer treatment. Atovaquone targets the mitochondrial complex III in breast cancer cells, inhibiting further proliferation.¹⁹ Furthermore, it was shown to have potential in the treatment of gynecologic cancers by inhibiting oxidative phosphorylation,²⁰ as well as the treatment of several forms of leukemia *in vitro* as well as in *in vivo* mouse models.²¹ Since the targets of atovaquone reside within the cytosol, controlling the intracellular targeting could improve the drug's efficacy. Conjugating drug molecules covalently to nanoparticles prevents drug leakage and burst-release of the cargo, which is often observed for nanoparticles with encapsulated drugs.²²⁻²³ For efficient conjugation, drug molecules can be converted into prodrugs by attaching a handle for conjugation through a linker.²⁴⁻²⁶ After cleavage, the drug is released in its active

form. Targeted release of therapeutics can even be controlled by modifying the type of functional linker, to induce drug release at a specific trigger.²⁷⁻²⁸ This concept has been extensively used in the field of drug delivery, especially for anti-cancer therapy.²⁹⁻³¹ Furthermore, atovaquone has already been synthetically modified into a prodrug to modify bioavailability³²⁻³³ or connect it to other active pharmaceuticals,³⁴⁻³⁵ for increased therapeutic effectiveness.

In this Chapter, we evaluate the potential of SCNPs to deliver therapeutics to cancer cells (HeLa) and we investigate the influence of intracellular SCNPs location on drug efficacy. A set of SCNPs with increasing content of tertiary amines, as well as quaternary ammonium moieties, is prepared and conjugated with an atovaquone prodrug. SCNP uptake and intracellular location are studied and the efficacy of the drug-conjugated SCNPs is evaluated to understand the influence of their (sub)cellular location on apoptotic activity.

4.2 Results and discussion

PFP-SCNPs were synthesized as previously described in Chapter 2 and were functionalized with 15 and 40 % tertiary amines to yield **SCNP-15** and **SCNP-40**. Remaining PFP-esters were end-capped with aminoglycerol to fully passivate the SCNPs and further increase their water-solubility (Scheme 4.1, top). Furthermore, **SCNP-40Q** with quaternized ammonium groups was synthesized by methylating the tertiary amines. To circumvent *O*-methylation of the alcohol-groups, quaternization of the tertiary amines was performed before end-capping the remaining PFP-esters with 1-aminoglycerol (Scheme 4.1, bottom). Converting the tertiary amines into quaternary ammonium groups allows us to differentiate between the effect of buffer capacity and positive charge of the functional side groups on the cellular interactions.



Scheme 4.1. Schematic representation of the functionalization of **PFP-SCNPs** with increasing amounts of tertiary amines, followed by end-capping of remaining functional esters with 1-aminoglycerol. To synthesize **SCNP-40Q**, quaternization was performed by methyl iodide before end-capping with 1-aminoglycerol (followed by counter-anion exchange).

The set of three distinct SCNPs was characterized by ¹H NMR spectroscopy. Upon increasing the tertiary amine content, an increasing signal is observed at δ 2.3 ppm, which disappears after quaternization of the amines (Figure 4.1a). Instead, a new downfield signal appears at δ 3.1 ppm, indicative of the conversion into ammonium groups. Subsequently, zeta-potential of the SCNPs was measured at different pH values to carefully analyze the surface charge and take the protonation state of the tertiary amines into account (Figure 4.1b). At pH 7.4, an increase in surface charge from **SCNP-15** to **SCNP-40** was observed and only a minor increase between **SCNP-40** and **SCNP-40Q**. At pH 9.5 and 13.5, the difference in zeta-potential between **SCNP-40** and **SCNP-40Q** becomes more pronounced, as the tertiary amines are increasingly deprotonated under these basic conditions, while quaternized amines maintain their positive charge. Together with the ¹H NMR data, this confirms successful introduction of permanent charges on **SCNP-40Q**. To enable in vitro analysis of the SCNPs, a fluorescent label (fluorescein derivative 5-DTAF) was conjugated onto all SCNPs.

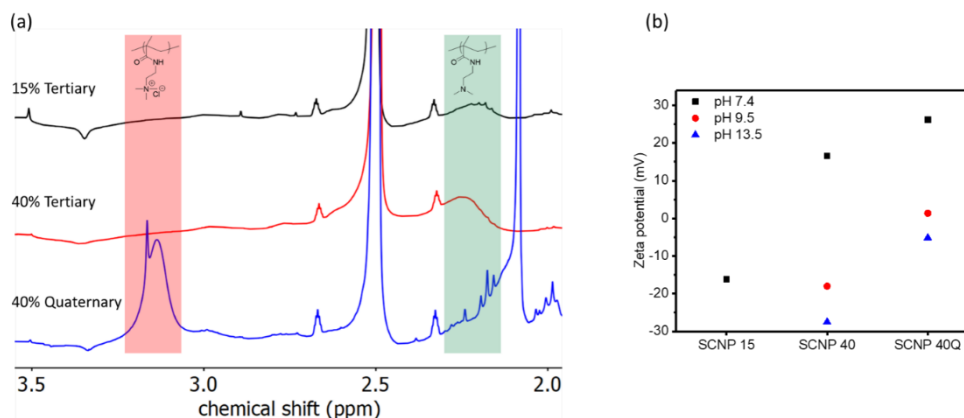


Figure 4.1. Characterization of the set of SCNPs. (a) stacked ¹H NMR spectra, indicating the presence and disappearance of the tertiary amines (green band) and quaternary ammoniums (red band) and (b) zeta potential measurements at different pH values.

To be able to function as a drug delivery system, the SCNPs need to be biocompatible. Therefore, we first assessed cell viabilities for the entire set of SCNPs on HeLa cells, a model cancer human cell line. No significant decrease in cell viability was observed, even at 500 $\mu\text{g}/\text{mL}$ after a 24 h incubation period (Figure 4.2a). Cellular uptake was investigated next and quantified by flow cytometry, as depicted in Figure 4.2b. Similarly as described in Chapter 2, **SCNP-40** shows a stronger fluorescent signal than **SCNP-15**, which is also in line with early studies demonstrating that positively charged nanoparticles promote cellular uptake.^{4, 15, 36} Interestingly, cells incubated with **SCNP-40Q** display a significantly higher fluorescent intensity as compared to **SCNP-40**. The permanent charge of the quaternized amines promotes the interaction of SCNPs with the cell membrane more strongly than the tertiary amines.

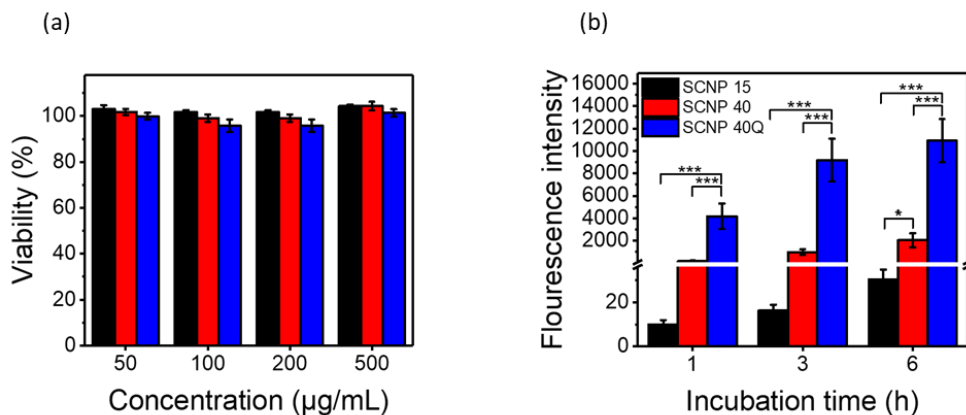


Figure 4.2. (a) Viability of HeLa cells after 24 h incubation. (b) Fluorescence intensity per event of HeLa cells after 1, 3 and 6 h incubation with SCNPs measured by flow cytometry. Asterisks indicate significant higher uptake, * $p < 0.05$, ** $p < 0.01$ and *** $p < 0.001$ ($n=9$).

We further studied the cellular interactions by confocal microscopy. Due to the considerable differences in cellular association measured by flow cytometry, the incubation times for the different particles were adapted accordingly for the confocal microscopy experiments. The images confirm the observed low cellular internalization of **SCNP-15**, as barely any green fluorescent signal is visible (Figure 4.3, top row). As shown in Figure 4.3, middle row, cytosolic delivery of **SCNP-40** occurs, as indicated by the diffuse green signal throughout the cell. Interestingly, the quaternized **SCNP-40Q** shows strong cellular association, but the particles are only found on the cell membranes (Figure 4.3, bottom row). These results indicate that the permanent charge on **SCNP-40Q** causes strong adherence to the negatively charged cell membrane due to electrostatic interaction, but does not promote subsequent internalization. These findings were confirmed by employing a calcein assay (Figure S4.1). Calcein is a membrane-impermeable fluorescein derivative, that can be taken up by endosomes and only be released into the cytosol in the case of membrane leakage.³⁷ Whereas **SCNP-15** and **SCNP-40Q** showed very little calcein signal, **SCNP-40** induced a diffuse calcein signal throughout the cell, indicative of endosomal escape.

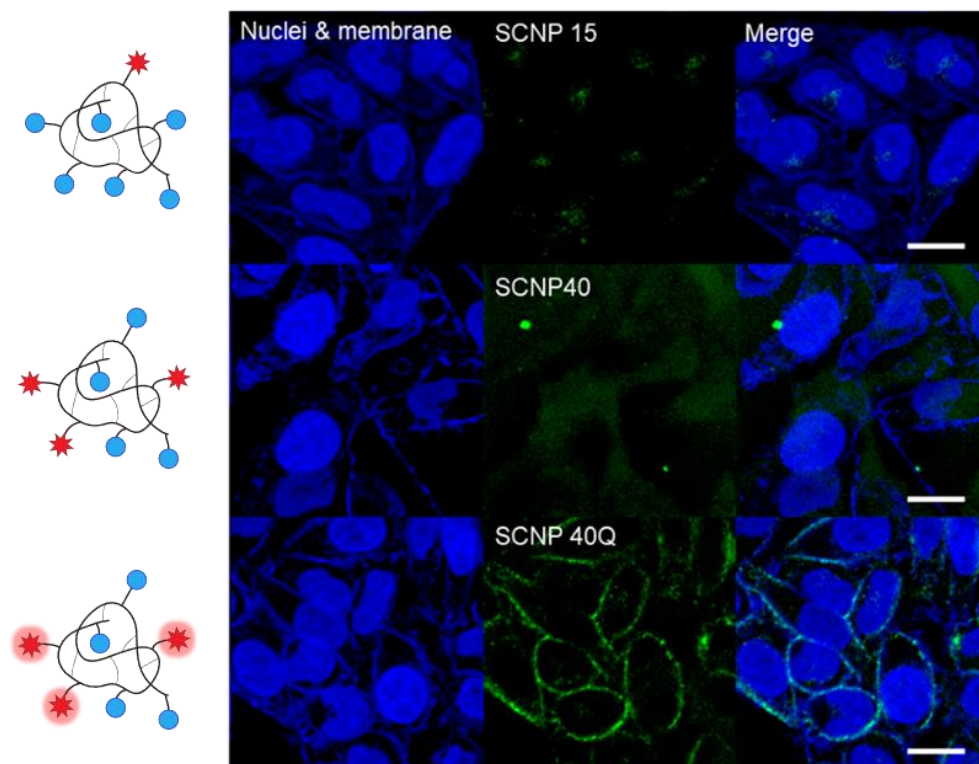
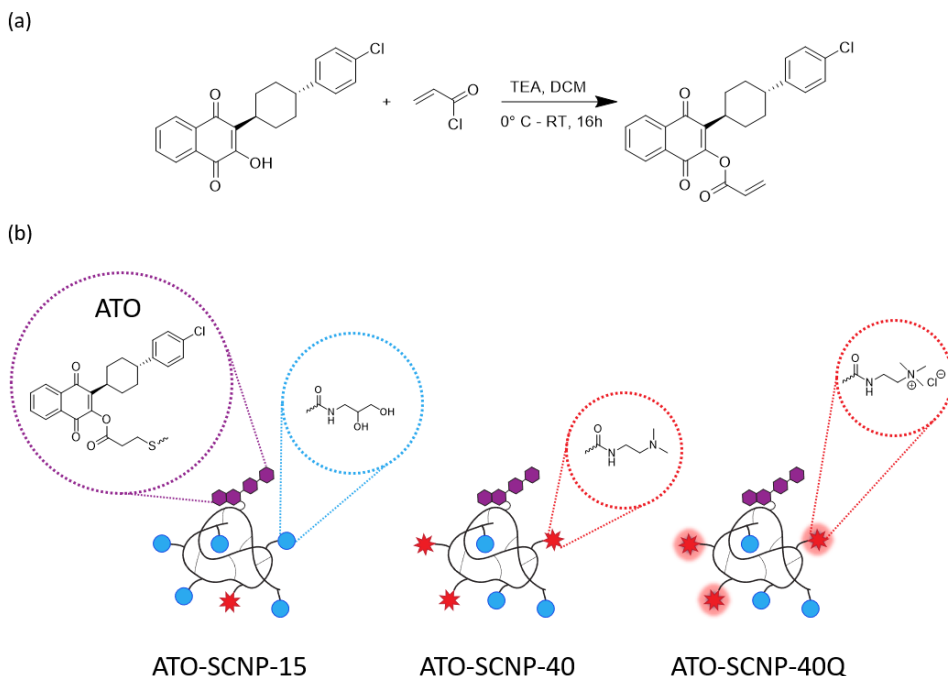


Figure 4.3. Confocal microscopy images of HeLa cells incubated with either **SCNP-15**, **40** or **40Q** for 4 h, 1 h or 30 min respectively. Cells were stained with nuclei and membrane staining in blue and the SCNPs have a green fluorescent label (DTAF). The scale bar is 20 μm .

In order to study the SCNPs as a drug carrier system, we conjugated an atovaquone-prodrug (**ATO**) to the **PFP-SCNPs**. The prodrug was synthesized by attaching an acrylate group to the enol moiety (Scheme 4.2a). The prodrug was then added as an end-capping agent directly after the intramolecular crosslinking of the parent PFP-SCNPs, and before end-capping with methyl acrylate, to react with the remaining free thiols in a thiol-Michael addition. The resulting **PFP-ATO-SCNPs** contained 1.3 wt% drug loading, as determined by ^1H NMR spectroscopy. The batch of precursor SCNPs was split in three parts, to be subsequently functionalized in the same manner as for the empty carriers to yield **ATO-SCNP-15**, **ATO-SCNP-40** and **ATO-SCNP-40Q** (Scheme 4.2b), all containing the same quantity of **ATO**. Size exclusion chromatography analysis on the empty and loaded nanocarriers revealed similar elution times, indicating that pro-drug conjugation does not markedly affect particle size (Figure S4.2, quaternized SCNPs were not measured, due to incompatibility with the eluent). Furthermore, the zeta potential of the **ATO-SCNPs** was measured and the values are well in line with the results obtained for the empty nanocarriers

(Figure S4.3). Lastly, confocal microscopy revealed no significant changes in the cellular location of the SCNPs after ATO-conjugation (Figure S4.4)



Scheme 4.2. (a) Synthesis of atovaquone-acrylate (ATAO) and (b) Schematic representation of the atovaquone-functionalized **SCNPs** with different surface functionality.

Since the prodrug is conjugated through an ester linkage, release of atovaquone can be triggered by acidic conditions, such as the lowered pH in endo/lysosomes.³⁸⁻³⁹ In order to explore atovaquone release, **ATO-SCNP 40** was incubated under acidic conditions for 24 h. In the HPLC traces given in Figure S4.5, the atovaquone release from **ATO-SCNP-40** is shown. Next, we studied the influence of subcellular targeting upon the atovaquone efficiency via Annexin/PI staining. As a start, the set of empty nanocarriers was evaluated on HeLa cells. After 24 h incubation, no significant toxicity was observed (Figure S4.6a). Furthermore, free atovaquone was also not able to induce (early) apoptosis (Figure S4.6b, top left). Upon exposing HeLa cells to ATO-loaded SCNPs, no significant increase in Annexin-V signal was visible for **ATO-SCNPs** functionalized with 15% tertiary amines or 40% quaternary ammoniums. However, when HeLa cells were incubated with **ATO-SCNP-40**, a strong shift of the cell population towards early apoptosis is observed, which is significant compared to the other nanocarriers (see Figure 4.4 and Figure S4.6b). To validate specificity for cancer targeting, the empty and ATO-loaded **SCNPs** were also incubated with NIH/3T3 mouse fibroblasts and uptake and apoptosis was

studied. The uptake of **ATO-SCNPs** is shown in Figure S4.7, revealing a similar cellular location as observed for the HeLa cells. Interestingly, apoptosis of NIH/3T3 cells after incubation with the set of **ATO-SCNPs** differs slightly (see Figure S4.8). A shift of the NIH/3T3 cell population towards higher Annexin-V signal is presented for nanocarrier **ATO-SCNP-40**, which is however also observed for unloaded **SCNP-40**. This shift is most likely due to their entry into the cell cytosol. Therefore, NIH/3T3 cells are more sensitive to the carrier itself compared to HeLa cells. However, addition of the atovaquone prodrug did not significantly increase early apoptosis in these cells. Therefore, these results indicate a specificity of the ATO delivery strategy for cancerous HeLa cells.

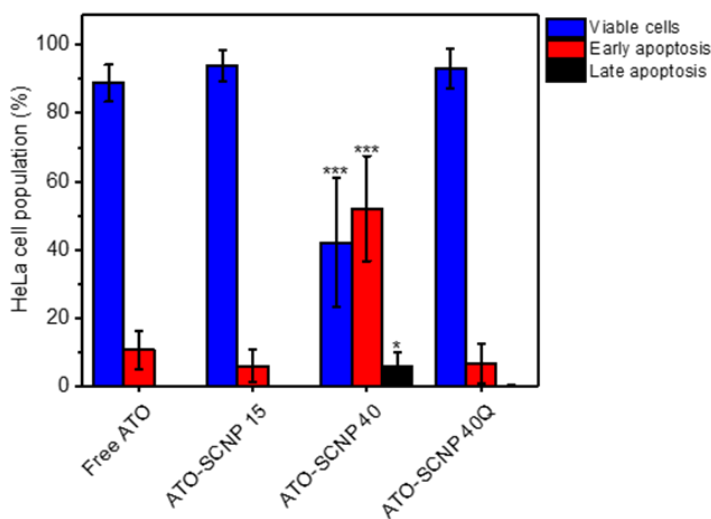


Figure 4.4. flow cytometry plots of HeLa cell populations after incubation with **ATO-SCNPs** or free atovaquone for 24 h and stained by annexin-V and propidium iodide. Percentages of viable or apoptotic HeLa populations with asterisks indicate significance, * $p < 0.05$, ** $p < 0.01$ and *** $p < 0.001$.

4.3 Conclusions

In this work, we synthesized a set of functional single-chain polymer nanoparticles from the same parent active ester precursor. The SCNPs were evaluated on HeLa cells to probe the influence of the different type of surface charge on cellular interactions. SCNPs with a low incorporation ratio of tertiary amines (**SCNP-15**) were only sparingly taken up into the endosomes, whereas a higher content of tertiary amines (**SCNP-40**) lead to higher cellular uptake and cytosolic release of SCNPs. Interestingly, SCNPs with permanently charged quaternized ammonium side groups (**SCNP-40Q**) exhibited high cellular associations, but remained on the cell membranes. Therefore, we conclude that the tertiary amines induce high cellular uptake and that protonatability is essential for cytosolic release. After pro-drug

conjugation, only **ATO-SCNP-40**, which is released in the cytosol induced apoptosis in HeLa cells. Cytosolic release is crucial for therapeutics that work in specific cell organelles, and this work demonstrates efficient targeting of subcellular locations with SCNPs, which may lead to improved drug efficacies in a variety of applications.

To further improve drug delivery, the current drug-loading strategy requires for optimization. In this work, the **ATO-SCNPs** were conjugated with an ester linkage, which can be hydrolyzed under acidic conditions, but the choice of linker can be tailored towards a specific signal for release. For example, a valine-citrulline linker is susceptible to cleavage by proteases, which would facilitate intracellular release, but provides otherwise stability during blood circulation.⁴⁰ An alternative is to use redox-active linkers. Since the concentration of glutathione in cancer cells can be up to a 7-fold higher than in regular cells, the reductive environment can be used to induce drug release.⁴¹ This has already been widely exploited for different carrier systems,⁴² but is particularly interesting in our case because of the efficient intracellular delivery of the SCNPs. However, disulfide-linkers are not compatible with this design, since the SCNPs are crosslinked by thiol-chemistry. This could be circumvented by a different reducible moiety, such as azo-compounds,⁴³ or by using conjugating through the PFP-groups. Overall, the versatility of the PFP-SCNP system can be further exploited for the intracellular delivery of different drugs and release triggers.

4.4 Materials and methods

Tetrahydrofuran (THF, >99%), acetonitrile (ACN, >99%), heptane (>99%) and methanol (>99%) were purchased from LPS b.v. *N,N*-dimethylformamide (DMF, >99.8%) and dichloromethane (>99%) were purchased from VWR. Triethylamine (TEA, 99%), *N,N*-dimethylethylenediamine (DMEN, 95%), 3-amino-1,2-propanediol (1-aminoglycerol, 97%), DMSO (anhydrous, 99.9%), 1,4-butanediol diacrylate (>90.0%), methyl acrylate (99%), tri-*n*-butylphosphine (97%), acryloyl chloride (>97.0%), methyl iodide (99%), 1,3,5-trioxane (>99%), ethanolamine (>99.0%), chloroform-*d* (99.8% atom % D), *d*₆-acetone (99.9 atom % D) DMSO-*d*₆ (99.9 atom % D), atovaquone (>98%), Dulbecco's modified Eagles medium (DMEM), fetal bovine serum (FBS), penicillin-streptomycin (containing 10.000 units penicillin, 10 mg streptomycin mL⁻¹), phosphate buffered saline (PBS, pH 7.4), Hanks' balanced salt solution (HBSS), calcein, Trypsin-EDTA solution (sterile filtered, BioReagent) and 4,6-diamidino-2-phenylindole dihydrochloride (DAPI, 98%) were purchased from Sigma-Aldrich. Fluorescent label 5-(4,6-Dichlorotriazinyl) aminofluorescein (DTAF) and Lyso Tracker™ Deep Red were purchased from ThermoFisher Scientific. CF® 405M Wheat Germ Agglutinin (WGA) was purchased from Biotium. Annexin V-DY-634/PI Apoptosis detection kit was purchased from Abcam. All chemicals were used without further purification unless stated otherwise. When stated as dry, solvents were treated with molecular sieves (3 Å) 24 h before usage

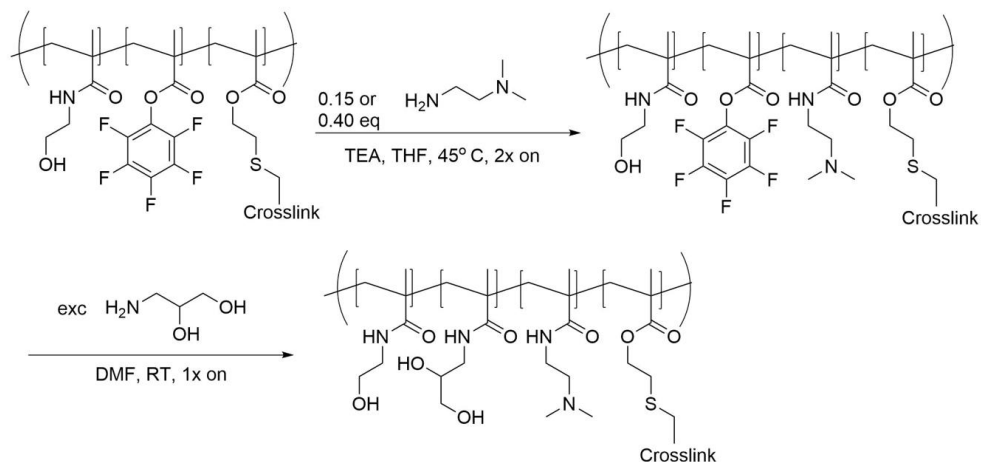
and stored under nitrogen. SnakeSkin™ dialysis tubing (10 K MWCO) from ThermoFisher was employed for dialysis and disposable PD-10 desalting columns were purchased from GE healthcare.

¹H-NMR (400 MHz), ¹⁹F-NMR (376 MHz) and ¹³C-NMR (101 MHz) spectra were recorded on a Bruker 400 spectrometer. Size exclusion chromatography (SEC) analysis was performed on a Waters e2695 Separations Module equipped with an Agilent PLgel 5 μm MIXED-D 300 × 7.5 mm column and Waters photodiode array detector (PDA 2998) and refractive index detector (RI 2414) and DMF was employed as eluent. Zeta potential measurements were performed on a Malvern Instruments Zetasizer ZS. Samples for SEC and DLS were filtered using a GE Healthcare Whatman SPARTAN 13/0.2 RC 0.2 μm syringe filter prior to measurements. RP-HPLC analysis was performed on a Waters 2535 Quaternary Gradient Module equipped with a Waters XBridge C18, 5 μm, 4.6 mm x 250 mm column and a Waters photodiode array detector (PDA 2998), using a H₂O + 0.1% TFA : acetonitrile gradient (95:5 to 5:95). Mass spectra were obtained on an Advion Expression-L Compact Mass Spectrometer featured with either electrospray ionization (ESI) or Atmospheric Pressure Chemical Ionization (APCI).

Synthesis of SCNPs with pentafluorophenyl active esters (PFP-SCNPs)

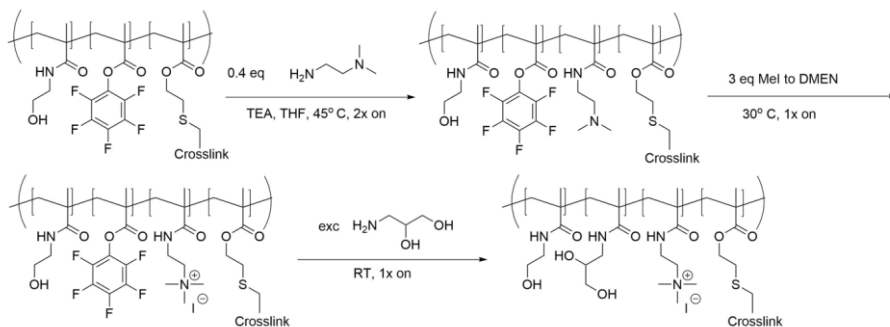
PFP-SCNPs were synthesized as previously reported¹⁴ utilizing a co-polymer (600 mg, DP=236, 0.24 mmol xanthate groups, 1 eq.), containing pentafluorophenyl and xanthate pendant side-groups. The xanthate moieties were deprotected by ethanolamine (87 μL, 1.44 mmol, 6 eq.) to obtain free thiols. After precipitation of the polymer in MeOH (130 mL), the polymer was redissolved in THF (12 mL) and intramolecularly crosslinked via a thiol-Michael addition, by slow addition of the co-polymer to a solution of 1,4-butanediol diacrylate (47 mg, 0.24 mmol, 1 eq.) as crosslinker and tri(*n*-butyl)phosphine (10 mg, 0.04 mmol, 0.2 eq) as initiator in DCM (130 mL). After stirring for an additional 2 hours, the remaining thiols were end-capped by methyl acrylate (1 mL, 12 mmol, 50 eq.). The SCNPs were obtained as a white powder after repeated precipitations in MeOH (60 mL) (320 mg, 55% yield).

Synthesis of SCNP-15 and SCNP-40



A particle set with different surface charges was obtained by functionalization of PFP-SCNPs with either 15 or 40% tertiary amines following an earlier reported method.¹⁵ In brief, for 15% substituted SCNPs, 50 mg of PFP-SCNPs (0.17 mmol PFP, 1 eq) was dissolved in dry THF (3 mL) under nitrogen atmosphere. To the solution triethylamine (96 μL , 0.069 mmol, 4 eq.) and *N,N*-dimethylethylenediamine (DMEN) (2.3 mg, 0.026 mmol, 0.15 eq., from a 5.0 wt% stock solution in dry THF) were added and the solution was stirred for 24 h at 45 $^\circ\text{C}$. After confirmation of full conversion by ^{19}F NMR, 3-amino-1,2-propanediol (157 mg, 1.72 mmol, 10 eq., 10 wt% solution in DMF) was added to the solution to substitute all residual reactive PFP-groups. The solution was left stirring overnight and was afterwards dialyzed against 1 wt% NaCl for 24 h and then against demineralized water for 48 h. The SCNPs were obtained via lyophilization yielding a white powder (25 mg, 79% yield). For SCNP-40 double the amount of PFP-SCNP was functionalized (100 mg).

Synthesis of SCNP-40Q

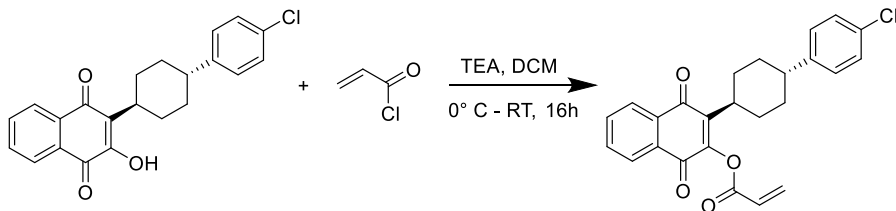


To circumvent *O*-methylation of alcohol moieties, SCNPs with tertiary amine side groups were first quaternized and then remaining pentafluorophenyl esters were reacted with aminoglycerol. PFP-SCNPs with and without atovaquone (50 mg, 0.173 mmol PFPMA, 1 eq.) were dissolved in 3.5 mL dry THF, followed by addition of TEA (96 μ L, 0.67 mmol, 4 eq.) and DMEN (6.65 mg, 0.075 mmol, 0.45 eq.) dissolved in 200 μ L dry THF. The mixture was stirred for 48 h at 45 °C. After determining conversion by ^{19}F NMR, the temperature was lowered to 30 °C, and 3 mL dry DMF was added, followed by methyl iodide (33.1 mg, 0.23 mmol, 3 eq.) dissolved in 150 μ L dry THF and the mixture was stirred overnight. The particles were subsequently reacted with aminoglycerol (393 mg, 4.3 mmol, 25 eq.) dissolved in 6 mL dry DMF. After stirring overnight at room temperature, the mixture was dialyzed against 1 wt% NaCl for 24 h, followed by another 48 h against demineralized water. The clear solution was lyophilized to yield a white powder (non-atovaquone) or a faint yellow powder (particles with atovaquone).

Fluorescent labeling of SCNPs

Each of the functionalized SCNPs (10 mg) was dissolved in carbonate-bicarbonate buffer (2 mL, 0.1 M, pH 9.5) and 5-DTAF (0.02 eq. to alcohol groups, 10 mg/mL stock solution in dry DMSO) was added and the solution was stirred overnight. Afterwards, the SCNPs were purified on a PD10 column by elution with water and the SCNPs were obtained after lyophilization yielding a yellow powder.

Synthesis of atovaquone-acrylate (ATOA)



To a stirred solution of atovaquone (200 mg, 0.55 mmol) in dichloromethane (8 mL) under nitrogen atmosphere, triethylamine (92 μ L, 0.66 mmol) was added and the solution was cooled on an ice bath. Acryloyl chloride (53 μ L, 0.66 mmol) was added dropwise and the solution was stirred overnight while warming up to room temperature. The mixture was diluted with dichloromethane (15 mL) and washed with water (2 \times 5 mL) and brine (1 \times 5 mL), dried over MgSO_4 and concentrated under reduced pressure. The residue was purified by flash column chromatography (silica gel, heptane:dichloromethane 2:1) to give ATOA as yellow crystals in 140 mg yield (60%).

^1H NMR (400 MHz, CDCl_3): δ (ppm) 8.08, 7.75, 7.28 and 7.16 (m, 8H, ArH), 6.74, (d, 1H, $\text{CH}_2=\text{CH}$) 6.45 (m, 1H, $\text{CH}=\text{CH}_2$), 6.17 (d, 1H, $\text{CH}_2=\text{CH}$), 3.11 (m, 1H, $(\text{CH}_2)_2\text{-CH-PhCl}$), 2.58 (m, 1H, $(\text{CH}_2)_2\text{-CH-C=C}$), 1.98 (m, 4H, $\text{CH}_2\text{-CH}_2\text{-CH-PhCl}$), 1.85 (m, 2H, $\text{CH}_2\text{-CH}_2\text{-CH-C=C}$) and 1.55 (m, 2H, $\text{CH}_2\text{-CH}_2\text{-CH-C=C}$), ^{13}C NMR (101 MHz, CDCl_3) δ (ppm) 184.6, 178.3, 163.4, 151.4, 145.7, 142.2, 134.7, 134.3, 133.9, 132.5, 131.8, 130.8, 128.6, 128.3, 127.1, 126.7, 126.7, 43.4 36.0, 34.3, 30.1.

ATO-SCNP preparation and functionalization

Atovaquone functionalized PFP-SCNPs were prepared as described for non-functionalized PFP-SCNPs, with the extra addition of atovaquone as functional agent by a thiol-Michael addition. After slow addition of the deprotected polymer to the crosslinker solution and stirring for an additional 2 hours, the residual thiols were reacted with atovaquone acrylate (40 mg, 0.1 mmol, 0.4 eq. to xanthate groups) and stirred overnight, followed by end-capping with methyl acrylate (1 mL, 12 mmol, 50 eq.) and the SCNPs were obtained after repeated precipitation in methanol as a faint yellow powder (319 mg, 55% yield).

The atovaquone drug loading was determined by ^1H NMR spectroscopy. ATO-SCNPs ($M_n = 59$ kDa, 7.45 mg, 1.26×10^{-4} mmol) were dissolved in d_6 -acetone. Trioxane was added from a stock solution as internal standard (0.026 mg, 2.9×10^{-4} mmol). The ratio between the 6 trioxane protons and 4 of the atovaquone protons was determined at 1:0.5, resulting in 2.3×10^{-4} mmol atovaquone in the sample, which is a drug loading of approximately 2 atovaquone moieties per SCNP (1.3 wt%).

Cell culture

HeLa cells (p.4-15) were cultured in DMEM medium with 10% FBS, L-glutamine and Pen/Strep.

Cytotoxicity

HeLa cells were seeded at 10×10^3 cells per well in 100 μL medium in 96-well plates and incubated overnight at 37 $^\circ\text{C}$ in humidified 5% CO_2 -containing atmosphere. Sample solutions containing SCNP 15, 40, and 40Q were prepared from 1 mg/mL stock solution in medium to final concentrations of 50, 100, 200 and 500 $\mu\text{g/mL}$. The medium in the 96-well plates was aspirated and 100 μL of the sample solutions were added per well in triplicates. In the reference wells the medium was exchanged with fresh medium. The SCNPs were incubated for 24 or 48 h, afterwards the cells were washed with PBS. A resazurin assay was used to analyze the viability of the cells, 100 μL of the resazurin solution was added per well and incubated with the cells for 2 h. The fluorescence intensity was measured by an EnSpire plate reader at excitation and emission wavelength of 560/590 nm.

Cellular uptake by FACS

In 300 μL medium HeLa cells were seeded at 30×10^3 in 48-well plates and incubated overnight. The SCNPs were added in sample solution of 100 $\mu\text{g}/\text{mL}$ after removal of the medium, the SCNPs were incubated for 1, 3 and 6 h. Afterwards, the cells were washed with PBS and harvested with trypsin. In the preparation of the FACS experiment PI staining was added to the cell solutions to analyze the cell viability. The FACS measurements were performed using a BD Bioscience FACS Aria II with excitation and emission filter of 488-530/30 and 630-660/30 nm.

Statistical analysis

Statistical analysis for *in vitro* results ($n=9$) was performed utilizing SPSS 22, via One-way analysis of variance (ANOVA) with Tukey post hoc analysis. Classifications of the differences were reported as following: significant ($p < 0.05$), very significant ($p < 0.01$) and extremely significant ($p < 0.001$).

Confocal laser scanning microscopy

HeLa cells were cultured at 10×10^3 cells per well in 100 μL in 96-well plates and incubated overnight. For HeLa cells SCNPs or ATO-SCNPs were incubated at 100 $\mu\text{g}/\text{mL}$ for 4h, 1h or 30 min in the case of SCNP 15, SCNP 40 or SCNP 40Q respectively. In the case of NIH/3T3 cells, ATO-SCNP 15 and ATO-SCNP 40 were incubated for 5 h and ATO-SCNP 40Q was incubated for 30 min at 100 $\mu\text{g}/\text{mL}$. The cells were washed and stained with lysostaining for 20 min before fixation with 4% PFA. Afterwards, WGA and DAPI stainings were employed. The samples were analyzed using a Nikon confocal microscope A1, equipped with the following laser wavelengths: 375, 488 and 561 nm.

Calcein assay

HeLa cells were seeded at 7.5×10^3 cells per well in 100 μL in 96-well plates and incubated overnight. SCNPs (without DTAF label) were incubated at 100 $\mu\text{g}/\text{mL}$ with calcein (200 μM) in 100 μL medium for 3 h. Then the cells were washed with PBS and fixated with 4% PFA. The cells were imaged using a fluorescent microscope Olympus IX 71.

Drug release

ATO-SCNP-40 was incubated at 5 mg/mL in 1 M acetic acid and stirred for 24 h. The sample was centrifuged at 12000 rpm for 20 min and the drug release was measured by HPLC and compared to free atovaquone and **SCNP-40**.

ATO-SCNP activity analysis

HeLa cells were seeded at 30×10^3 cells in 300 μL in 48-well plates and incubated overnight. Sample solutions of ATO-SCNPs and references of SCNPs, as well as free ATO, were incubated with the cells at 100 $\mu\text{g}/\text{mL}$ for the SCNPs and 5 $\mu\text{g}/\text{mL}$ for the free ATO. After 24 h incubation the cells were washed with PBS and harvested with trypsin. The samples were prepared for FACS using an Annexin V-DY-634/PI Apoptosis detection kit. The ATO activity was analyzed using a BD Bioscience FACS Aria II with excitation and emission filter of 375-450/30, 488-530/30 and 630-660/30 nm.

4.5 Supplementary information

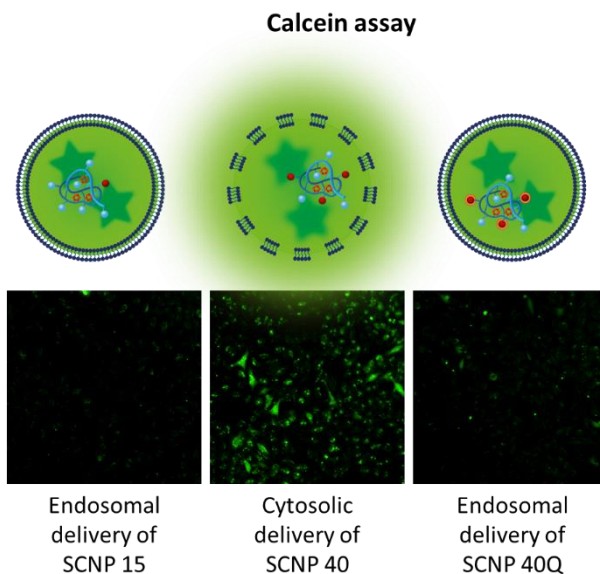


Figure S4.1. Fluorescent microscopy images of calcein assay. HeLa cells were incubated with SCNPs and calcein for 3 h.

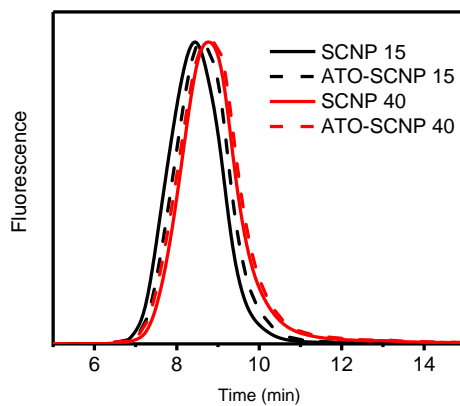


Figure S4.2. Size exclusion chromatography traces of **SCNP-15**, **SCNP-40** and **ATO-SCNP-15** and **ATO-SCNP-40**.

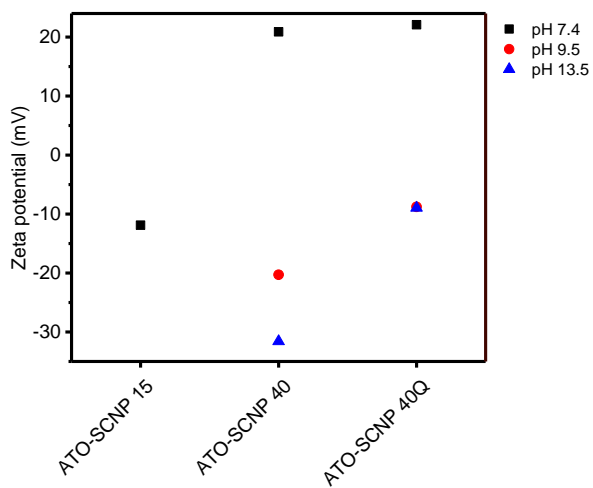


Figure S4.3. Zeta-potential of **ATO-SCNPs** at different pH values.

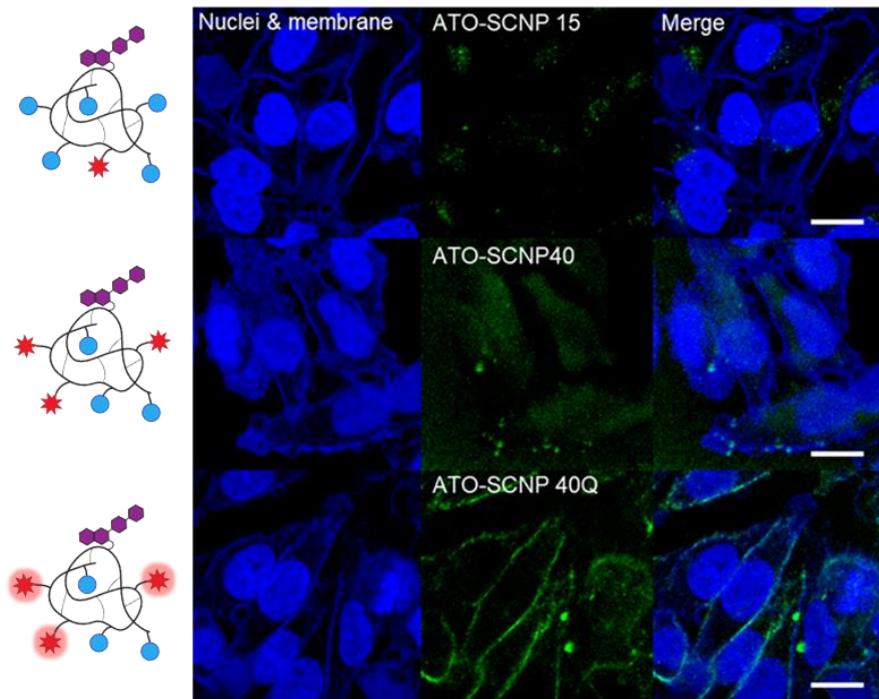


Figure S4.4. Confocal microscopy images of **ATO-SCNPs** in HeLa cells with nuclei and membrane in blue and SCNPs signal in green. ATO-SCNP15 and SCNP 40 were incubated for 5h and SCNP 40Q was incubated for 30 min. The scale bar is 20 μ m.

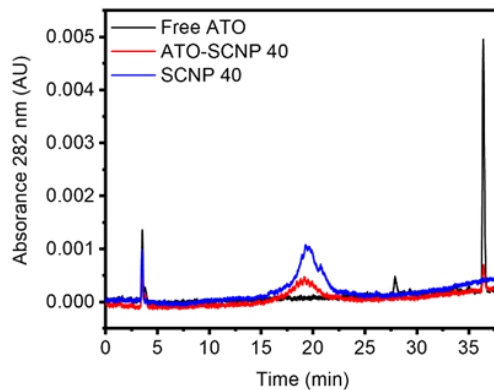


Figure S4.5. HPLC chromatogram of **ATO-SCNP-40**, free ATO and **SCNP-40** at 282 nm.

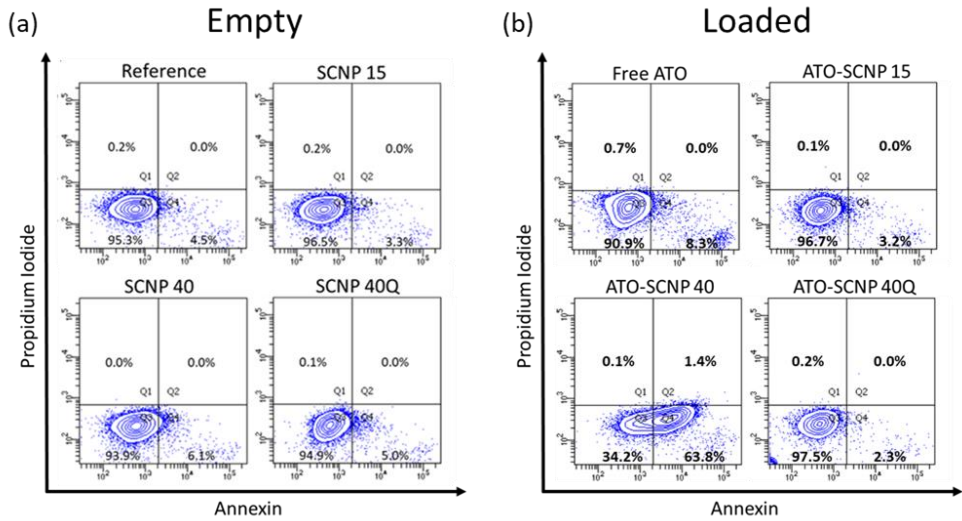


Figure S4.6. HeLa cell populations measured by flow cytometry after incubation with (a) empty (no atovaquone) nanocarriers and (b) **ATO-SCNPs (15, 40 and 40Q)** or free atovaquone for 24 h and stained by annexin-V and propidium iodide.

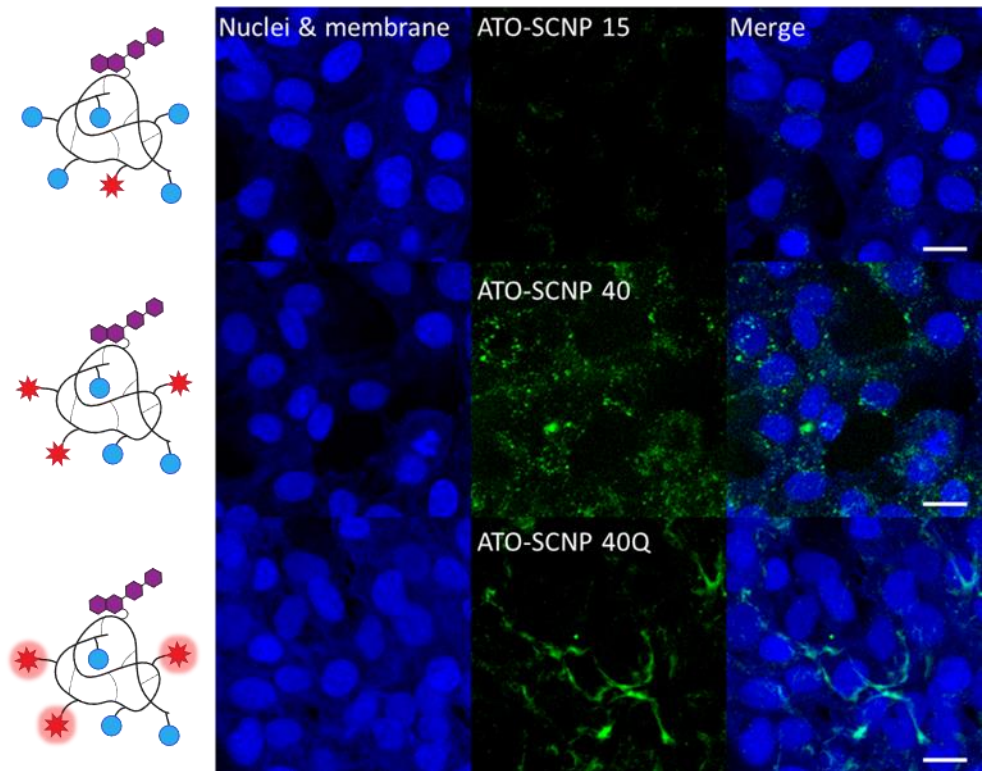


Figure S4.7. CLSM images of **ATO-SCNPs** in NIH/3T3 cells with nuclei and membrane in blue and SCNPs signal in green. **ATO-SCNP-15** and **ATO-SCNP-40** were incubated for 5h and **ATO-SCNP-40Q** was incubated for 30 min. The scale bar is 20 μ m.

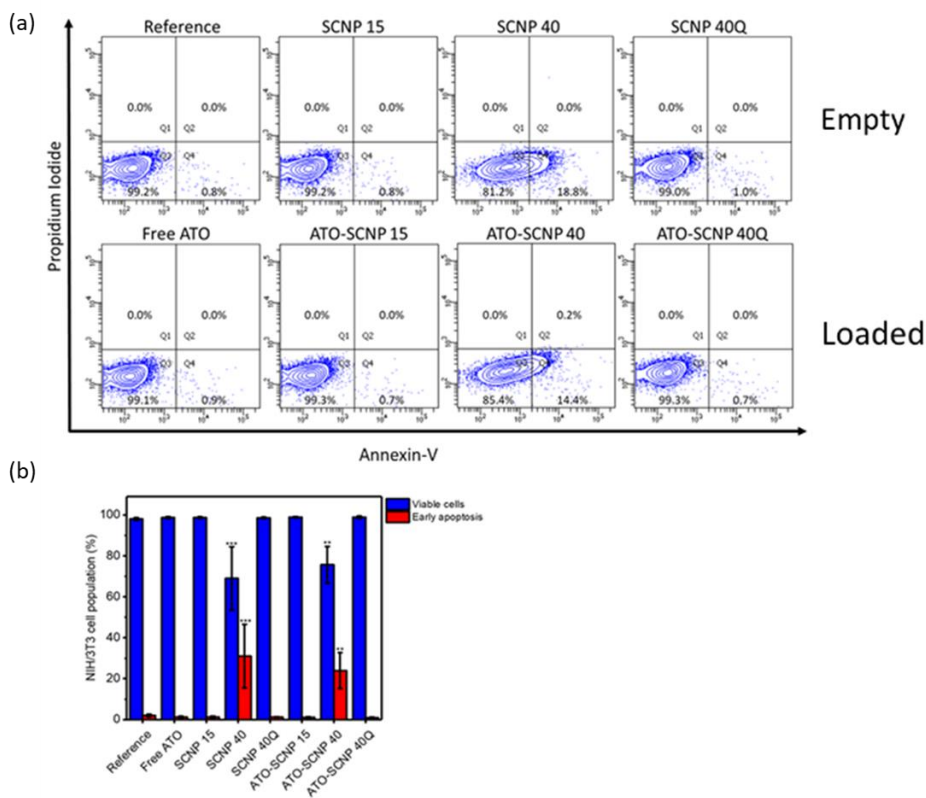


Figure S4.8. a) Representative flow cytometry dot plots of NIH/3T3 cell populations after incubation with **SCNPs**, **ATO-SCNPs** or free atovaquone for 24 h and stained by Annexin V and Propidium Iodide. b) Percentages of viable and apoptotic NIH/3T3 cell populations, asterisks indicate significant lower cell population in percentage relative to the reference, ** $p < 0.01$ and *** $p < 0.001$.

4.6 References

1. Banik, B. L.; Fattahi, P.; Brown, J. L., Polymeric nanoparticles: the future of nanomedicine. *Wiley Interdiscip Rev Nanomed Nanobiotechnol* **2016**, *8* (2), 271-99.
2. Zhang, C.; Yan, L.; Wang, X.; Zhu, S.; Chen, C.; Gu, Z.; Zhao, Y., Progress, challenges, and future of nanomedicine. *Nano Today* **2020**, *35*, 101008.
3. van der Meel, R.; Sulheim, E.; Shi, Y.; Kiessling, F.; Mulder, W. J. M.; Lammers, T., Smart cancer nanomedicine. *Nature Nanotechnology* **2019**, *14* (11), 1007-1017.
4. Lee, Y. W.; Luther, D. C.; Goswami, R.; Jeon, T.; Clark, V.; Elia, J.; Gopalakrishnan, S.; Rotello, V. M., Direct Cytosolic Delivery of Proteins through Coengineering of Proteins and Polymeric Delivery Vehicles. *J Am Chem Soc* **2020**, *142* (9), 4349-4355.
5. Luther, D. C.; Nagaraj, H.; Goswami, R.; Cicek, Y. A.; Jeon, T.; Gopalakrishnan, S.; Rotello, V. M., Direct Cytosolic Delivery of Proteins Using Lyophilized and Reconstituted Polymer-Protein Assemblies. *Pharm Res* **2022**, *39* (6), 1197-1204.
6. Hamilton, S. K.; Harth, E., Molecular Dendritic Transporter Nanoparticle Vectors Provide Efficient Intracellular Delivery of Peptides. *ACS Nano* **2009**, *3* (2), 402-410.

7. Chen, J.; Li, K.; Shon, J. S. L.; Zimmerman, S. C., Single-Chain Nanoparticle Delivers a Partner Enzyme for Concurrent and Tandem Catalysis in Cells. *J Am Chem Soc* **2020**, *142* (10), 4565-4569.
8. Jiao, Y.; Niu, L. N.; Ma, S.; Li, J.; Tay, F. R.; Chen, J. H., Quaternary ammonium-based biomedical materials: State-of-the-art, toxicological aspects and antimicrobial resistance. *Prog Polym Sci* **2017**, *71*, 53-90.
9. Hamelmann, N. M.; Paulusse, J. M. J., Single-chain polymer nanoparticles in biomedical applications. *J Control Release* **2023**.
10. Alqarni, M. A. M.; Waldron, C.; Yilmaz, G.; Becer, C. R., Synthetic Routes to Single Chain Polymer Nanoparticles (SCNPs): Current Status and Perspectives. *Macromol Rapid Commun* **2021**, e2100035.
11. Chen, R.; Berda, E. B., 100th Anniversary of Macromolecular Science Viewpoint: Re-examining Single-Chain Nanoparticles. *ACS Macro Letters* **2020**, *9* (12), 1836-1843.
12. Kroger, A. P. P.; Paulusse, J. M. J., Single-chain polymer nanoparticles in controlled drug delivery and targeted imaging. *J Control Release* **2018**, *286*, 326-347.
13. Bai, Y.; Hang, X.; Wu, P.; Feng, X.; Hwang, K.; Lee, J. M.; Phang, X. Y.; Lu, Y.; Zimmerman, S. C., Chemical Control over Cellular Uptake of Organic Nanoparticles by Fine Tuning Surface Functional Groups. *ACS Nano* **2015**, *9* (10), 10.
14. Kröger, A. P. P.; Paats, J.-W. D.; Boonen, R. J. E. A.; Hamelmann, N. M.; Paulusse, J. M. J., Pentafluorophenyl-based single-chain polymer nanoparticles as a versatile platform towards protein mimicry. *Polym. Chem.* **2020**, *11* (37), 6056-6065.
15. Hamelmann, N. M.; Paats, J. D.; Paulusse, J. M. J., Cytosolic Delivery of Single-Chain Polymer Nanoparticles. *ACS Macro Lett* **2021**, *10* (11), 1443-1449.
16. Liu, Y.; Pujals, S.; Stals, P. J. M.; Paulohrl, T.; Presolski, S. I.; Meijer, E. W.; Albertazzi, L.; Palmans, A. R. A., Catalytically Active Single-Chain Polymeric Nanoparticles: Exploring Their Functions in Complex Biological Media. *J Am Chem Soc* **2018**, *140* (9), 3423-3433.
17. Nakato, H.; Vivancos, R.; Hunter, P. R., A systematic review and meta-analysis of the effectiveness and safety of atovaquone - Proguanil (Malarone) for chemoprophylaxis against malaria. *Journal of Antimicrobial Chemotherapy* **2007**, *60* (5), 929-936.
18. Blanshard, A.; Hine, P., Atovaquone-proguanil for treating uncomplicated Plasmodium falciparum malaria. *Cochrane Database of Systematic Reviews* **2021**, *2021* (1).
19. Fiorillo, M.; Lamb, R.; Tanowitz, H. B.; Mutti, L.; Krstic-Demonacos, M.; Cappello, A. R.; Martinez-Outschoorn, U. E.; Sotgia, F.; Lisanti, M. P., Repurposing atovaquone: Targeting mitochondrial complex III and OXPHOS to eradicate cancer stem cells. *Oncotarget; Vol 7, No 23* **2016**.
20. Kapur, A.; Mehta, P.; Simmons, A. D.; Ericksen, S. S.; Mehta, G.; Palecek, S. P.; Felder, M.; Stenerson, Z.; Nayak, A.; Dominguez, J. M. A.; Patankar, M.; Barroilhet, L. M., Atovaquone: An Inhibitor of Oxidative Phosphorylation as Studied in Gynecologic Cancers. *Cancers (Basel)* **2022**, *14* (9).
21. Xiang, M.; Kim, H.; Ho, V. T.; Walker, S. R.; Bar-Natan, M.; Anahtar, M.; Liu, S.; Toniolo, P. A.; Kroll, Y.; Jones, N.; Giaccone, Z. T.; Heppler, L. N.; Ye, D. Q.; Marineau, J. J.; Shaw, D.; Bradner, J. E.; Blonquist, T.; Neuberger, D.; Hetz, C.; Stone, R. M.; Soiffer, R. J.; Frank, D. A., Gene expression-based discovery of atovaquone as a STAT3 inhibitor and anticancer agent. *Blood* **2016**, *128* (14), 1845-1853.
22. Fredenberg, S.; Wahlgren, M.; Reslow, M.; Axelsson, A., The mechanisms of drug release in poly(lactic-co-glycolic acid)-based drug delivery systems—A review. *International Journal of Pharmaceutics* **2011**, *415* (1), 34-52.
23. Yoo, J.; Won, Y.-Y., Phenomenology of the Initial Burst Release of Drugs from PLGA Microparticles. *ACS Biomaterials Science & Engineering* **2020**, *6* (11), 6053-6062.
24. Yin, Q.; Tong, R.; Xu, Y.; Baek, K.; Dobrucki, L. W.; Fan, T. M.; Cheng, J., Drug-initiated ring-opening polymerization of O-carboxyanhydrides for the preparation of anticancer drug-poly(O-carboxyanhydride) nanoconjugates. *Biomacromolecules* **2013**, *14* (3), 920-9.
25. Tong, R.; Cheng, J., Drug-Initiated, Controlled Ring-Opening Polymerization for the Synthesis of Polymer-Drug Conjugates. *Macromolecules* **2012**, *45* (5), 2225-2232.

26. Tong, R.; Cheng, J., Paclitaxel-initiated, controlled polymerization of lactide for the formulation of polymeric nanoparticulate delivery vehicles. *Angew Chem Int Ed Engl* **2008**, *47* (26), 4830-4.
27. Sheyi, R.; de la Torre, B. G.; Albericio, F., Linkers: An Assurance for Controlled Delivery of Antibody-Drug Conjugate. *Pharmaceutics* **2022**, *14* (2).
28. Ulbrich, K.; Hola, K.; Subr, V.; Bakandritsos, A.; Tucek, J.; Zboril, R., Targeted Drug Delivery with Polymers and Magnetic Nanoparticles: Covalent and Noncovalent Approaches, Release Control, and Clinical Studies. *Chem Rev* **2016**, *116* (9), 5338-431.
29. Feng, Q.; Tong, R., Anticancer nanoparticulate polymer-drug conjugate. *Bioeng Transl Med* **2016**, *1* (3), 277-296.
30. Alven, S.; Nqoro, X.; Buyana, B.; Aderibigbe, B. A., Polymer-Drug Conjugate, a Potential Therapeutic to Combat Breast and Lung Cancer. *Pharmaceutics* **2020**, *12* (5).
31. Yang, Y.; Wang, S.; Ma, P.; Jiang, Y.; Cheng, K.; Yu, Y.; Jiang, N.; Miao, H.; Tang, Q.; Liu, F.; Zha, Y.; Li, N., Drug conjugate-based anticancer therapy - Current status and perspectives. *Cancer Lett* **2023**, *552*, 215969.
32. El Hage, S.; Ane, M.; Stigliani, J. L.; Marjorie, M.; Vial, H.; Baziard-Mouysset, G.; Payard, M., Synthesis and antimalarial activity of new atovaquone derivatives. *Eur J Med Chem* **2009**, *44* (11), 4778-82.
33. Comley, J. C.; Yeates, C. L.; Frend, T. J., Antipneumocystis activity of 17C91, a prodrug of atovaquone. *Antimicrobial Agents and Chemotherapy* **1995**, *39* (10), 2217-2219.
34. Romeo, S.; Parapini, S.; Dell'Agli, M.; Vaiana, N.; Magrone, P.; Galli, G.; Sparatore, A.; Taramelli, D.; Bosisio, E., Atovaquone-statine "double-drugs" with high antiplasmodial activity. *ChemMedChem* **2008**, *3* (3), 418-20.
35. Ouji, M.; Nguyen, M.; Mustiere, R.; Jimenez, T.; Augereau, J. M.; Benoit-Vical, F.; Deraeve, C., Novel molecule combinations and corresponding hybrids targeting artemisinin-resistant Plasmodium falciparum parasites. *Bioorg Med Chem Lett* **2021**, *39*, 127884.
36. Sprouse, D.; Reineke, T. M., Investigating the Effects of Block versus Statistical Glycopolycations Containing Primary and Tertiary Amines for Plasmid DNA Delivery. *Biomacromolecules* **2014**, *15* (7), 2616-2628.
37. Hausig-Punke, F.; Richter, F.; Hoernke, M.; Brendel, J. C.; Traeger, A., Tracking the Endosomal Escape: A Closer Look at Calcein and Related Reporters. *Macromol Biosci* **2022**, *22* (10), e2200167.
38. Hu, Y. B.; Dammer, E. B.; Ren, R. J.; Wang, G., The endosomal-lysosomal system: from acidification and cargo sorting to neurodegeneration. *Translational neurodegeneration* **2015**, *4*, 18.
39. Wang, C.; Zhao, T.; Li, Y.; Huang, G.; White, M. A.; Gao, J., Investigation of endosome and lysosome biology by ultra pH-sensitive nanoprobe. *Adv Drug Deliv Rev* **2017**, *113*, 87-96.
40. Su, F. Y.; Srinivasan, S.; Lee, B.; Chen, J.; Convertine, A. J.; West, T. E.; Ratner, D. M.; Skerrett, S. J.; Stayton, P. S., Macrophage-targeted drugamers with enzyme-cleavable linkers deliver high intracellular drug dosing and sustained drug pharmacokinetics against alveolar pulmonary infections. *J Control Release* **2018**, *287*, 1-11.
41. Wu, C.; Gong, M. Q.; Liu, B. Y.; Zhuo, R. X.; Cheng, S. X., Co-delivery of multiple drug resistance inhibitors by polymer/inorganic hybrid nanoparticles to effectively reverse cancer drug resistance. *Colloids Surf B Biointerfaces* **2017**, *149*, 250-259.
42. Guo, X.; Cheng, Y.; Zhao, X.; Luo, Y.; Chen, J.; Yuan, W. E., Advances in redox-responsive drug delivery systems of tumor microenvironment. *J Nanobiotechnology* **2018**, *16* (1), 74.
43. Zhu, J.; Guo, T.; Wang, Z.; Zhao, Y., Triggered azobenzene-based prodrugs and drug delivery systems. *J Control Release* **2022**, *345*, 475-493.

Chapter 5

Dual-reactive single-chain polymer nanoparticles for orthogonal functionalization through active ester and click chemistry

Glucose has been extensively studied as a targeting ligand for biomedical nanoparticles. A promising nanocarrier platform are single-chain polymer nanoparticles (SCNPs). SCNPs are well-defined 5-20 nm semi-flexible nano-objects, formed by intramolecularly crosslinked linear polymers. Functionality can be incorporated by introducing labile pentafluorophenyl (PFP) esters in the polymer backbone, which can be readily substituted by functional amine-ligands. However, not all ligands are compatible with PFP-chemistry, requiring different ligation strategies for increasing the versatility of surface functionalization.

Here, we combine active PFP-ester chemistry with copper(I)-catalyzed azide alkyne cycloaddition (CuAAC) click chemistry to yield dual-reactive SCNPs. First, the SCNPs are functionalized with increasing amounts of amino-butyne groups through PFP-chemistry, leading to a range of butyne-SCNPs with increasing terminal alkyne-density. Subsequently, azido-propylglucose is conjugated through the glucose C1- or C6-position by CuAAC click chemistry, yielding two sets of glyco-SCNPs. Cellular uptake is evaluated in HeLa cancer cells, revealing increased uptake upon higher glucose-surface density, with no apparent positional dependence. The general conjugation strategy proposed here can be readily extended to incorporate a wide variety of functional molecules to create vast libraries of multifunctional SCNPs.

5.1 Introduction

Polymeric nanoparticles (NPs) are materials ranging from 1 to 100 nm, that have gained significant attention in recent decades, due to their high surface to volume ratio, modularity and biocompatibility.¹⁻⁴ Owing to these favorable characteristics, they have been widely explored in controlled drug delivery,⁵⁻⁶ imaging⁷⁻⁸ and as antimicrobial agents.⁹⁻¹⁰ To further tailor NPs towards specific applications, their characteristics can be altered by incorporating additional ligands and modifying the surface chemistry. For studying the influence of ligands on structural properties, a straightforward way to introduce functionality, is by direct polymerization of functional monomers. This is the most efficient strategy, omitting the need for additional synthetic steps. However, direct incorporation requires compatibility between the functional groups and the polymerization conditions. Although the introduction of new polymerization techniques has resulted in greatly expanding the functional group tolerance,¹¹⁻¹⁴ a wide variety of ligands of interest still remains incompatible with the currently available polymerization toolbox. Likewise, post-polymerization modification (PPM) has emerged as an attractive alternative, circumventing the limitations imposed by direct polymerization.¹⁵⁻¹⁶ Expanding the concept of PPM to polymeric nanoparticles, post-formation modification enables modification of a particle's exterior, without altering the nanoparticle backbone structure, thereby dramatically reducing synthetic complexity by being able to start from the same reactive precursor.

Over the years, a plethora of PPM techniques has been developed and utilized, spanning a wide range of different chemistries, such as thiol-ene reactions,¹⁷ epoxide ring openings¹⁸ and Diels-Alder cyclo-additions.¹⁹ One particularly useful PPM-methodology is using active pentafluorophenyl (PFP) esters, owing to their facile substitution with primary amines forming stable amide linkages, their high tolerance towards radical polymerizations and the ability to follow the reaction by background-free ¹⁹F NMR spectroscopy.²⁰⁻²² However, not every functional ligand is compatible with active ester chemistry, and different conjugation strategies are still needed. An alternative is to use copper(I)-catalyzed azide alkyne cycloaddition (CuAAC), one of the most versatile reactions in "click chemistry". Since the first reports in 2002,²³⁻²⁴ the reaction has been exploited in the synthesis of functional macromolecules, such as dendrimers,²⁵ polymers,²⁶ micelles²⁷ and protein-conjugates,²⁸ with many ligands of interest already (commercially) available. Although the reaction conditions are mild and tolerant towards a wide range of conditions, the ligation requires incorporation of an azide- or alkyne-moiety on the backbone of the macromolecule. Especially for biomolecules, incorporation of a precise number of azide or alkyne-moieties is often not feasible, nor is the incorporation easily quantified.

Besides surface functionalization, many other NP characteristics are important to consider for biomedical applications, such as stiffness,²⁹ shape³⁰ and especially their size.³¹⁻³² Bai et al. demonstrated an inverse relationship between polymeric NP size and cellular uptake, with 7 nm NPs showing a 3-fold higher uptake than 40 nm NPs.³³ This underlines the value of scaling down particle size to promote endocytosis. However, only limited synthetic strategies are available to synthesize NPs in this size range. One elegant way towards sub-20 nm particles is to use single-chain polymer nanoparticles (SCNPs). SCNPs are formed from polymer-precursors through exclusive intramolecular crosslinks, forming soft and semi-flexible NPs with excellent control over size and dispersity.³⁴⁻³⁶ SCNPs have found widespread application in for example cellular targeting,³⁷⁻³⁹ catalysis,⁴⁰⁻⁴² and imaging.⁴³⁻⁴⁵ We have recently shown that we can equip SCNPs with active PFP-esters for quantitative functionalization with primary amines.⁴⁶⁻⁴⁷ However, incorporation is not straightforward, since not every functional moiety is compatible with an amine group. Therefore, the possibility of combining PFP-chemistry with CuAAC is very appealing, since it further increases the modularity regarding choice of ligand, solvent polarity, and provides excellent control over ligand density, all starting from the same scaffold. This would allow for the systematic investigation of a wide range of surface functionalities.

Molecular interactions between sugars and sugar-binding proteins (lectins) are essential for many recognition events in the human body, which is the start for numerous biological processes.⁴⁸⁻⁴⁹ This makes glucose a highly interesting surface ligand for investigating cellular interactions. Furthermore, since glucose is the main energy source in living systems, cell surfaces are decorated with a variety of glucose-transporters (GLUTs) for enabling efficient uptake.⁵⁰ Since GLUTs are often upregulated in tissues with a high metabolic activity (e.g. cancer cells or brain endothelial cells), it is not surprising that decorating NPs with sugar-moieties has become a popular strategy to achieve efficient cellular targeting.⁵¹⁻⁵² Simple monovalent sugars generally display low affinity constants for binding with cellular receptors. However, by using glyco-macrostructures, multiple binding events between cell surfaces and NPs can be induced. This enhanced activity through multivalency, coined the “cluster glycoside effect”, can therefore be exploited to circumvent the inherent weak binding limitations by single saccharide-units and still offer strong interactions.⁵³ However, increasing overall binding strengths does not necessarily lead to higher cellular uptake and often hampers selectivity.⁵⁴ Furthermore, when using NPs for crossing barriers, very strong NP binding to cellular receptors can even be detrimental to transcytosis.⁵⁵ This stresses the need for ligand density optimization with respect to the prospected biological targets.

An important additional parameter is the position through which glucose is conjugated. Binding studies on erythrocytes revealed hydrogen bonding between

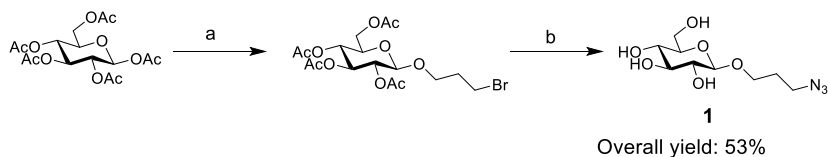
C1-O, C3-O, C4-OH and C6-O of glucose and the glucose transporter (GLUT1).⁵⁶ Furthermore, alkyl substitutions on the C-6 position even increased the affinity of GLUT1 for glucose, whereas a propyl-group at β -C1-O rendered the glucopyranoside with no ability to any longer compete with native glucose on the outside of cells.⁵⁷⁻⁵⁸ This suggests that modification at the C6-position with a (hydrophobic) linker is a good starting point for effective glucose-binding on cell surfaces, a strategy which has been adopted for other glucose-decorated nanocarriers.⁵⁹⁻⁶¹ Similarly, galactose-containing self-assembled NPs revealed a positional dependence (C1 vs C6) on intracellular pathways, reaching different endo- and lysosomal structures depending on the conjugation position.⁶² However, modification at the C1-position with a short alkyl linker is synthetically more convenient than at the C6-position, because of its anomeric reactivity. Furthermore, studies in a different GLUT1-upregulated cell-line (HeLa cancer cells) suggested little difference between C1 and C6-modification for the amount of cellular uptake of glucose-decorated platinum-conjugates.⁶³⁻⁶⁴

To this end, we combine here active PFP ester chemistry with CuAAC click chemistry to develop a range of SCNPs with increasing alkyne-ligand density from the same precursor SCNPs. To shed more light on the positional dependency of the conjugation site, the SCNPs are subsequently ligated with D-glucose through an azidopropyl-linker at two different positions (C1 and C6) and at different ligand densities to arrive at a set of **glyco-SCNPs**. The SCNPs are characterized by ¹H NMR spectroscopy and size exclusion chromatography, and lectin binding assays are performed. The positional dependence, as well as the influence of ligand density are finally evaluated by cellular uptake studies in HeLa cancer cells.

5.2 Results and discussion

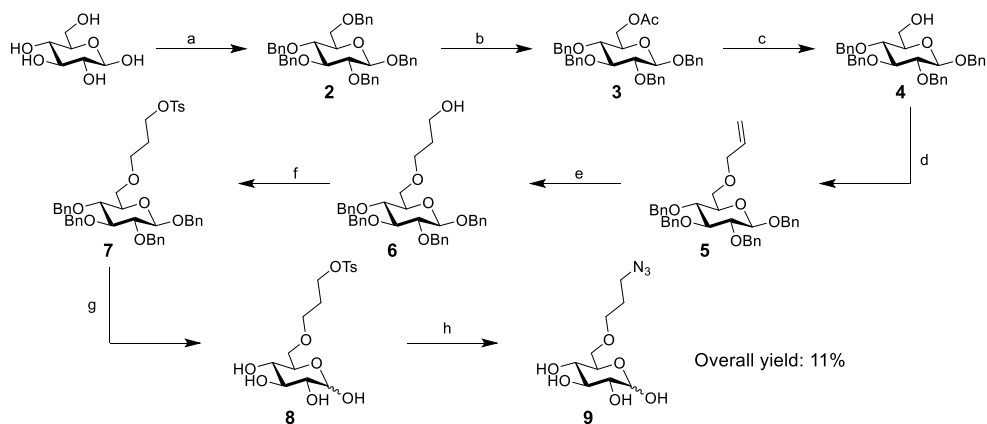
Synthesis of glucose-ligands

In order to evaluate the positional dependence of cell-nanoparticle interactions, glucose-ligands were designed with the same spacer for conjugation, only differing in the conjugation position. Modification at the C1-position is fairly straightforward, by exploiting the Lewis acid catalyzed reactivity of the OAc-group at the anomeric position. Subsequent azidation and Zemplén deacetylation yielded target compound **1** (see Scheme 5.1).



Scheme 5.1. Synthesis of azide-functional glucose via the 1-position. Reagents and conditions: (a) 1) 3-bromo-1-propanol, $\text{BF}_3\text{-Et}_2\text{O}$, DCM, N_2 , 0°C – r.t., overnight; (b) 1) NaN_3 , DMF, 50°C , argon, overnight; 2) 20 mM NaOMe in MeOH, r.t., overnight.

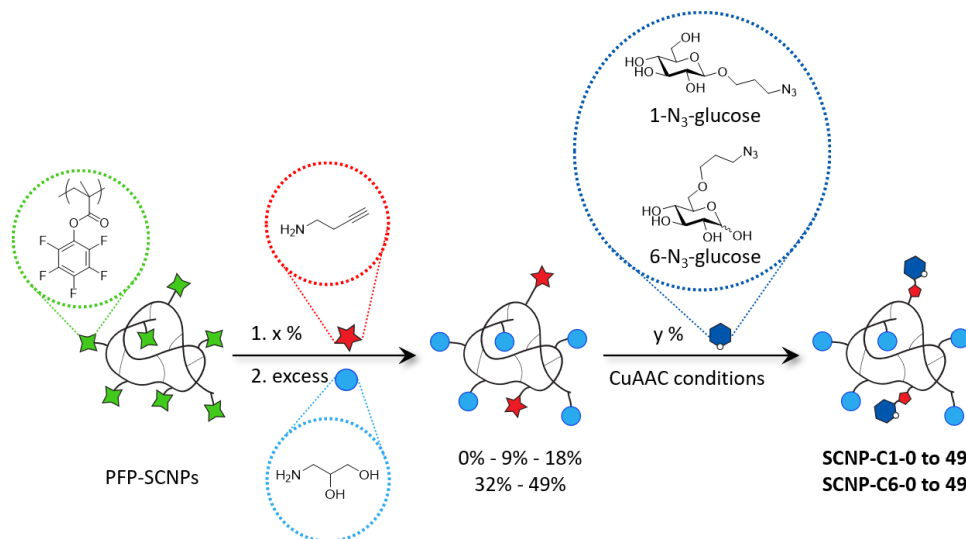
For modification at the C6-position, a new synthetic route had to be established (Scheme 5.2). Starting from D-glucose, compound **4** was synthesized according to a literature procedure with comparable yield.⁶⁵ Chain extension by allyl bromide, followed by hydroboration, yielded compound **6**, as well as compound **4** as a deprotection product.⁶⁴ Converting the alcohol into a bromide by an Appel reaction resulted in 10% loss of the halogen upon the subsequent hydrogenation. Although the by-product would be inert, compound **6** was tosylated, followed by subsequent Zemplén deacetylation, hydrogenation and azidation, to yield target compound **9** in 11% overall isolated yield (characterization data can be found in Figure S5.1 and Figure S5.2).



Scheme 5.2. Synthesis of azide-functional glucose via the 6-position. Reagents and conditions: (a) 1) NaH, DMF, N_2 ; 2) BnBr, N_2 , 0°C – r.t., overnight; (b) AcOH:Ac₂O 1:5, ZnCl_2 , 2.5h, r.t.; (c) 25 mM NaOMe in MeOH, r.t., 5h; (d) 1) NaH, DMF, N_2 ; 2) allyl-Br, N_2 , 0°C – r.t., overnight; (e) 1) NaBH_4 , $\text{BF}_3\text{-Et}_2\text{O}$, THF, N_2 , r.t. overnight; 2) H_2O , 4 M NaOH, H_2O_2 30%, 0°C – r.t., 3h; (f) *p*-TsCl, pyridine, DCM, N_2 , 0°C – r.t., overnight; (g) H_2 8 bar, Pd/C 10%, MeOH, EtOAc, r.t., overnight; (h) NaN_3 , DMF, N_2 , 50°C , overnight.

Synthesis and characterization of butyne-SCNPs

Conjugation of glucose-ligands onto the SCNPs through copper-catalyzed azide-alkyne cycloaddition (CuAAC) first requires introduction of alkyne moieties on the nanoparticles. To this end, active-ester **PFP-SCNPs** were prepared as previously described,⁴⁶ to subsequently conjugate an amino-alkyne onto the SCNPs. However, this conjugation was severely hampered. The use of commercially available alkyne-PEG4-amine resulted in crosslinking between particles, as observed by size exclusion chromatography (SEC) (see Figure S5.3). This is possibly a result of intermolecular Glaser coupling taking place. Although Glaser couplings are normally catalyzed by copper,⁶⁶ metal-free variants have also been reported.⁶⁷⁻⁶⁸ Since the conjugation was performed at elevated temperature for 24 h in the presence of a base, it is not unlikely that alkyne-alkyne dimerization occurred. Since the prospected number of alkyne groups on a single nanoparticle can be well above 100 moieties, and the flexible tetraethylene glycol linker ensures accessibility of these moieties, minor intermolecular coupling would already result in multi-chain aggregates, as evidenced by increased crosslinking upon increased alkyne-incorporation. Therefore, conjugation of different amino-alkynes was investigated as well. Conjugation of propargylamine, however, resulted in very low incorporation ratios, whereas propargyl-terminated 4-amino-butan-1-ol seemed to lead only to partial hydrolysis, since the incorporation ratio was low and largely independent of the concentration of amino-alkyne (see Figure S5.3). Furthermore, no evidence of conjugation was observed in the ¹H NMR spectra (*data not shown*). Incorporation of 1-amino-3-butyne was attempted next, which did result in appreciable conjugation. Although the conjugation was relatively sluggish as compared to earlier investigated functional amines, the amino-alkyne could be titrated towards the desired ligand density (Table S5.1). After determining the conversion by ¹⁹F NMR (Figure S5.4), remaining reactive PFP-esters were endcapped with a large excess of 1-aminoglycerol, quenching the reaction and increasing the particles' water solubility (Scheme 5.3).



Scheme 5.3. Schematic representation of the functionalization of **PFP-SCNPs** with increasing amounts of 1-amino-3-butyne, followed by endcapping of remaining functional esters with 1-aminoglycerol. The range was conjugated with either 1-N₃-glucose or 6-N₃-glucose forming a set of 2x4 particles, as well as a 100% 1-aminoglycerol version (**SCNP-0**).

The range of 3-butyamide-SCNPs was studied by ¹H NMR spectroscopy. Successful incorporation of alkyne-groups is observed in the ¹H NMR spectra as shown in Figure 5.1a. Signals corresponding to the 3-butyamide groups, i.e. the terminal alkyne proton at $\delta = 2.8$ ppm and the adjacent methylene group at $\delta = 2.3$ ppm, increased with increasing ligand density, whereas the signals for 1-aminoglycerol incorporation, observed at $\delta = 4.9-4.4$, 3.5 and 3.0 ppm, diminished in intensity. The absence of signals in the ¹⁹F NMR spectra (*data not shown*) further indicates successful functionalization of SCNPs with increasing amounts of alkyne-ligands, while no reactive PFP groups remained. SEC-analysis showed a monomodal trace with a slight shift towards shorter elution times upon higher alkyne-content, indicative of a slightly increased hydrodynamic radius, but importantly without discernible dimerization of nanoparticles (Figure 5.1b).

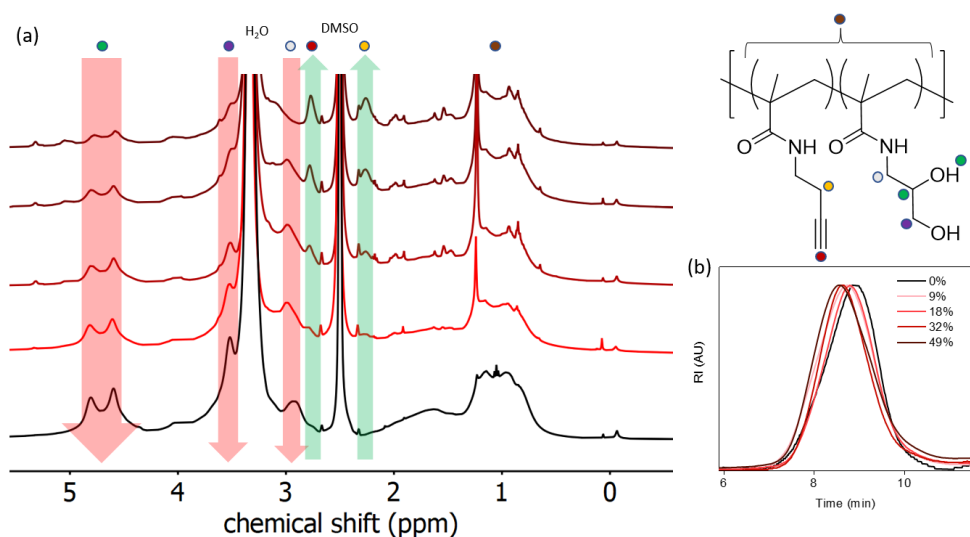


Figure 5.1. (a) Overlaid NMR-spectra of 1-amino-3-butynyl functionalized SCNPs, indicating the increase (green) and decrease (red) of respective functional groups with increasing alkyne incorporation. (b) SEC-trace of functionalized SCNPs.

Synthesis and Characterization of glyco-SCNPs

The range of butynamide-SCNPs was subsequently conjugated with either **1-azidopropylglucoside** or **6-azidopropylglucoside** (Scheme 5.3). Conjugation was performed on the same SCNP parent precursor, eliminating batch-to-batch differences. The CuAAC ligation was conducted with an excess of azido-glucose, in the presence of a base and without any additional copper-chelating agent. Successful incorporation of glucose is observed by ^1H NMR spectroscopy. The resonances associated with the alkyne-moiety disappeared after conjugation (Figure S5.5). For the 1-position, an shift of the anomeric proton signal to $\delta = 4.1$ ppm can be observed, as well as an increasing signal corresponding to the triazole ring at $\delta = 7.9$ ppm (Figure 5.2a), upon increased glucose-content. Similarly for the 6-position, an increased triazole resonance is observed at $\delta = 7.9$ ppm. Furthermore, because ring-opening is not blocked in this glucoside, the anomeric proton is seen at $\delta = 6.6$ ppm and $\delta = 6.3$ ppm, for β - and α -glucose respectively, in approximately 2:1 ratio (Figure 5.2b). However, conjugation of 6-azido-glucose onto the highest substituted alkyne-SCNP (**SCNP-C6-49**) proved unsuccessful, resulting in insoluble material. Furthermore, ^1H NMR analysis indicated a distinctly different structure than the lower substituted versions, and it was therefore omitted from further analysis (*data not shown*).

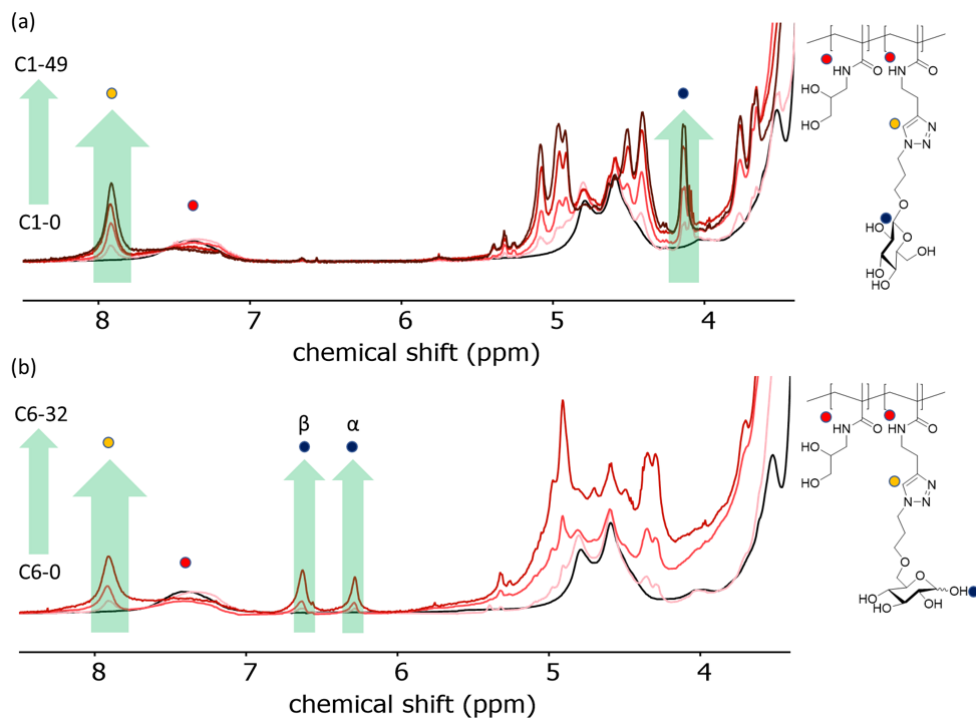


Figure 5.2. Overlaid NMR-spectra of (a) 1-azidopropylglucoside functionalized SCNPs and (b) 6-azidopropylglucoside functionalized SCNPs, normalized by backbone intensity, indicating the increase (green) of respective functional groups with increasing glucose conjugation.

SEC-analysis on both sets of **glyco-SCNPs** revealed the appearance of higher molecular weight species upon increasing the ligand density (Figure 5.3a and b). This effect is more pronounced for **glyco-SCNPs** conjugated through the C6-position. Most likely, alkyne-dimerization occurs under the applied CuAAC-conditions, resulting in crosslinking between SCNPs. Since Glaser-couplings also require Cu(I) and a base,⁶⁹ this would explain the observed dimerization (and possibly even larger structures) in the SEC-traces. Furthermore, by in situ reduction of Cu(II) to Cu(I) by sodium ascorbate, reactive oxygen species are generated which are potentially harmful for biomacromolecules.⁷⁰⁻⁷² This would be more severe for 6-azido-glucose, since it is still a reducing sugar compared to 1-azido-glucose, and this may lead to more undefined structures by being oxidized. For future experiments, the conjugation should be conducted with a Cu(I)-binding ligand present,⁷³ more azido-sugar,⁷⁴ less sodium ascorbate and at lower temperatures.

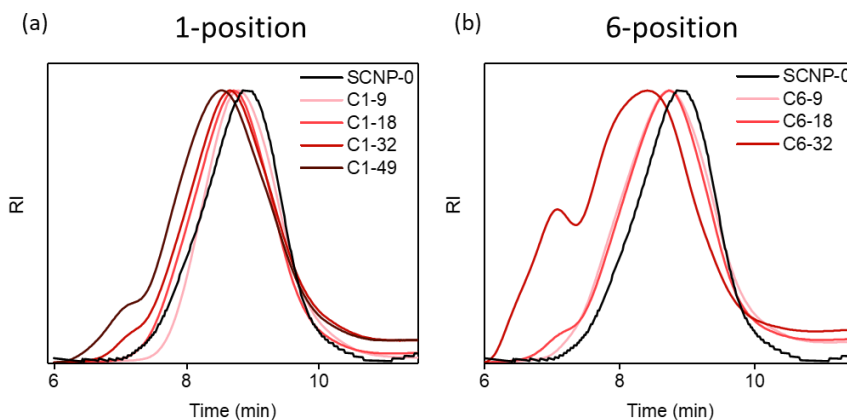


Figure 5.3 Overlaid SEC-traces of (a) **SCNP-C1-0 to 49** and (b) **SCNP-C6-0 to 32**.

Lectin binding study

To probe the availability of the glucose ligands on the SCNP surfaces for lectin binding, we employed a quantitative precipitation assay using the model lectin concanavalin A (Con A). Con A exists as a tetramer at neutral pH, with 4 identical binding sites for glucose.⁷⁵⁻⁷⁶ Upon binding between Con A and **glyco-SCNPs**, aggregates can form, which can be quantified by UV-Vis spectroscopy and are an indication of the accessibility of the glucose ligands. Figure 5.4 shows increased Con A binding for **glyco-SCNPs** conjugated through the C1-position, upon increased ligand density. For the C6-range, **SCNP-C6-32** is omitted, since it did not yield a clear solution at the required concentration. No Con A precipitation was observed for **SCNP-C6-9** and **SCNP-C6-18**, which is in line with previous work on C6-glucose modified SCNPs from our group.⁷⁷ This result shows the importance of including a non-substituted glucose primary alcohol (C6) in the Con A binding assay.

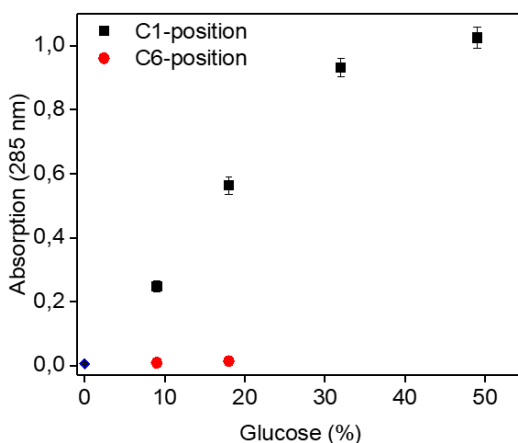


Figure 5.4. Con A precipitation assay for C1 and C6-functionalized **glyco-SCNPs** with increasing ligand density

Cell studies

However, the complexation behavior of **glyco-SCNPs** with the model lectin Con A is not representative for the immense complexity of biological systems. Therefore, the influence of position and ligand-density was further studied in cell culture models. **SCNP-C6-32** is omitted to arrive at a more fair comparison, since these nanoparticles showed significant inter-particle crosslinking as compared to its C1-counterpart (Figure S5.6). The two series of **glyco-SCNPs** were fluorescently labelled with 5-(4,6-dichlorotriazinyl) aminofluorescein (DTAF) for subsequent biological evaluations. SEC-analysis indicated no free dye present, which could interfere with subsequent cell experiments (Figure S5.7).

Evaluation on cancer cells

Since glucose-decorated nanoparticles have found widespread application in cancer treatment,⁷⁸⁻⁸¹ we further assessed the applicability of our range of **glyco-SCNPs** on HeLa cells. HeLa cells overexpress GLUT1 and are therefore expected to display enhanced binding interactions with glucose-decorated SCNPs.⁸² A resazurin assay revealed no apparent cytotoxicity after 24 h of incubation, even at the highest concentrations of SCNPs (Figure S5.8). Next, cellular uptake was studied by flow cytometry (see Figure 5.5). No significant increases in uptake are observed for SCNPs **C1-9** and **C6-9** with the lowest ligand densities, as compared to **SCNP-0**. However, both **C1-18** and **C6-18** show significantly higher uptake, already after 3 h of incubation. Interestingly, in contrast to the strong influence of ligand density, no positional dependency is observed between **C1-18** and **C6-18**. Although examined on different GLUT1 overexpressing cancer cell lines, this is also in line with earlier

work on platinum-conjugated sugars through alkyl-linkages, where no difference in uptake was observed between the two conjugation positions.⁶³ On the other hand, Kröger et al. showed superior uptake for C6-conjugated **glyco-SCNPs** as compared to the C1-position in HeLa cells.⁷⁷ An important difference, however, is the employed short linker in this earlier study, and the apparent positional dependency may thus have a different origin.

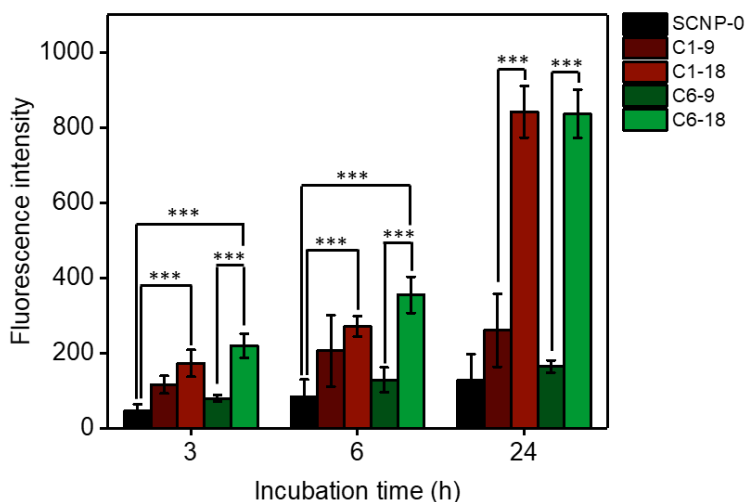


Figure 5.5. Cellular uptake in HeLa cells at different timepoints measured by flow cytometry. *** indicates $p < 0.001$

To further confirm cellular uptake and gain insights into the mode of cellular entry, uptake was further evaluated by confocal microscopy (see Figure 5.6). In agreement with the flow cytometry results, the SCNPs were observed inside the cells. Furthermore, the green fluorescence of the SCNPs co-localizes well with vesicular structures, indicating endosomal uptake, and resembling previous observations by our group for glycerol- and glycoside-modified SCNPs.^{37, 77} Overall, these results suggest glucose-conjugation through the C1-position would suffice for effective targeting, while ligand density is the determining factor for efficient cellular uptake in HeLa cells.

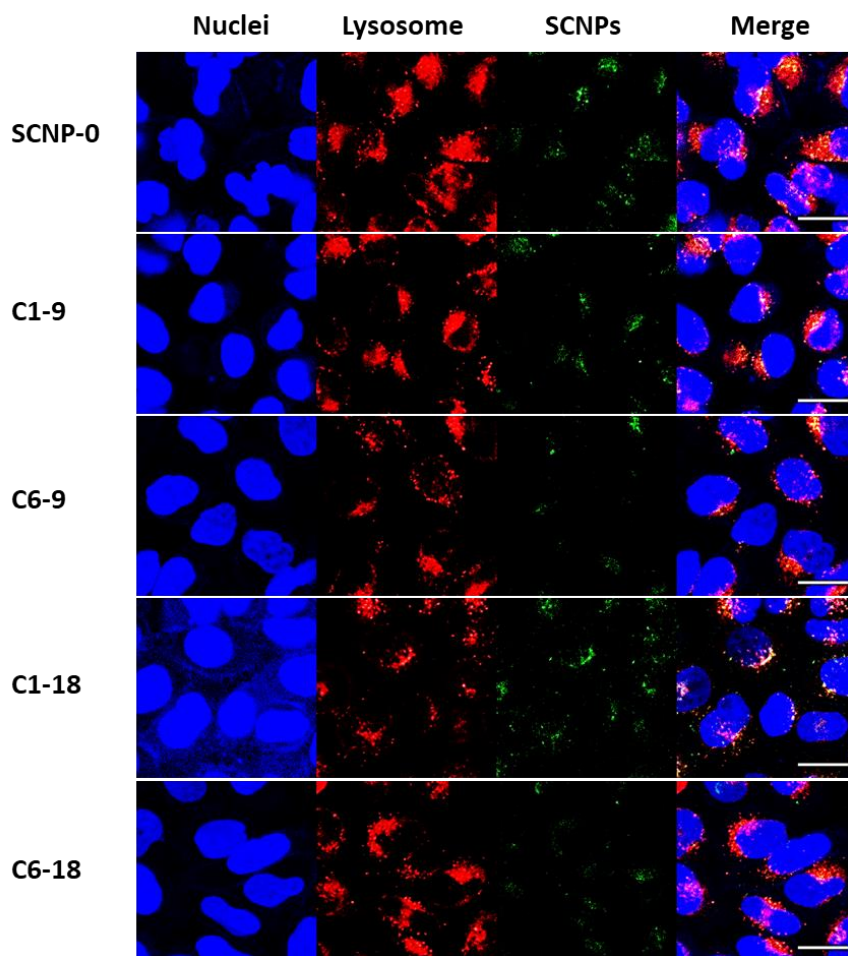


Figure 5.6. Confocal microscopy images of **glyco-SCNPs** and **SCNP-0**. Nuclei are stained in blue, lysosomes in red and SCNPs are labeled green fluorescent. Scale bar is 20 μm .

5.3 Conclusion

In this work, single-chain polymer nanoparticles were decorated with increasing amounts of terminal alkynes for subsequent copper(I)-catalyzed alkyne-azide cycloaddition. Although incorporation was slow, the required ligand density could be reached by choosing the right amino-alkyne moiety. Two different azido-glucose-ligands (functionalization on C1 and C6) were synthesized and subsequently conjugated under CuAAC-conditions. The click reaction revealed the importance of choosing the right conditions to prevent Glaser couplings and other oxidative side-reactions. The resulting **glyco-SCNPs** exhibited no discernible cytotoxicity in cancer cells (HeLa). Uptake in cancer cells did increase substantially upon increasing the

density of glucose-ligands on the particle surface, but proved largely independent of conjugation position. This could indicate that ligand-density is more important than conjugation position for cellular uptake, although a wider range of ligand density, as well as incubation conditions should be studied to substantiate this.

The general synthetic strategy proposed here can be readily extended to incorporate a wide variety of functional molecules. By combining active ester chemistry and click chemistry, multifunctional nanoparticles can be synthesized with precise control over ligand type and ligand density, which would otherwise remain synthetically unattainable due to incompatibilities with polymerization conditions or non-orthogonal post-polymerization modification. Moreover, since one can start from the same precursor SCNP, vast libraries can be readily created, having the same macromolecular template. This could provide a powerful combinatorial approach to study complex structure-activity relationships, in which different types of azido-sugars are employed, through linkers of different lengths and polarity, and even combined with additional surface functionality, such as charges or peptides.

5.4 Materials and Methods

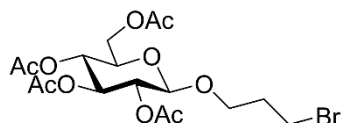
BF₃-Et₂O (46% BF₃), 3-bromo-1-propanol (97%), D-(+)-glucose (>99.5%), 3-amino-1,2-propanediol benzyl bromide (98%), NaH 60% in mineral oil, acetic acid (AcOH, >99%), acetic anhydride (Ac₂O, >98%), ZnCl₂ (anhydrous, >98%), allyl bromide (99%), NaBH₄ (99%), NaOH (>98%), H₂O₂ 30% in H₂O, *p*-toluenesulfonyl chloride (*p*-TsCl, >99%), pyridine (>99.0%), 1-amino-3-butyne (95%), 4-amino-1-butanol (98%), di-*tert*-butyl dicarbonate (Boc₂O, >98%), propargyl bromide (80 wt% in toluene), 3-amino-1,2-propanediol (1-aminoglycerol, 97%), Pd/C 10%, NaOMe in MeOH 25 wt%, NaN₃ (>99.5%), CuSO₄ (>99%), sodium ascorbate (>98%), Amberlyst® A21 free base, trifluoroacetic acid (TFA, 99%), Concanavalin A from *Canavalia ensiformis* (Type VI), *N,N*-diisopropylethylamine (DIPEA, >99%), chloroform-*d* (CDCl₃, 99.8% atom % D), acetone-*d*₆ (99.9% atom % D), D₂O (99.9 atom % D) and DMSO-*d*₆ (99.9 atom % D), fetal bovine serum (FBS), Dulbecco modified Eagles medium (DMEM), penicillin-streptomycin (containing 10.000 units penicillin, 10 mg streptomycin mL⁻¹), resazurin sodium salt (BioReagent), phosphate buffered saline (PBS, pH 7.4), Trypsin-EDTA solution (sterile filtered, BioReagent), 4,6-diamidino-2-phenylindole dihydrochloride (DAPI, 98%), hydrocortisone (#H0888) and ascorbic acid were purchased from Sigma-Aldrich. EBM-2 was purchased from Lonza. Collagen I rat tail was purchased from Enzo Life Sciences. CD lipid concentrate (#11905-031), Hanks' Balanced Salt Solution (HBSS) and HEPES (#15630080) were purchased from Gibco/Thermo. Alkyne-PEG4-Amine was purchased from Lumiprobe. Fluorescent label 5-(4,6-dichlorotriazinyl) aminofluorescein (DTAF), propidium iodide, Lyso Tracker™ Deep Red and SnakeSkin™ dialysis tubing (10K MWCO) were purchased from ThermoFisher

Scientific. Human FGF-basic (#100-10B) was purchased from Preprotech. Tetrahydrofuran (THF, >99%), ethyl acetate (EtOAc, >99%), dichloromethane (DCM, >99%) and methanol (>99%) were purchased from LPS B.V. *N,N*-dimethylformamide (DMF, >99.8%) was purchased from VWR. Chloroform (>99.8%) was purchased from Merck. Disposable PD-10 desalting columns were purchased from GE healthcare All chemicals were used without further purification unless stated otherwise. When stated as dry, solvents were treated with molecular sieves (3 Å) 24 h before usage and stored under nitrogen.

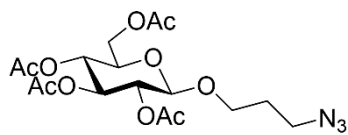
¹H-NMR (400 MHz), ¹³C-NMR (101 MHz) and ¹⁹F-NMR (376 MHz) spectra were recorded on a Bruker 400 spectrometer. Size exclusion chromatography (SEC) analysis was performed on a Waters e2695 Separations Module equipped with an Agilent PLgel 5 μm MIXED-D 300x7.5 mm column and Waters photodiode array detector (PDA 2998), fluorescence detector (FLR 2475) and refractive index detector (RI 2414). Chloroform and DMF with 50 mM LiCl were employed as eluent. Samples for SEC were filtered using a GE Healthcare Whatman SPARTAN 13/0.2 RC 0.2 μm syringe filter prior to measurements. UV-measurements were performed on a Shimadzu 1 UV-2401PC UV-VIS Recording Spectrophotometer. Mass spectra were obtained on a Advion Expression-L Compact Mass Spectrometer featured with either electrospray ionization (ESI) or Atmospheric Pressure Chemical Ionization (APCI).

Synthesis of glucose-ligands

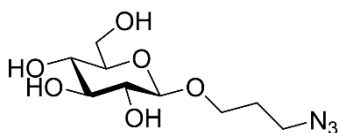
Compound 1. A 250 mL three neck flask was charged with 3-bromo-1-propanol (1.43 g, 10.2 mmol, 2.0 eq.) and brought under nitrogen. Dry dichloromethane (80 mL) was added, followed by the addition of β-D-glucose-pentaacetate (2.0 g, 5.1 mmol, 1.0 eq.). After dissolving, BF₃-Et₂O (46%, 1.8 mL, 14.6 mmol, 2.9 eq.) was added



dropwise by syringe in 5 min. The mixture was stirred overnight, after which the light yellow solution was diluted with 300 mL DCM, transferred to a 2 L beaker and sat. NaHCO₃ (400 mL) was slowly added over 30 min. The organic layer was separated, dried over MgSO₄, filtered and concentrated under reduced pressure. Flash chromatography (SiO₂, 20% → 50% EtOAc in heptane) yielded a colorless oil, which slowly solidified to an off-white waxy solid (yield: 1.25g, 52%). ¹H NMR (CDCl₃) δ 5.21 (td, *J* = 9.4, 1.9 Hz, 1H), 5.08 (td, *J* = 9.8, 2.0 Hz, 1H), 5.05 – 4.93 (m, 1H), 4.51 (dd, *J* = 8.0, 1.9 Hz, 1H), 4.34 – 4.21 (m, 1H), 4.21 – 4.06 (m, 1H), 4.00 (m, 1H), 3.70 (m, 2H), 3.52 – 3.39 (m, 2H), 2.28 – 1.93 (m, 14H). ¹³C NMR (CDCl₃) δ 170.69, 170.27, 169.42, 101.07, 72.74, 71.84, 71.28, 68.41, 67.36, 61.93, 32.26, 30.09, 20.75, 20.71, 20.62, 20.60. ESI- MS (positive detection mode): *m/z* [M+Na]⁺ = 492.3, calculated [M+Na]⁺ = 492.3



A 100 mL three neck flask was charged brominated tetra-acetylglucose intermediate (1.25 g, 2.6 mmol, 1 eq.), brought under nitrogen and dissolved in 13 mL dry DMF. NaN_3 (0.85g, 13.0 mmol, 5 eq.) was added and the mixture was stirred overnight at 50° C. DMF was removed under reduced pressure and the residue was dissolved in 50 mL ethyl acetate. The mixture was washed consecutively with 2 x 20 mL H_2O , 5 x 20 mL 10% NH_4Cl , 20 mL brine, dried over MgSO_4 , filtered and concentrated under reduced pressure to yield a colorless oil (yield: 1.23 g, 98%). ^1H NMR (CDCl_3) δ 5.21 (m, 1H), 5.08 (m, 1H), 4.99 (m, 1H), 4.50 (d, $J = 7.9$, 1H), 4.26 (m, 1H), 4.19 – 4.09 (m, 1H), 4.00 – 3.89 (m, 1H), 3.70 (m, 1H), 3.60 (m, 1H), 3.37 (m, 2H), 2.09 – 1.98 (m, 12H), 1.85 (m, 2H). ^{13}C NMR (CDCl_3) δ 170.67, 170.27, 169.41, 169.33, 100.84, 72.79, 71.85, 71.28, 68.40, 66.48, 61.92, 47.93, 28.97, 20.62 (m). ESI- MS (positive detection mode): m/z $[\text{M}+\text{Na}]^+ = 454.3$, calculated $[\text{M}+\text{Na}]^+ = 454.4$

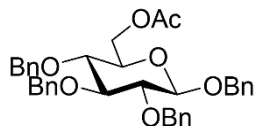


A 100 mL flask was charged with azido-tetra-acetylglucose intermediate (0.50 g, 1.16 mmol) and dissolved in 20 mL 20 mM NaOMe in MeOH and stirred overnight. The mixture was neutralized with Amberlyst 15 (H), filtered, rinsed with MeOH and concentrated under reduced pressure to a sticky colorless solid (yield: 0.3 g, quant). ^1H NMR (D_2O) δ 4.44 (d, $J = 8.0$ Hz, 1H), 3.98 (m, 1H), 3.90 (d, $J = 12.4$, 1H), 3.73 (m, 2H), 3.51 – 3.41 (m, 4H), 3.37 (d, $J = 9.6$ Hz, 1H), 3.29-3.19 (m, 1H), 1.90 (m, 2H). ^{13}C NMR (D_2O) δ 102.28, 75.91, 75.73, 73.11, 69.65, 67.32, 60.74, 48.85, 47.88, 28.23. APCI- MS (positive detection mode): m/z $[\text{M}+\text{H N}_2]^+ = 236.0$, calculated $[\text{M}+\text{H N}_2]^+ = 236.1$.

Compound 2. A 500 mL three neck flask was charged with D-glucose (9.0 g, 50.0 mmol, 1 eq) and brought under nitrogen. The glucose was dissolved in 250 mL of dry DMF, followed by the addition of NaH (60% in mineral oil, 6.0 g, 150 mmol, 3 eq). The suspension was stirred for 30 min and subsequently cooled on an ice bath. Benzyl bromide (29.9 g, 175 mmol, 3.5 eq.) was added by dropping funnel over 15 min, stirred for 10 min, after which the suspension was warmed to room temperature. After stirring for 150 min, a second portion of NaH (60% in mineral oil, 6.0 g, 150 mmol, 3 eq.) was added, The suspension was stirred for 30 min and subsequently cooled on an ice bath. Benzyl bromide (29.9 g, 175 mmol, 3.5 eq.) was added by dropping funnel over 15 min, stirred for 10 min, after which the suspension was warmed to room temperature. After stirring for 150 min, a third portion of NaH (60% in mineral oil, 4.0 g, 100 mmol, 2 eq.) was added, The suspension was stirred for 30 min and subsequently cooled on an ice bath. Benzyl bromide (17.1 g, 100 mmol, 2 eq.) was added by dropping funnel over 15 min, stirred for 10 min, after which the suspension was warmed to room temperature and stirred overnight.

MeOH (10 mL) was added slowly to quench the excess NaH and the suspension was concentrated under reduced pressure. The residue was dissolved in 250 mL DCM and washed consecutively with 3 × 125 mL water and 1 × 125 mL brine, dried over MgSO₄, filtered and concentrated to a dark red oil. Flash chromatography (SiO₂, 10% → 40% EtOAc in heptane) yielded a white powder (yield: 22.3 g, 71%). ¹H NMR (CDCl₃) δ 7.43 – 7.09 (m, 25H), 5.08 – 4.47 (m, 11H), 3.87 – 3.41 (m, 6H).

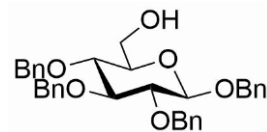
Compound 3. A 250 mL flask was charged with ZnCl₂ (5.48 g, 40.2 mmol, 5.2 eq.).



The ZnCl₂ was fused under high vacuum, 30 mL 5:1 Ac₂O / AcOH was added and the suspension was cooled on an ice bath. Compound **2** (4.88 g, 7.7 mmol, 1 eq.) was dissolved in 30 mL 5:1 Ac₂O / AcOH and added to the ZnCl₂ suspension over 30 min by dropping funnel. The ice bath was removed

and the suspension was stirred for 150 min at r.t. and then poured in 200 mL ice water. The white precipitate was filtered and washed with ice cold water and dried in the back of the fume hood. The product was used as such for the next step without further purification (yield: 4.1 g, 91%). ¹H NMR (400 MHz, CDCl₃) δ 7.46 – 7.12 (m, 20H), 5.07 – 4.43 (m, 9H), 4.37 (dd, *J* = 12.0, 2.1 Hz, 1H), 4.24 (dd, *J* = 11.9, 4.7 Hz, 1H), 3.78 – 3.59 (m, 1H), 3.61 – 3.35 (m, 3H), 2.06 (s, 3H).

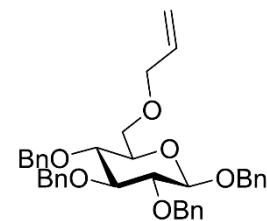
Compound 4. A 250 mL flask was charged with compound **3** (4.1g, 7.0 mmol, 1 eq.) and NaOMe in MeOH (60 mL, 25 mM) was added to give a white suspension and the mixture was stirred for 5 h,



becoming a yellow clear solution. The solution was poured in 240 mL ice water, filtered and washed with sat. NaHCO₃ and water to form a white sticky powder. Flash chromatography (SiO₂, 10% → 60% EtOAc in heptane) yielded a white powder

(yield: 2.1 g, 55%). ¹H NMR (400 MHz, Chloroform-d) δ 7.40 – 7.22 (m, 20H), 5.07 – 4.51 (m, 9H), 3.87 (dd, *J* = 11.9, 2.7 Hz, 1H), 3.80 – 3.61 (m, 2H), 3.57 (t, *J* = 9.3 Hz, 1H), 3.49 (t, *J* = 8.4 Hz, 1H), 3.37 (m, 1H).

Compound 5. A 50 mL three neck flask was charged with NaH (60% in mineral oil, 0.50 g, 12.5 mmol, 2 eq.) and brought under nitrogen,

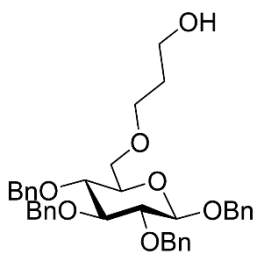


followed by the addition of 5 mL dry DMF, stirred for 15 min and subsequently cooled on an ice bath. Compound **4** (3.38 g, 6.3 mmol, 1 eq.) was brought under nitrogen, dissolved in 7 mL DMF and dropwise added to the NaH suspension by cannula. The ice bath was removed and the mixture was stirred for 60 min, after which it was cooled again on an ice

bath. Allyl bromide (1.13 g, 9.4 mmol, 1.5 eq.) was added dropwise and the mixture was stirred overnight at room temperature. The mixture was quenched with saturated NH₄Cl solution (80 mL), extracted with EtOAc (125 mL) and the organic

layer was washed consecutively 3 × 30 mL saturated NH₄Cl solution, 40 mL H₂O, 20 mL brine, dried over MgSO₄, filtered and concentrated under reduced pressure to yield a white solid (yield: 3.55 g, 98%). ¹H NMR (CDCl₃) δ 7.40 – 7.21 (m, 20H), 5.92 (ddd, *J* = 11.7, 10.4, 5.2 Hz, 1H), 5.29 (dq, *J* = 17.3, 1.7 Hz, 1H), 5.18 (dq, *J* = 10.4, 1.5 Hz, 1H), 5.05 – 4.58 (m, 8H), 4.50 (d, *J* = 7.8 Hz, 1H), 4.05 (ddt, *J* = 11.2, 5.6, 1.5 Hz, 2H), 3.82 – 3.36 (m, 6H).

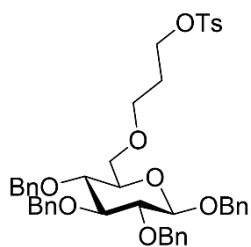
Compound 6. A 250 mL three neck flask was charged with compound **5** (3.2 g, 5.5



mmol, 1 eq.), brought under nitrogen and dry THF (40 mL) was added. was added to form a suspension and the mixture was stirred for 45 min, followed by the addition of BF₃·Et₂O (2.8 g, 19.8 mmol, 3.6 eq.). The cloudy mixture was stirred overnight, placed on an ice bath and H₂O (3.5 mL) was slowly added, followed by the addition of 4M NaOH solution (14 mL) and 30% H₂O₂ in water (10.6 mL). The mixture was stirred 60 min on the ice bath, then the ice bath was removed and

the mixture was stirred for another 2 h and subsequently transferred to a separatory funnel. The water layer was extracted with EtOAc (1 × 175 mL and 1 × 50 mL). The combined organic layers were washed with 3 × 100 mL water and 1 × 25 mL brine, dried over MgSO₄, filtered and concentrated under reduced pressure to a dark oil. Flash chromatography (SiO₂, 10% → 60% EtOAc in heptane) yielded a white powder (yield: 2.2 g, 66%). ¹H NMR (CDCl₃) δ 7.41 – 7.23 (m, 20H), 5.07 – 4.42 (m, 9H), 3.93 – 3.40 (m, 10H), 2.43 (t, *J* = 5.7 Hz, 1H), 1.84 (d, *J* = 6.7 Hz, 2H). Compound **3** (0.6 g, yield: 20%) was isolated as well.

Compound 7. A 100 mL three neck flask was charged with compound **6** (0.60 g, 1.0

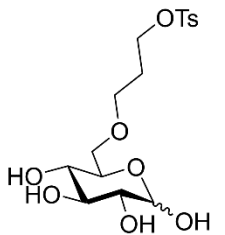


mmol, 1 eq.), brought under nitrogen and dissolved in dry DCM (20 mL). was added, followed by pyridine (566 μL, 7.0 mmol, 7 eq.) and the mixture was stirred overnight. Saturated NH₄Cl solution (6 mL) was added, stirred for 2 h and the mixture was brought into a separatory funnel. The organic layer was washed consecutively with 3 × 5 mL 1M HCl, 1 × 5 mL 5% NaHCO₃, 1 × 5mL brine, dried over MgSO₄, filtered and concentrated under reduced pressure. Flash

chromatography (SiO₂, 5% → 40% EtOAc in heptane) yielded a white powder (yield: 0.48 g, 66%). ¹H NMR (CDCl₃) δ 7.75 (d, *J* = 8.3 Hz, 2H), 7.51 – 7.19 (m, 22H), 5.04 – 4.40 (m, 9H), 4.14 (t, *J* = 6.3 Hz, 2H), 3.73 – 3.31 (m, 8H), 2.38 (s, 3H), 1.92 (td, *J* = 6.2, 3.0 Hz, 2H).

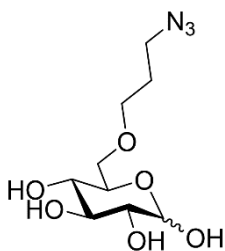
Compound 8. A 100 mL flask was charged with compound **7** (0.47 g, 0.63 mmol), 12 mL MeOH and 4 mL EtOAc. The solution was purged with nitrogen for 15 min, followed by addition 100 mg Pd/C 10 wt%. The flask was placed in an autoclave and filled with 8 bar H₂ and stirred overnight. Next, the solution was purged with nitrogen for 15 min and filtered over Celite S, rinsed with MeOH and concentrated to yield a transparent solid (yield: 0.25 g, 100%).

¹H NMR (D₂O) δ 7.85 (d, *J* = 8.0 Hz, 2H), 7.51 (d, *J* = 8.1 Hz, 2H), 5.16 (d, *J* = 3.7 Hz, 1H, H1-α), 4.56 (d, *J* = 7.9 Hz, 1H, H1-β), 4.21 (t, *J* = 6.3 Hz, 2H), 3.86 – 3.18 (m, 8H), 2.46 (s, 3H), 1.90 (m, 2H).

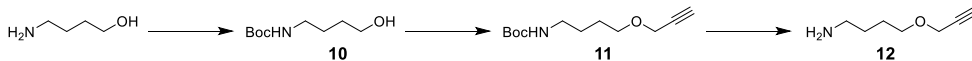


Compound 9. A 100 mL three neck flask was charged with compound **8** (0.25 g, 0.63 mmol, 1 eq.), brought under nitrogen and 12 mL dry DMF was added. NaN₃ (0.13 g, 1.9 mmol, 3 eq.) was added and the suspension was stirred overnight at 60° C. The excess NaN₃ was quenched by the addition of ethyl-4-bromobutyrate (0.27 mL, 1.9 mmol, 3 eq.) and the solution was stirred overnight. The solvent was removed under reduced pressure to yield a white powder, which was redissolved in 25 mL water. The water layer was washed with 3 × 10 mL diethyl ether and lyophilized to yield a sticky white powder. Flash chromatography (SiO₂, 10% MeOH in DCM) yielded a white powder (yield: 0.12 g, 72%).

¹H NMR (D₂O) δ 5.12 (d, *J* = 3.7 Hz, 1H, H1-α), 4.53 (d, *J* = 7.8 Hz, 1H, H1-β), 3.89 – 3.06 (m, 10H), 1.79 (q, *J* = 6.4 Hz, 2H). ¹³C NMR (D₂O) δ 95.9, 92.0, 75.6, 74.7, 74.0, 72.7, 71.4, 70.2, 69.8, 69.5, 69.3, 68.4, 68.3, 48.1, 27.9. ESI- MS (negative detection mode): *m/z* [M-H]⁻ = 262.1, calculated [M-H]⁻ = 262.1



Synthesis of alkyne-linker



Compound 10. A 250 mL three neck flask was charged with 4-amino-1-butanol (5.3g, 59 mmol, 1 eq.) and dry DCM (70 mL) and cooled down on an ice bath. Boc₂O was dissolved in DCM (40 mL) and added dropwise over 30 min. Triethylamine (7.2g, 71 mmol, 1.2 eq.) was added and the solution was slowly warmed to r.t. and stirred overnight. The solution was concentrated under reduced pressure to a yellow oil and used as such without additional purification (yield: 11.0 g, 98%). ¹H NMR (CDCl₃) δ 3.67 (m, 2H), 3.14 (m, 2H), 1.57 (m, 4H), 1.44 (s, 9H).

Compound 11. A 250 mL three neck flask was charged with compound **10** (2.2 g, 11.7 mmol, 1 eq.), brought under nitrogen and 30 mL dry THF and 30 mL dry DMF were added. The solution was cooled on an ice bath, NaH (60% in mineral oil, 1.1 g,

28.2 mmol, 2.4 eq.) was added and the suspension was stirred for 2h. Propargyl bromide (80 wt% in toluene, 2.6 g, 17.6 mmol, 1.5 eq.) was diluted in dry THF (10 mL), added slowly by dropping funnel and the mixture was stirred at r.t. overnight. The mixture was quenched with 75 mL H₂O, the organic solvents were removed under reduced pressure and the water layer was extracted with diethyl ether (4 × 50 mL). The combined organic layers were washed with 10 wt% NH₄Cl (5 × 50 mL), brine (1 × 50 mL brine), dried over MgSO₄, filtered and concentrated under reduced pressure to a brown oil. Flash chromatography (SiO₂, 30% EtOAc in heptane) yielded a yellow oil (yield: 0.3 g, 11%). ¹H NMR (400 MHz, CDCl₃) δ 4.57 (s, 1H), 4.13 (d, *J* = 2.4 Hz, 2H), 3.53 (t, *J* = 6.1 Hz, 2H), 3.14 (d, *J* = 6.5 Hz, 2H), 2.42 (t, *J* = 2.4 Hz, 1H), 1.82 – 1.55 (m, 4H), 1.44 (s, 9H).

Compound 12. A 100 mL three neck flask was charged with compound **11** (0.3 g, 1.3 mmol, 1 eq.) was brought under argon, dissolved in 14 mL dry DCM and cooled on an ice bath. TFA was added (4 mL) and the solution was warmed up to r.t. and stirred overnight. Saturated NaHCO₃ (15 mL) was added and the water layer was extracted with diethyl ether (15 mL) and ethyl acetate (15 mL). The combined organic layers were washed with brine (1 × 15 mL), dried over MgSO₄, filtered and concentrated under reduced pressure. The orange oil was dissolved in DCM (10 mL), Amberlyst A21 was added (6.4 mL, 8.3 mmol amines, 10 eq.), stirred for 60 min, filtered and concentrated under reduced pressure to a yellow oil (0.12 g, 72% yield). ¹H NMR (CDCl₃) δ 4.16 (d, *J* = 2.3 Hz, 2H), 3.58 (td, *J* = 6.8 Hz, 2H), 3.01 (t, *J* = 6.8 Hz, 2H), 2.47 (t, *J* = 2.3 Hz, 1H), 1.87 – 1.69 (m, 4H).

Alkyne functionalized SCNPs

The range of SCNPs with increasing alkyne density was made from the same batch **PFP-SCNPs**. The actual amounts per sample are listed in Table S5.1. Conversion was not quantitative and was therefore titrated towards the desired conversion. For example, for the 18% substituted SCNPs (**SCNP-18**), 60 mg of **PFP-SCNPs** (0.21 mmol PFP, 1 eq.) was dissolved in 6 mL dry THF under nitrogen atmosphere. Triethylamine was added 116 μL, 0.83 mmol, 4 eq.), followed by 1-amino-3-butyne (10.0 mg, 0.145 mmol, 0.7 eq.) from a 66 mg/mL stock solution in dry THF. The solution was stirred for 72h at 45° C. Conversion was determined by ¹⁹F NMR analysis, followed by the addition of 3-amino-1,2,-propanediol (566 mg, 6.2 mmol, 30 eq., 10 wt% solution in DMF) to endcap the remaining reactive PFP-groups. After stirring overnight at room temperature, the mixture was dialyzed against 1 wt% NaCl for 24 hours, followed by another 48 hours against demineralized water. The clear solutions were lyophilized to yield a white powder (40 mg, 98% yield).

Dual-reactive single-chain polymer nanoparticles for orthogonal functionalization through active ester and click chemistry

Table S5.1. Overview of equivalents, conversion and final incorporation ratio of 1-amino-3-butyne.

	Eq.	Conversion	# alkyne-moieties
SCNP-9	0.28	9%	19
SCNP-18	0.7	18%	38
SCNP-32	1.5	32%	68
SCNP-49	3.25	49%	104

Copper(I)-catalyzed Azide-Alkyne Cycloaddition (CuAAC)

The CuAAC click reaction was performed in a mixture of DMF and H₂O. For example, for the 18% alkyne-substituted SCNPs (**SCNP-18-1**) with 1-azido-aminoglucose (compound **1**), 18 mg SCNP-18 (0.024 mmol alkynes, 1 eq.) was dissolved in 2 mL DMF under argon atmosphere. DIPEA (43 μ L, 0.24 mmol, 10 eq.), CuSO₄ (12.4 mg, 0.048 mmol, 2 eq., from 50 mg/mL stock solution in H₂O), sodium ascorbate (49.1 mg, 0.24 mmol, 10 eq., from a 100 mg/mL stock solution in H₂O) and azido-glucose (compound **1**) (19.6 mg, 0.072 mmol, 3 eq., from a 19 mg/mL stock solution in DMF) were added and the mixture was stirred for 72h under argon atmosphere, followed by dialysis against 1 wt% NaCl for 24 hours, followed by another 48 hours against demineralized water. The clear solutions were lyophilized to yield a white powder (20 mg, 94% yield).

Table S5.2. Overview of molecular weight and number of glucose ligands of **Glyco-SCNPs** and **SCNP-0**.

	Molecular weight (kDa)	# glucose-moieties
SCNP-0	39.8	0
SCNP-9 (C1 and C6)	42.7	19
SCNP-18 (C1 and C6)	48.8	38
SCNP-32 (C1 and C6)	55.5	68
SCNP-49 (C1 and C6)	66.6	104

Concanavalin A precipitation assay

Concanavalin A (Con A) was dissolved in HEPES Buffer pH 7.4 (140 mM NaCl, 20 mM HEPES, 1.0 mM MgCl₂, 2.5 mM KCl, 1.8 mM CaCl₂ and 1 mM MnCl₂) to reach a 60 mM concentration (assuming tetramers of 104 kDa). **Glyco-SCNPs** were dissolved in the buffer to reach 17 μM concentrations. Equal volumes (150 μL) of SCNP-solution and Con A were thoroughly mixed and incubated for 20h at r.t at 500 rpm. The samples were centrifuged (15 min x 7000 rpm) and the supernatant was carefully removed. The pellets were washed with 200 μL cold buffer, followed by centrifugation (15 min x 7000 rpm). The supernatant was carefully removed and the washing step was repeated. The pellets were dissolved in 600 μL 100 mM methyl α-D-mannopyranoside to help dissolving the aggregates, incubated for 2h at r.t at 1400 rpm, diluted with 500 μL buffer and the UV-absorbance was measured at 285 nm (λ_{max}). Measurements are the average of 3 experiments with 2 scans performed for each data point.

Fluorescent labelling

Glyco-SCNPs (between 7-9 mg) were dissolved in 2 mL of 0.1 M carbonate-bicarbonate buffer (pH 9.7). 5-DTAF (0.02 eq. to SCNPs, 10 mg/mL stock solution in dry DMSO) was added and the solutions were stirred under ambient conditions overnight, after which they were purified by elution with water from a PD10 column and subsequently lyophilized to yield yellow powders (90% yield).

Cytotoxicity of SCNPs on HeLa cells

HeLa cells were seeded in 100 μL medium at 10.000 cells per well in 96 well plates and incubated at 37 °C in humidified 5% CO₂-containing atmosphere overnight. Sample solutions of SCNPs were prepared with concentrations of 1, 3, 6 and 9 μM. The medium was aspirated from the cells and the SCNPs were added in the sample solutions in 100 μL and 100 μL medium was added to reference cells. The cells were incubated for 24 h with the SCNPs, then the medium was aspirated and a resazurin assay solution (44 μM) was added in fresh medium to the cells. The fluorescence intensity was measured by an Enspire plate reader at excitation and emission wavelength of 560/590 nm.

Cellular uptake of SCNPs in HeLa cells by flow cytometry

HeLa cells were seeded at 30.000 cells per well in 300 μL medium in 24 well plates and incubated overnight. SCNP sample solutions were prepared at 3 μM and incubated with the cells for 3, 6 and 24 h. Then, the cells were harvested with trypsin and resuspended in PBS. For the flow cytometry measurement PI staining was added to the sample solutions, to detect dead cells. The flow cytometry

measurements were performed on a BD Bioscience FACS Aria II with excitation and emission filter of 488-530/30 and 630-660/30 nm.

Statistical analysis

Statistical analysis for flow cytometry data was performed utilizing SPSS 22, via One-way analysis of variance (ANOVA) and Tukey post hoc analysis. Classifications of the differences were noted as following: ($p < 0.05$), very significant ($p < 0.01$) and extremely significant ($p < 0.001$).

Confocal microscopy of SCNP uptake in HeLa cells

In 100 μ L medium HeLa cells were seeded at 10,000 cells per well in 96 well plate and incubated overnight. The SCNPs were incubated with the HeLa cells at 3 μ M for 3 h. Afterwards, the cells were washed with PBS and incubated with lysosome staining for 20 min before fixation using 4% PFA. Then DAPI staining was used to stain the cell nuclei. The cells were analyzed using a Nikon confocal microscope A1, equipped with the following laser wavelengths: 375, 488 and 561 nm.

5.5 Supplementary information

Characterization compound 9

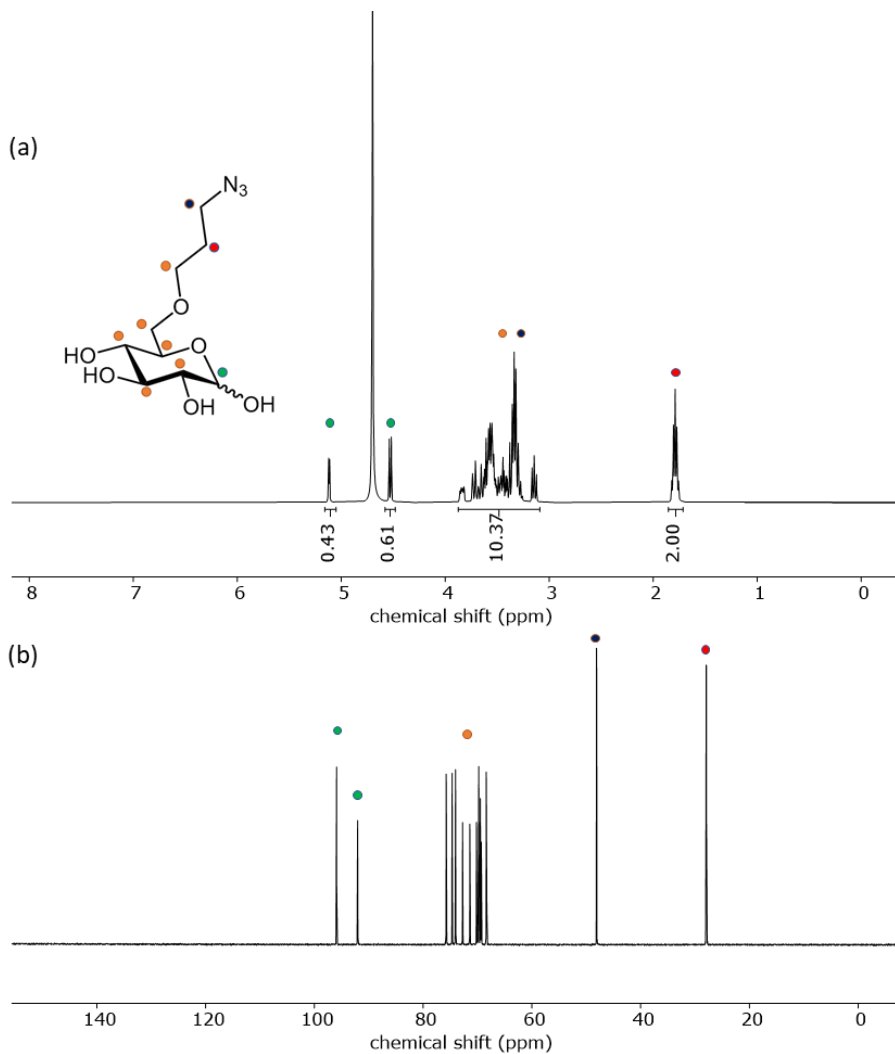


Figure S5.1. (a) ^1H NMR and (b) ^{13}C NMR spectra of compound **9** in D_2O .

Dual-reactive single-chain polymer nanoparticles for orthogonal functionalization through active ester and click chemistry

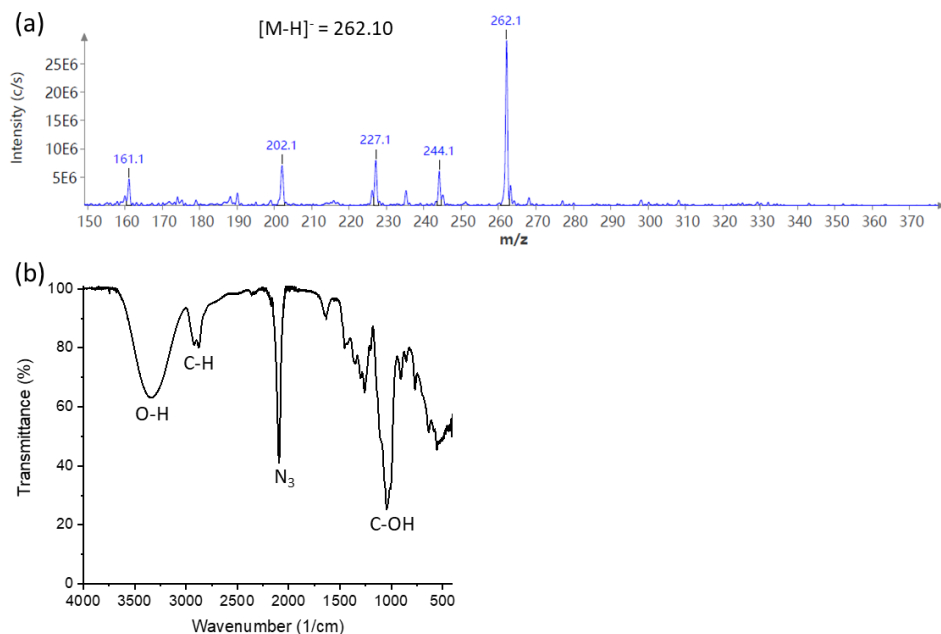


Figure S5.2. (a) Mass spectrum in negative ionization mode and (b) FTIR spectrum of compound **9**.

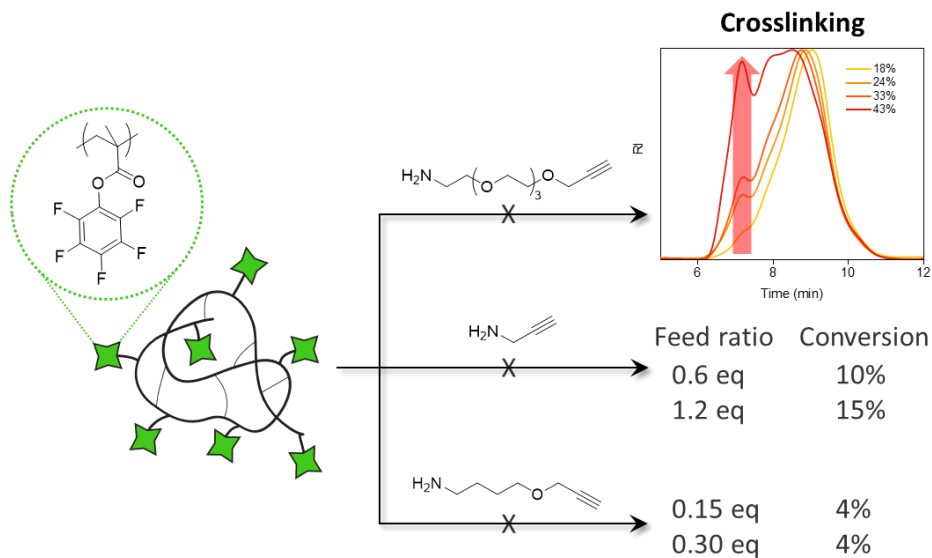


Figure S5.3. Conjugation strategies with amino-alkynes on **PFP-SCNPs** that did not yield satisfactory results.

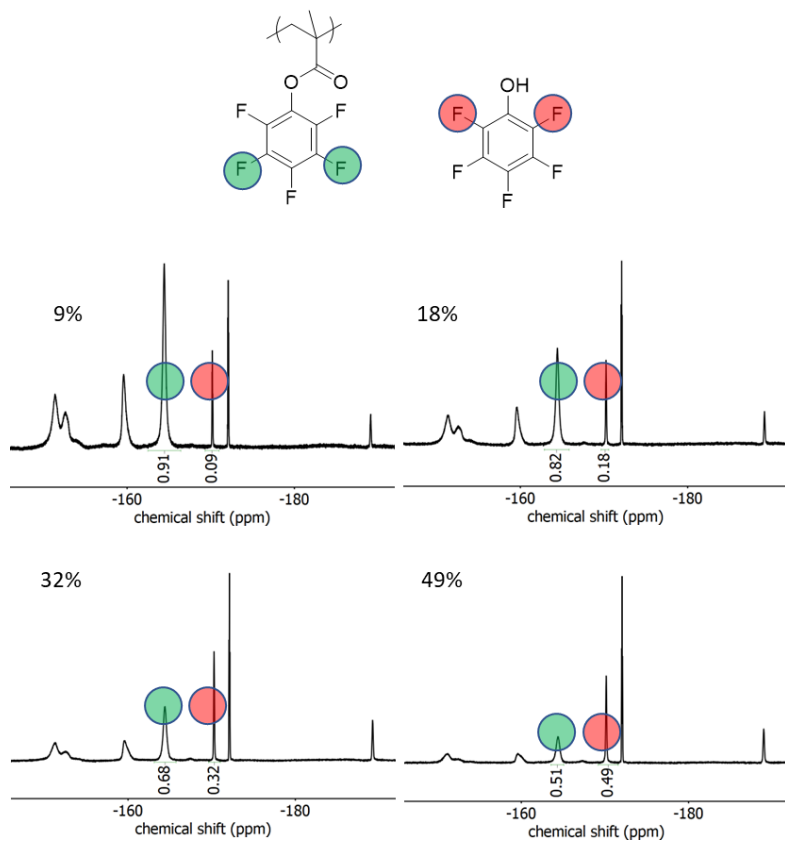


Figure S5.4. Conversion of active PFP-esters quantified by ^{19}F NMR-spectroscopy.

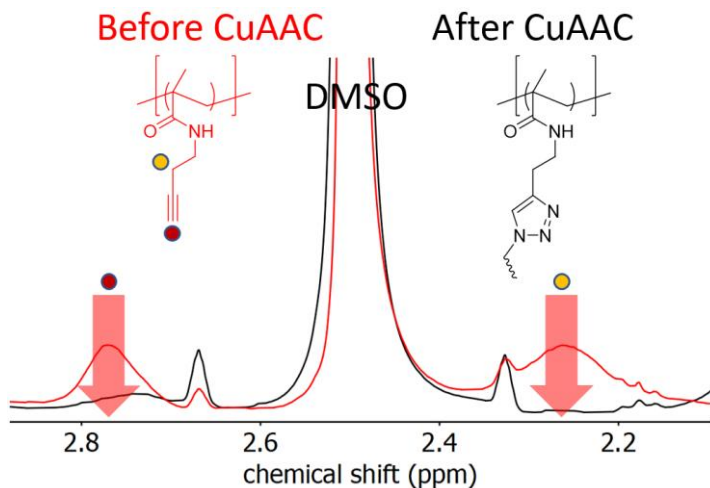


Figure S5.5. Comparison between SCNP with 49% 1-amino-3-butyne, before and after CuAAC-reaction, indicating disappearance of the triple bond.

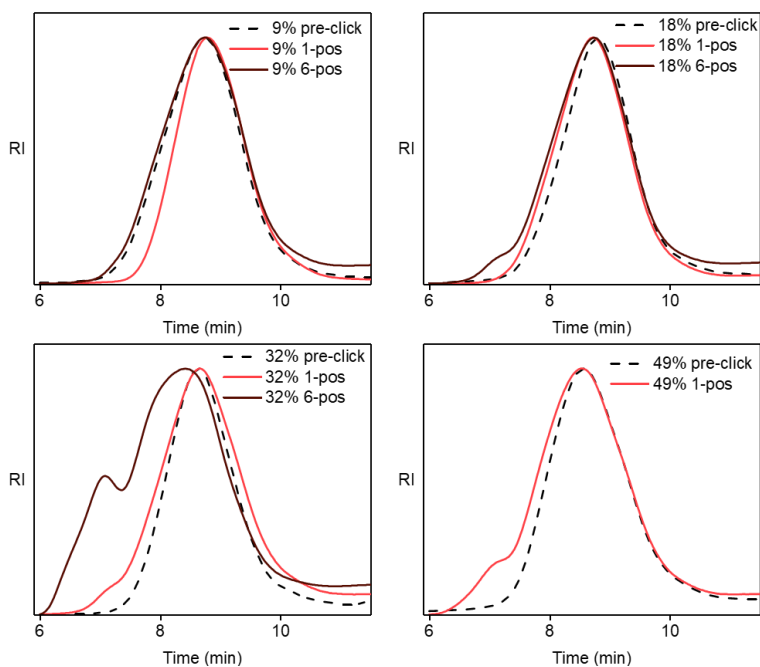


Figure S5.6. SEC-traces comparing butyne-functionalized SCNPs with the subsequent glucose-clicked SCNPs. **SCNP-C6-49** was omitted from analysis since it was not adequately soluble for SEC analysis.

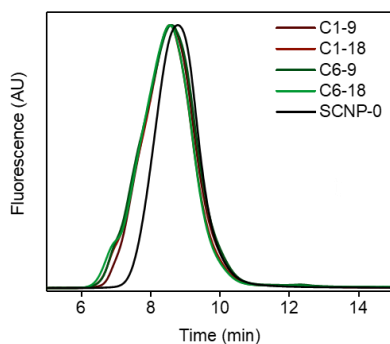


Figure S5.7. SEC-traces of fluorescent glyco-SCNPs, excitation at 492 nm, emission at 516 nm, indicating no free dye present.

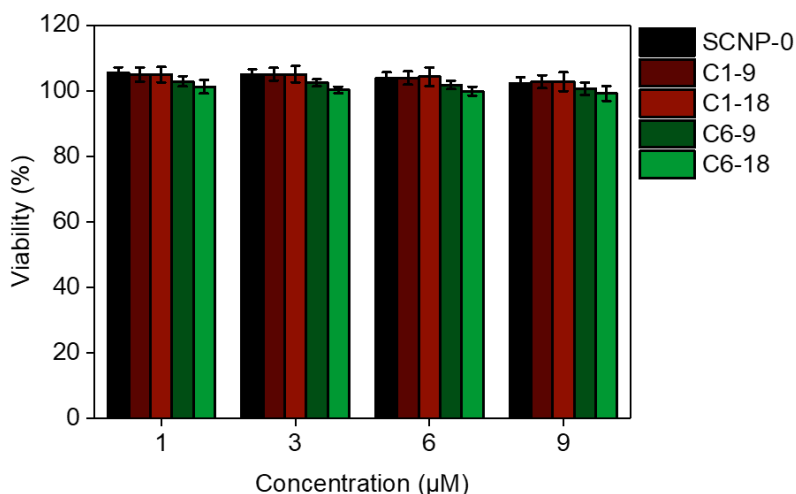


Figure S5.8. Resazurin assay on HeLa cells for different concentrations after 24 h incubation.

5.6 References

- Zielinska, A.; Carreiro, F.; Oliveira, A. M.; Neves, A.; Pires, B.; Venkatesh, D. N.; Durazzo, A.; Lucarini, M.; Eder, P.; Silva, A. M.; Santini, A.; Souto, E. B., Polymeric Nanoparticles: Production, Characterization, Toxicology and Ecotoxicology. *Molecules* **2020**, *25* (16).
- Crucho, C. I. C.; Barros, M. T., Polymeric nanoparticles: A study on the preparation variables and characterization methods. *Mater Sci Eng C Mater Biol Appl* **2017**, *80*, 771-784.
- Farokhzad, O. C.; Langer, R., Impact of Nanotechnology on Drug Delivery. *ACS Nano* **2009**, *3* (1), 16-20.
- Ribovski, L.; Hamelmann, N. M.; Paulusse, J. M. J., Polymeric Nanoparticles Properties and Brain Delivery. *Pharmaceutics* **2021**, *13* (12).
- Elsabagy, M.; Wooley, K. L., Design of polymeric nanoparticles for biomedical delivery applications. *Chem Soc Rev* **2012**, *41* (7), 2545-61.

6. Gagliardi, A.; Giuliano, E.; Venkateswararao, E.; Fresta, M.; Bulotta, S.; Awasthi, V.; Cosco, D., Biodegradable Polymeric Nanoparticles for Drug Delivery to Solid Tumors. *Front Pharmacol* **2021**, *12*, 601626.
7. Ong, S. Y.; Zhang, C.; Dong, X.; Yao, S. Q., Recent Advances in Polymeric Nanoparticles for Enhanced Fluorescence and Photoacoustic Imaging. *Angew Chem Int Ed Engl* **2021**, *60* (33), 17797-17809.
8. Sarcan, E. T.; Silindir-Gunay, M.; Ozer, A. Y., Theranostic polymeric nanoparticles for NIR imaging and photodynamic therapy. *Int J Pharm* **2018**, *551* (1-2), 329-338.
9. Spirescu, V. A.; Chircov, C.; Grumezescu, A. M.; Andronescu, E., Polymeric Nanoparticles for Antimicrobial Therapies: An Up-To-Date Overview. *Polymers (Basel)* **2021**, *13* (5).
10. Lam, S. J.; Wong, E. H. H.; Boyer, C.; Qiao, G. G., Antimicrobial polymeric nanoparticles. *Progress in Polymer Science* **2018**, *76*, 40-64.
11. Tian, X.; Ding, J.; Zhang, B.; Qiu, F.; Zhuang, X.; Chen, Y., Recent Advances in RAFT Polymerization: Novel Initiation Mechanisms and Optoelectronic Applications. *Polymers (Basel)* **2018**, *10* (3).
12. Truong, N. P.; Jones, G. R.; Bradford, K. G. E.; Konkolewicz, D.; Anastasaki, A., A comparison of RAFT and ATRP methods for controlled radical polymerization. *Nature Reviews Chemistry* **2021**, *5* (12), 859-869.
13. Gonçalves, S. d. Á.; Vieira, R. P., Current status of ATRP-based materials for gene therapy. *Reactive and Functional Polymers* **2020**, *147*.
14. Chen, Y.; Abdellatif, M. M.; Nomura, K., Olefin metathesis polymerization: Some recent developments in the precise polymerizations for synthesis of advanced materials (by ROMP, ADMET). *Tetrahedron* **2018**, *74* (6), 619-643.
15. Kubo, T.; Easterling, C. P.; Olson, R. A.; Sumerlin, B. S., Synthesis of multifunctional homopolymers via sequential post-polymerization reactions. *Polymer Chemistry* **2018**, *9* (37), 4605-4610.
16. Shahrokhinia, A.; Biswas, P.; Reuther, J. F., Orthogonal synthesis and modification of polymer materials. *Journal of Polymer Science* **2021**, *59* (16), 1748-1786.
17. Campos, L. M.; Killops, K. L.; Sakai, R.; Paulusse, J. M. J.; Damiron, D.; Drockenmuller, E.; Messmore, B. W.; Hawker, C. J., Development of Thermal and Photochemical Strategies for Thiol-Ene Click Polymer Functionalization. *Macromolecules* **2008**, *41* (19), 7063-7070.
18. Muzammil, Ezzah M.; Khan, A.; Stuparu, M. C., Post-polymerization modification reactions of poly(glycidyl methacrylate)s. *RSC Advances* **2017**, *7* (88), 55874-55884.
19. Hall, D. J.; Van Den Berghe, H. M.; Dove, A. P., Synthesis and post-polymerization modification of maleimide-containing polymers by 'thiol-ene' click and Diels-Alder chemistries. *Polymer International* **2011**, *60* (8), 1149-1157.
20. Eberhardt, M.; Mruk, R.; Zentel, R.; Théato, P., Synthesis of pentafluorophenyl(meth)acrylate polymers: New precursor polymers for the synthesis of multifunctional materials. *European Polymer Journal* **2005**, *41* (7), 1569-1575.
21. Das, A.; Theato, P., Activated Ester Containing Polymers: Opportunities and Challenges for the Design of Functional Macromolecules. *Chem Rev* **2016**, *116* (3), 1434-95.
22. Kakuchi, R.; Theato, P., Post-Polymerization Modifications via Active Esters. In *Functional Polymers by Post-Polymerization Modification*, 2012; pp 45-64.
23. Tornøe, C. W.; Christensen, C.; Meldal, M., Peptidotriazoles on Solid Phase: [1,2,3]-Triazoles by Regiospecific Copper(I)-Catalyzed 1,3-Dipolar Cycloadditions of Terminal Alkynes to Azides. *The Journal of Organic Chemistry* **2002**, *67* (9), 3057-3064.
24. Rostovtsev, V. V.; Green, L. G.; Fokin, V. V.; Sharpless, K. B., A Stepwise Huisgen Cycloaddition Process: Copper(I)-Catalyzed Regioselective "Ligation" of Azides and Terminal Alkynes. *Angewandte Chemie International Edition* **2002**, *41* (14), 2596-2599.
25. Arseneault, M.; Wafer, C.; Morin, J. F., Recent advances in click chemistry applied to dendrimer synthesis. *Molecules* **2015**, *20* (5), 9263-94.

26. Tunca, U., Orthogonal multiple click reactions in synthetic polymer chemistry. *Journal of Polymer Science Part A: Polymer Chemistry* **2014**, *52* (22), 3147-3165.
27. Dai, Y.; Chen, X.; Zhang, X., Recent advances in stimuli-responsive polymeric micelles via click chemistry. *Polymer Chemistry* **2019**, *10* (1), 34-44.
28. Lutz, J. F.; Zarafshani, Z., Efficient construction of therapeutics, bioconjugates, biomaterials and bioactive surfaces using azide-alkyne "click" chemistry. *Adv Drug Deliv Rev* **2008**, *60* (9), 958-70.
29. Hui, Y.; Yi, X.; Hou, F.; Wibowo, D.; Zhang, F.; Zhao, D.; Gao, H.; Zhao, C. X., Role of Nanoparticle Mechanical Properties in Cancer Drug Delivery. *ACS Nano* **2019**, *13* (7), 7410-7424.
30. Albanese, A.; Tang, P. S.; Chan, W. C., The effect of nanoparticle size, shape, and surface chemistry on biological systems. *Annu Rev Biomed Eng* **2012**, *14*, 1-16.
31. Dolai, J.; Mandal, K.; Jana, N. R., Nanoparticle Size Effects in Biomedical Applications. *ACS Applied Nano Materials* **2021**, *4* (7), 6471-6496.
32. Hoshyar, N.; Gray, S.; Han, H.; Bao, G., The effect of nanoparticle size on in vivo pharmacokinetics and cellular interaction. *Nanomedicine* **2016**, *11* (6), 673-692.
33. Bai, Y.; Hang, X.; Wu, P.; Feng, X.; Hwang, K.; Lee, J. M.; Phang, X. Y.; Lu, Y.; Zimmerman, S. C., Chemical Control over Cellular Uptake of Organic Nanoparticles by Fine Tuning Surface Functional Groups. *ACS Nano* **2015**, *9* (10), 10.
34. Alqarni, M. A. M.; Waldron, C.; Yilmaz, G.; Becer, C. R., Synthetic Routes to Single Chain Polymer Nanoparticles (SCNPs): Current Status and Perspectives. *Macromol Rapid Commun* **2021**, e2100035.
35. Chen, J.; Garcia, E. S.; Zimmerman, S. C., Intramolecularly Cross-Linked Polymers: From Structure to Function with Applications as Artificial Antibodies and Artificial Enzymes. *Acc Chem Res* **2020**, *53* (6), 1244-1256.
36. Kroger, A. P. P.; Paulusse, J. M. J., Single-chain polymer nanoparticles in controlled drug delivery and targeted imaging. *J Control Release* **2018**, *286*, 326-347.
37. Kroger, A. P. P.; Hamelmann, N. M.; Juan, A.; Lindhoud, S.; Paulusse, J. M. J., Biocompatible Single-Chain Polymer Nanoparticles for Drug Delivery-A Dual Approach. *ACS Appl Mater Interfaces* **2018**, *10* (37), 30946-30951.
38. Gracia, R.; Marradi, M.; Salerno, G.; Pérez-Nicado, R.; Pérez-San Vicente, A.; Dupin, D.; Rodriguez, J.; Loinaz, I.; Chiodo, F.; Nativi, C., Biocompatible single-chain polymer nanoparticles loaded with an antigen mimetic as potential anticancer vaccine. *ACS Macro Letters* **2018**, *7* (2), 196-200.
39. Chen, X.; Li, R.; Wong, S. H. D.; Wei, K.; Cui, M.; Chen, H.; Jiang, Y.; Yang, B.; Zhao, P.; Xu, J.; Chen, H.; Yin, C.; Lin, S.; Lee, W. Y.; Jing, Y.; Li, Z.; Yang, Z.; Xia, J.; Chen, G.; Li, G.; Bian, L., Conformational manipulation of scale-up prepared single-chain polymeric nanogels for multiscale regulation of cells. *Nat Commun* **2019**, *10* (1), 2705.
40. Chen, J.; Li, K.; Shon, J. S. L.; Zimmerman, S. C., Single-Chain Nanoparticle Delivers a Partner Enzyme for Concurrent and Tandem Catalysis in Cells. *J Am Chem Soc* **2020**, *142* (10), 4565-4569.
41. Knofel, N. D.; Rothfuss, H.; Willenbacher, J.; Barner-Kowollik, C.; Roesky, P. W., Platinum(II)-Crosslinked Single-Chain Nanoparticles: An Approach towards Recyclable Homogeneous Catalysts. *Angew Chem Int Ed Engl* **2017**, *56* (18), 4950-4954.
42. Zeng, R.; Chen, L.; Yan, Q., CO₂-Folded Single-Chain Nanoparticles as Recyclable, Improved Carboxylase Mimics. *Angew Chem Int Ed Engl* **2020**.
43. Perez-Baena, I.; Loinaz, I.; Padro, D.; Garcia, I.; Grande, H. J.; Odriozola, I., Single-chain polyacrylic nanoparticles with multiple Gd(III) centres as potential MRI contrast agents. *Journal of Materials Chemistry* **2010**, *20* (33).
44. Benito, A. B.; Aiertza, M. K.; Marradi, M.; Gil-Iceta, L.; Shekhter Zahavi, T.; Szczupak, B.; Jimenez-Gonzalez, M.; Reese, T.; Scanziani, E.; Passoni, L.; Matteoli, M.; De Maglie, M.; Orenstein, A.; Oron-Herman, M.; Kostenich, G.; Buzhansky, L.; Gazit, E.; Grande, H. J.; Gomez-Vallejo, V.; Llop, J.; Loinaz, I., Functional Single-Chain Polymer Nanoparticles: Targeting and Imaging Pancreatic Tumors in Vivo. *Biomacromolecules* **2016**, *17* (10), 3213-3221.

45. Gracia, R.; Marradi, M.; Cossío, U.; Benito, A.; Pérez-San Vicente, A.; Gómez-Vallejo, V.; Grande, H. J.; Llop, J.; Loinaz, I., Synthesis and functionalization of dextran-based single-chain nanoparticles in aqueous media. *Journal of Materials Chemistry B* **2017**, *5* (6), 1143-1147.
46. Kröger, A. P. P.; Paats, J. D.; Boonen, R. J. E. A.; Hamelmann, N. M.; Paulusse, J. M. J., Pentafluorophenyl-based single-chain polymer nanoparticles as a versatile platform towards protein mimicry. *Polymer Chemistry* **2020**, *11* (37), 6056-6065.
47. Hamelmann, N. M.; Paats, J. D.; Paulusse, J. M. J., Cytosolic Delivery of Single-Chain Polymer Nanoparticles. *ACS Macro Lett* **2021**, *10* (11), 1443-1449.
48. Ladmiraal, V.; Melia, E.; Haddleton, D. M., Synthetic glycopolymers: an overview. *European Polymer Journal* **2004**, *40* (3), 431-449.
49. Ghazarian, H.; Idoni, B.; Oppenheimer, S. B., A glycobiology review: carbohydrates, lectins and implications in cancer therapeutics. *Acta Histochem* **2011**, *113* (3), 236-47.
50. Thorens, B.; Mueckler, M., Glucose transporters in the 21st Century. *Am J Physiol Endocrinol Metab* **2010**, *298* (2), E141-5.
51. Zhao, T.; Terracciano, R.; Becker, J.; Monaco, A.; Yilmaz, G.; Becer, C. R., Hierarchy of Complex Glycomacromolecules: From Controlled Topologies to Biomedical Applications. *Biomacromolecules* **2022**, *23* (3), 543-575.
52. Kang, B.; Opatz, T.; Landfester, K.; Wurm, F. R., Carbohydrate nanocarriers in biomedical applications: functionalization and construction. *Chem Soc Rev* **2015**, *44* (22), 8301-25.
53. Lundquist, J. J.; Toone, E. J., The Cluster Glycoside Effect. *Chemical Reviews* **2002**, *102* (2), 555-578.
54. Tjandra, K. C.; Thordarson, P., Multivalency in Drug Delivery-When Is It Too Much of a Good Thing? *Bioconjug Chem* **2019**, *30* (3), 503-514.
55. Haqqani, A. S.; Thom, G.; Burrell, M.; Delaney, C. E.; Brunette, E.; Baumann, E.; Sodja, C.; Jezierski, A.; Webster, C.; Stanimirovic, D. B., Intracellular sorting and transcytosis of the rat transferrin receptor antibody OX26 across the blood-brain barrier in vitro is dependent on its binding affinity. *J Neurochem* **2018**, *146* (6), 735-752.
56. Barnett, J. E. G.; Holman, G. D.; Munday, K. A., Structural requirements for binding to the sugar-transport system of the human erythrocyte. *The Biochemical journal* **1973**, *131* 2, 211-21.
57. Barnett, J. E.; Holman, G. D.; Chalkley, R. A.; Munday, K. A., Evidence for two asymmetric conformational states in the human erythrocyte sugar-transport system. *Biochem J* **1975**, *145* (3), 417-29.
58. Barnett, J. E.; Holman, G. D.; Munday, K. A., An explanation of the asymmetric binding of sugars to the human erythrocyte sugar-transport systems. *Biochem J* **1973**, *135* (3), 539-41.
59. Kumar, P.; Shustov, G.; Liang, H.; Khlebnikov, V.; Zheng, W.; Yang, X. H.; Cheeseman, C.; Wiebe, L. I., Design, synthesis, and preliminary biological evaluation of 6-O-glucose-azomycin adducts for diagnosis and therapy of hypoxic tumors. *J Med Chem* **2012**, *55* (13), 6033-46.
60. Xie, F.; Yao, N.; Qin, Y.; Zhang, Q.; Chen, H.; Yuan, M.; Tang, J.; Li, X.; Fan, W.; Zhang, Q.; Wu, Y.; Hai, L.; He, Q., Investigation of glucose-modified liposomes using polyethylene glycols with different chain lengths as the linkers for brain targeting. *Int J Nanomedicine* **2012**, *7*, 163-75.
61. Xie, J.; Gonzalez-Carter, D.; Tockary, T. A.; Nakamura, N.; Xue, Y.; Nakakido, M.; Akiba, H.; Dirisala, A.; Liu, X.; Toh, K.; Yang, T.; Wang, Z.; Fukushima, S.; Li, J.; Quader, S.; Tsumoto, K.; Yokota, T.; Anraku, Y.; Kataoka, K., Dual-Sensitive Nanomicelles Enhancing Systemic Delivery of Therapeutically Active Antibodies Specifically into the Brain. *ACS Nano* **2020**, *14* (6), 6729-6742.
62. Sun, P.; He, Y.; Lin, M.; Zhao, Y.; Ding, Y.; Chen, G.; Jiang, M., Glyco-regioisomerism Effect on Lectin-Binding and Cell-Uptake Pathway of Glycopolymer-Containing Nanoparticles. *ACS Macro Letters* **2013**, *3* (1), 96-101.
63. Patra, M.; Awuah, S. G.; Lippard, S. J., Chemical Approach to Positional Isomers of Glucose-Platinum Conjugates Reveals Specific Cancer Targeting through Glucose-Transporter-Mediated Uptake in Vitro and in Vivo. *J Am Chem Soc* **2016**, *138* (38), 12541-51.

64. Patra, M.; Johnstone, T. C.; Suntharalingam, K.; Lippard, S. J., A Potent Glucose-Platinum Conjugate Exploits Glucose Transporters and Preferentially Accumulates in Cancer Cells. *Angew Chem Int Ed Engl* **2016**, *55* (7), 2550-4.
65. Lu, W.; Navidpour, L.; Taylor, S. D., An expedient synthesis of benzyl 2,3,4-tri-O-benzyl-beta-D-glucopyranoside and benzyl 2,3,4-tri-O-benzyl-beta-D-mannopyranoside. *Carbohydr Res* **2005**, *340* (6), 1213-7.
66. Sindhu, K. S.; Anilkumar, G., Recent advances and applications of Glaser coupling employing greener protocols. *RSC Adv* **2014**, *4* (53), 27867-27887.
67. Schorgenhumer, J.; Waser, M., Transition metal-free coupling of terminal alkynes and hypervalent iodine-based alkyne-transfer reagents to access unsymmetrical 1,3-diynes. *Org Biomol Chem* **2018**, *16* (41), 7561-7563.
68. Kaldhi, D.; Vodnala, N.; Gujjarappa, R.; Kabi, A. K.; Nayak, S.; Malakar, C. C., Transition-metal-free variant of Glaser- and Cadiot-Chodkiewicz-type Coupling: Benign access to diverse 1,3-diynes and related molecules. *Tetrahedron Letters* **2020**, *61* (16).
69. Akhtar, R.; Zahoor, A. F., Transition metal catalyzed Glaser and Glaser-Hay coupling reactions: Scope, classical/green methodologies and synthetic applications. *Synthetic Communications* **2020**, *50* (22), 3337-3368.
70. Liu, P. Y.; Jiang, N.; Zhang, J.; Wei, X.; Lin, H. H.; Yu, X. Q., The oxidative damage of plasmid DNA by ascorbic acid derivatives in vitro: the first research on the relationship between the structure of ascorbic acid and the oxidative damage of plasmid DNA. *Chem Biodivers* **2006**, *3* (9), 958-66.
71. Hong, V.; Udit, A. K.; Evans, R. A.; Finn, M. G., Electrochemically protected copper(I)-catalyzed azide-alkyne cycloaddition. *ChemBiochem* **2008**, *9* (9), 1481-6.
72. Alemon-Medina, R.; Brena-Valle, M.; Munoz-Sanchez, J. L.; Gracia-Mora, M. I.; Ruiz-Azuara, L., Induction of oxidative damage by copper-based antineoplastic drugs (Casiopinas). *Cancer Chemother Pharmacol* **2007**, *60* (2), 219-28.
73. Ekholm, F. S.; Pynnonen, H.; Vilkmann, A.; Koponen, J.; Helin, J.; Satomaa, T., Synthesis of the copper chelator TGTA and evaluation of its ability to protect biomolecules from copper induced degradation during copper catalyzed azide-alkyne bioconjugation reactions. *Org Biomol Chem* **2016**, *14* (3), 849-52.
74. Ladmiral, V.; Mantovani, G.; Clarkson, G. J.; Cauet, S.; Irwin, J. L.; Haddleton, D. M., Synthesis of Neoglycopolymers by a Combination of "Click Chemistry" and Living Radical Polymerization. *J Am Chem Soc* **2006**, *128* (14), 4823-4830.
75. Cavada, B. S.; Osterne, V. J. S.; Lossio, C. F.; Pinto-Junior, V. R.; Oliveira, M. V.; Silva, M. T. L.; Leal, R. B.; Nascimento, K. S., One century of ConA and 40 years of ConBr research: A structural review. *Int J Biol Macromol* **2019**, *134*, 901-911.
76. Derewenda, Z.; Yariv, J.; Helliwell, J. R.; Kalb, A. J.; Dodson, E. J.; Papiz, M. Z.; Wan, T.; Campbell, J., The structure of the saccharide-binding site of concanavalin A. *EMBO J* **1989**, *8* (8), 2189-93.
77. Kroger, A. P. P.; Komil, M. I.; Hamelmann, N. M.; Juan, A.; Stenzel, M. H.; Paulusse, J. M. J., Glucose Single-Chain Polymer Nanoparticles for Cellular Targeting. *ACS Macro Lett* **2019**, *8* (1), 95-101.
78. Venturelli, L.; Nappini, S.; Bulfoni, M.; Gianfranceschi, G.; Dal Zilio, S.; Coceano, G.; Del Ben, F.; Turetta, M.; Scoles, G.; Vaccari, L.; Cesselli, D.; Cojoc, D., Glucose is a key driver for GLUT1-mediated nanoparticles internalization in breast cancer cells. *Sci Rep* **2016**, *6*, 21629.
79. Yi, Y.; Kim, H. J.; Zheng, M.; Mi, P.; Naito, M.; Kim, B. S.; Min, H. S.; Hayashi, K.; Perche, F.; Toh, K.; Liu, X.; Mochida, Y.; Kinoh, H.; Cabral, H.; Miyata, K.; Kataoka, K., Glucose-linked sub-50-nm unimer polyion complex-assembled gold nanoparticles for targeted siRNA delivery to glucose transporter 1-overexpressing breast cancer stem-like cells. *J Control Release* **2019**, *295*, 268-277.
80. Xu, S.; Zhang, P.; Heing-Becker, I.; Zhang, J.; Tang, P.; Bej, R.; Bhatia, S.; Zhong, Y.; Haag, R., Dual tumor- and subcellular-targeted photodynamic therapy using glucose-functionalized MoS₂ nanoflakes for multidrug-resistant tumor ablation. *Biomaterials* **2022**, *290*, 121844.

81. Morais, M.; Machado, V.; Dias, F.; Figueiredo, P.; Palmeira, C.; Martins, G.; Fernandes, R.; Malheiro, A. R.; Mikkonen, K. S.; Teixeira, A. L.; Medeiros, R., Glucose-Functionalized Silver Nanoparticles as a Potential New Therapy Agent Targeting Hormone-Resistant Prostate Cancer cells. *Int J Nanomedicine* **2022**, *17*, 4321-4337.
82. Rodriguez-Enriquez, S.; Marin-Hernandez, A.; Gallardo-Perez, J. C.; Moreno-Sanchez, R., Kinetics of transport and phosphorylation of glucose in cancer cells. *J Cell Physiol* **2009**, *221* (3), 552-9.

Chapter 6

Future outlook and additional findings

The PFP-SCNP platform developed and described in this thesis provides ample opportunities for rapid and precise functionalization and evaluation of SCNPs in biomedical applications. However, to further explore the possibilities, a wider range of functional SCNPs is needed. In this final chapter, we provide an outlook on methods for upscaling SCNP synthesis and for water-compatible functionalization strategies, to ensure a wider range of functional SCNPs can be synthesized and rapidly tested in *in vitro* assays. Furthermore, we performed an initial biodistribution study with the charged particle set from Chapter 2 to better understand the particle behavior *in vivo*. Despite their small size, SCNPs were still observed in the mice after 24 h. An increase in liver, kidney and spleen accumulation was found upon increasing the surface charge density on the particles. Overall, the results prompt the exploration of a wider range of functional SCNPs, which can be tested in *in vivo* models.

6.1 Introduction

In this thesis, we studied the influence of the surface functionalization of single-chain polymeric nanoparticles (SCNPs) on their cellular interactions. To this end, we developed pentafluorophenyl (PFP)-equipped SCNPs for facile incorporation of functional ligands, as described in Chapter 2. We modified the surface with protonatable tertiary amines to create a range of differently charged SCNPs (ranging from negative to positive zeta potential). We used this set to study cellular uptake in endothelial cells (Chapter 2), where we found that the surface charge dictated the intracellular fate of the SCNPs, as well as for transcytosis in a blood-brain barrier (BBB) model (Chapter 3). All SCNPs showed very high transcytosis rates, slightly diminishing upon increasing the surface charge. We further explored the potential for controlled drug delivery by attaching an anti-cancer drug atovaquone in Chapter 4 to achieve intracellular delivery to cancer cells. Selective killing of cancer cells was achieved, only upon cytosolic delivery of the nanoparticles. In Chapter 5, SCNPs were functionalized with increasing amounts of alkyne groups, which were subsequently used to conjugate different azidopropyl-glucose moieties through Cu(I)-catalyzed Alkyne-Azide Cycloaddition (CuAAC) click chemistry. The new series allowed us to study the positional dependence of glucose-ligands on uptake in cancer (HeLa) cells.

Combination of active ester and click chemistry already dramatically expands the range of ligands that can be incorporated and studied. Sets of SCNPs were developed by gradually increasing ligand density, which enabled systematic investigation into structure-activity relationships. Furthermore, the incorporation of functional ligands could be (indirectly) monitored and quantified in real-time through ^{19}F NMR spectroscopy. By drawing inspiration from the field of polymer chemistry, we transferred the concept of post-polymerization modification to modifying nanoparticles post-formation, thereby leaving the colloidal structure largely intact.¹ Starting from the same parent PFP-decorated precursors, we ensured decoupling of the particle's colloidal features from the functionalization step, which allowed for studying the relationship between functional surface groups and biological activity. Employing post-formation modification of NPs is a big step forward compared to traditional synthetic methods, where every functional NP requires a new specific precursor and likewise requires careful characterization to ensure the nanostructures are still comparable.²⁻⁸ However, to be able to optimize ligand density towards a specific application, more resolution in surface modification is needed. As seen for example in Chapter 2, increasing the ligand density already dramatically influences the biological interactions, where a 15% increase (from 30 to 45% tertiary amines) led to completely different cellular interactions. Therefore, the step-size in functionalization degree needs to be decreased to better discern changes. When looking at the synthesis of liposomes and solid lipid nanoparticles, vast libraries of

vesicles with gradually changing components can be created by simply adjusting the feed ratio of lipids and additives, although arguably, the nanostructures may still vary considerably in size, composition and morphology.⁹⁻¹⁴

Transferring this combinatorial approach to the synthesis of functional SCNPs, would require several improvements on the current synthesis routes. First, scale up of the reactive precursor-SCNP is required, to accommodate for the synthesis of a wide range of functional nanoparticles and to have sufficient material available for larger biological studies, for example *in vivo*. Additionally, this would allow studying the macroscopic properties of SCNPs. Compared to non-crosslinked linear polymer chains, SCNPs have shown interesting bulk properties, caused by the changed dynamics between the polymer chains.¹⁵⁻¹⁶ Yet, widespread application is hampered by the lack of sufficient available material. Secondly, rapid functionalization and subsequent reaction validation methods are required, which, in view of future biomedical applications, require the process to be carried out in water. Although active PFP-ester chemistry is versatile and mild, it does require organic solvents. To conduct large-scale structure-activity relationship studies, a water-compatible drop-in functionalization method is needed, as well as straightforward purification methods. Lastly, efficient screening of biological activity is needed, with many techniques having been developed by the pharmaceutical industry.¹⁷⁻¹⁸

6.2 Scale up of SCNP production

So far, production of SCNPs on 10-100 g scale has not yet been achieved. To prevent intermolecular crosslinking and gelation, generally ultra-dilute conditions are employed, but these conditions also impede scale up. Since the intramolecular chain collapse competes with the intermolecular crosslinking reaction, often concentrations as low as 20 mg per L (~0.002 wt%) are required,¹⁹ which means 500 L of solvent is needed to synthesize 10 g of SCNPs. For obvious reasons, this severely hampers commercialization and widespread macro-scale use of SCNPs. Recently, progress has been made by using flow chemistry for synthesis of SCNPs. Although a continuous process is synthetically convenient for large-scale production, still 20 L of solvent is required for the production of 10 g of SCNPs (~0.05 wt%).²⁰ Therefore, economically viable alternatives are required.

When turning to the PFP-SCNP crosslinking chemistry (the crosslinking concept which was initially explored by the Hawker group and adapted in Chapter 2 with thiol chemistry²¹), intramolecular crosslinking is performed under continuous addition of thiol-reactive polymer to a solution of bi-functional (di-acrylate) crosslinker (Figure 6.1). Because of the slow addition, the concentration of reactive polymers is kept at a minimum to prevent intermolecular reactions. Upon the first attachment of one side of the crosslinker to the polymer, the local concentration of reactive thiol-groups on the same backbone increases compared to thiols on different chains, favoring

intramolecular chain collapse. Previous work in our group showed that the majority of the free thiols had reacted within 30 minutes.²² After SCNP formation, the polymers do not participate in further crosslinking reactions and can be considered inert. Though, it should be noted that end-capping (with a large excess of monofunctional acrylate) still occurs, as evidenced by ¹H NMR spectroscopy. This indicates that there are still some reactive thiol-groups present, although presumably inaccessible for bulkier chemical moieties than the end-capping agent.

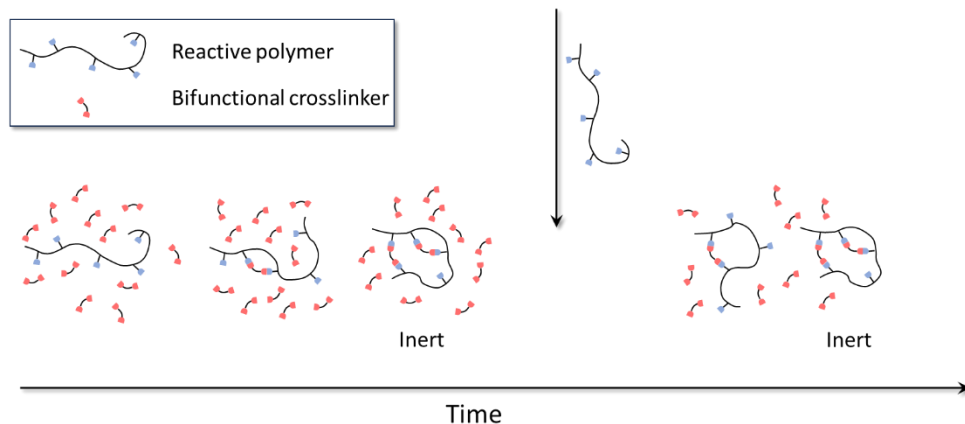


Figure 6.1. Schematic representation of intramolecular chain collapse using continuous addition of reactive polymer to a solution of bi-functional crosslinker. After crosslinking, the SCNPs are considered inert.

The SCNP's inertness is a huge advantage compared to attempting the simultaneous collapse of all polymer chains in one batch, which requires ultra-dilute conditions. However, in the current method, the total amount of crosslinker is already present in the solution at the start (see Figure 6.2a). When scaling up the reaction under these conditions, the ratio between crosslinker and added reactive polymer would therefore increase. Initial experiments showed that this leads predominantly to end-capping of the reactive polymers by one side of the di-acrylate crosslinker, because of the increased crosslinker concentration, especially in the beginning of the reaction. Therefore, the current process needs to be improved.

One method to circumvent the end-capping by the crosslinker is by controlled continuous addition of not only reactive polymer, but of reactive polymer and crosslinker to the same reaction mixture (Figure 6.2b). By careful controlling the flow, the composition of the reactive components in the reaction mixture can be kept within a specified range, allowing for the same ratio between crosslinker and reactive polymer throughout the entire reaction. Since the formed SCNPs are practically inert after crosslinking, the reaction concentration can therefore be dramatically increased, resulting in the synthesis of commercially interesting quantities of SCNPs.

If able to reach a 5 wt % reaction mixture, 100 mL of solvent would suffice to create 5 g of SCNPs. Since functionalization of 50 mg of SCNPs is more than enough for being able to perform characterization and biological assays, this amount would allow the creation of a library of 100 differently functionalized SCNPs from one batch (see 6.3 and 6.4 for methods to create such vast libraries). Furthermore, since the thiol-Michael addition is a very fast (click) reaction,²³ the chain collapse is swift and thus the rate of addition can be appropriately quick.

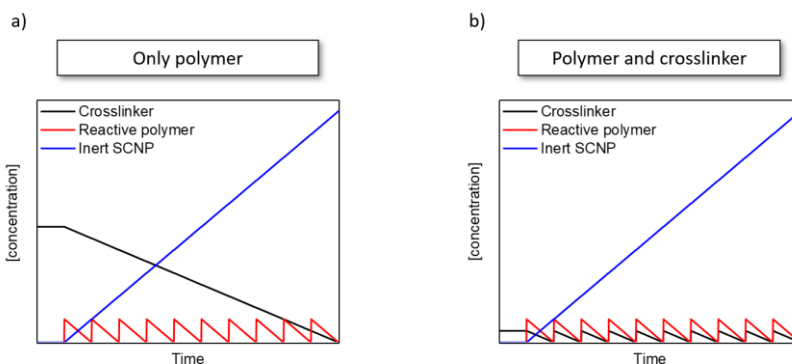


Figure 6.2. Concentration profiles of crosslinker, reactive thiol-polymer and formed inert SCNPs by continuous addition by a) only polymer and b) polymer and crosslinker.

6.3 Alternative functionalization strategies

Following the upscaling of the SCNPs, broader ranges of SCNPs with different surface functionality can be tested. A parent batch of reactive SCNPs could be functionalized and characterized by techniques from high throughput screening (HTS) to perform combinatorial chemistry. For example, the step-size for a specific parameter (e.g. surface charge, ligand density, drug loading) can be decreased, but also particles with combinations of different ligands can be developed, spanning a wider composition range. Such a combinatorial approach closely resembles the synthetic methods available for liposomes and other (solid) lipid nanoparticles, but with the benefit of keeping the colloidal structure constant and largely independent of the added surface ligands. Furthermore, characterization of self-assembled nanoparticles is generally done only by examining the morphology, whereas PFP-SCNP functionalization can be quantified by NMR spectroscopy, while the nanoparticle molecular weight is known. For rapid development of the library, water-soluble and oxygen-tolerant drop-in functionalization technology is needed, as well as a facile purification method. The current PFP-active ester system requires organic solvents and therefore a solvent switch from apolar to polar, and it releases persistent perfluorinated by-products, so a more polar and benign functionalization chemistry is desirable. Within the realm of active ester chemistry, there are several

water-soluble and/or less cytotoxic alternatives available (see Figure 6.3). Salicylic acid acrylate (SAA) has been employed for post-polymerization modification with primary and secondary amines.²⁴ Although the reaction kinetics are slower than for PFP-chemistry, full conversion could still be obtained within reasonable time periods. Cytotoxicity assays revealed substantially increased cell viability for SAA-derived polymers during post-polymerization functionalization as compared to PFP-polymers. Although less toxic, SAA is still poses limitations regarding water-solubility. An alternative option is the acrylate-version of the well-known sulfo-NHS (*N*-acryloxysulfosuccinimide, NASS).²⁵ NASS has been co-polymerized with different acrylates and successfully employed in the subsequent post-polymerization modification reactions. Although NHS is less hydrolytically stable than PFP,²⁶ the by-products are more innocuous and highly water-soluble. Another alternative is a sulfonated variant of PFP (2,3,5,6-tetrafluoro-4-sulfophenol, STFP). To the best of our knowledge, STFP has never been polymerized, but has been used for facile attachment of fluorophores to biomolecules.²⁷⁻²⁸ Even though post-formation modification would yield fluorinated by-products, quantification of conversion through ¹⁹F NMR is very convenient and straightforward. The choice for these alternative functionalization chemistries depends on the required scale and fidelity of the prospected final applications of the nanoparticles.

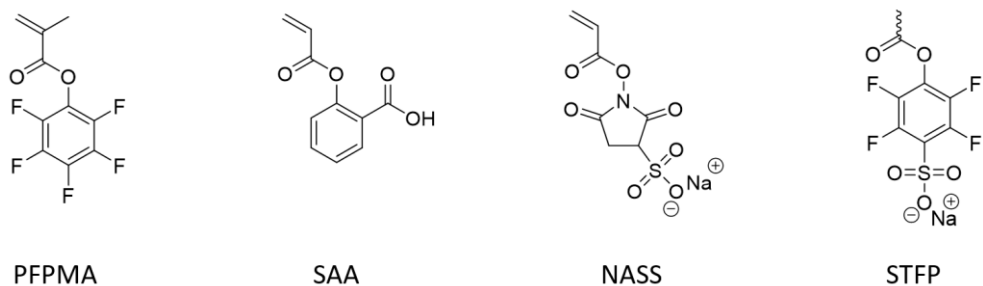


Figure 6.3. Alternative more benign and/or water-soluble activated esters for post-formation modification of SCNPs.

6.4 Combinatorial synthesis of libraries of SCNPs

Since SCNP functionalization is generally not quantitative when using more complex ligands (see Chapter 5), the incorporation of such ligands requires titration towards the desired degree of functionalization. Therefore, during functionalization, quick analysis is required. NMR spectroscopy has already proven to be a suitable method on multiple occasions, especially for fluorinated compounds. Furthermore, phenyl-moieties, as well as NHS-esters, both display well-resolved resonance signals in NMR spectroscopy, which allows for easy quantification of the incorporation of

functional groups.^{24, 29} Alternatively, the release of (sulfo-)NHS can be followed by HPLC to determine the degree of functionalization.³⁰ The information can be immediately used as a feedback to monitor and control the amount of incorporation (see Figure 6.4).

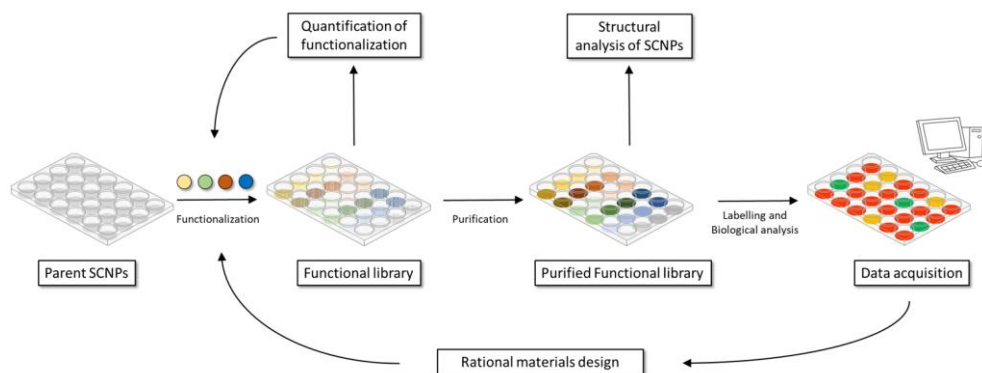


Figure 6.4. Flow scheme for rapid synthesis, characterization and screening of a library of functional SCNPs.

Since SCNPs are in the size range of proteins, purification can be easily performed by (disposable) size exclusion chromatography. This would separate the relatively large-sized functional SCNPs from the small molecule cleaved off by-products and allow for qualitative analysis of the degree of functionalization. Following an appropriate method of modification to be able to perform the subsequent analysis, such as fluorescent labelling or using DNA barcoding,³¹ the library can be investigated in quick biological assays and analysis, such as cytotoxicity, cellular uptake, antimicrobial activity, hydrophilicity or size.¹⁷ The acquired data set can subsequently be used for rational design of functional SCNPs, by finding optimum combinations of different surface ligands and gaining insights into structure-property relationships.³²

Employing active ester chemistry requires (primary) amine-terminated ligands, which restricts the flexibility in choice somewhat. In Chapter 5, we circumvented these limitations through a two-step functionalization: first alkyne (1-amino-3-butyne) groups were introduced at increasing density, following a CuAAC (Copper(I)-catalyzed Azide-Alkyne Cycloaddition) click conjugation to ligate azide-terminated glucose-moieties. However, the alkyne-decorated SCNPs were not water-soluble and attempts using PEGylated amino-alkynes resulted in large, insoluble agglomerates. As an alternative water-soluble azide-alkyne cycloaddition reagent, 7-membered rings containing a strained triple bond and a sulfoximine group have recently been developed.³³ These moieties showed improved reaction kinetics and lower log P values compared to the conventional strain-promoted click reagent

DBCO. However, whether conjugation of these moieties to SCNPs using active ester chemistry is feasible and whether the reactive groups are subsequently still accessible, remains to be explored.

6.5 In vivo studies

Although the potential of SCNPs has been demonstrated in *in vitro* assays on multiple occasions, in this thesis and by others, only scarce reports exist of SCNPs used *in vivo*.³⁴⁻³⁵ We therefore examined the pharmacokinetic properties of the particle set from Chapter 2, containing increasing amounts of tertiary amines, in a mouse model. To this end, the SCNPs were conjugated with a near-infrared Cy7 dye for fluorescent imaging. The mice were injected intravenously with equal concentrations of **SCNP-0**, **SCNP-15**, **SCNP-45**, **SCNP-60** or PBS and imaged after 30 min, 2 hours, 4 hours and 24 hours. **SCNP-30** was omitted, since it showed similar, but slightly diminished interactions in the *in vitro* assays as **SCNP-15**. Representative imaging of the mice is shown in Figure 6.5.

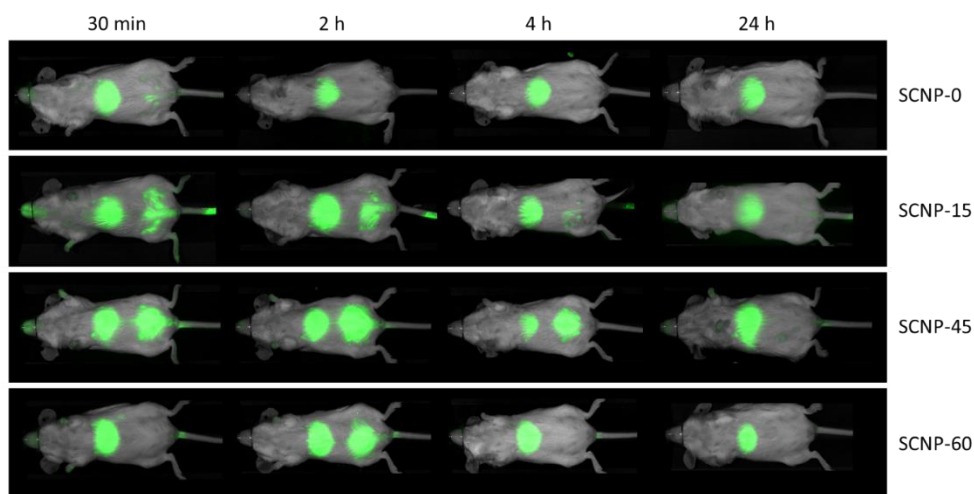


Figure 6.5. *In vivo* near-IR imaging of representative mice with the set of differently charged SCNPs from Chapter 2 at four different timepoints.

Visual inspection of the fluorescence images after 30 minutes already revealed strong accumulation in the liver, irrespective of the type of surface functionalization. After 24 h, the whole set of SCNPs is still present to certain extents in the liver. Accumulation in the bladder and kidneys is also observed, which indicates elimination of the SCNPs via the urine. After 24 h, the mice were sacrificed and the fluorescence intensity in the different organs was measured, corrected for the mass of the organ and intrinsic fluorescence of the injected SCNPs (Figure 6.6).

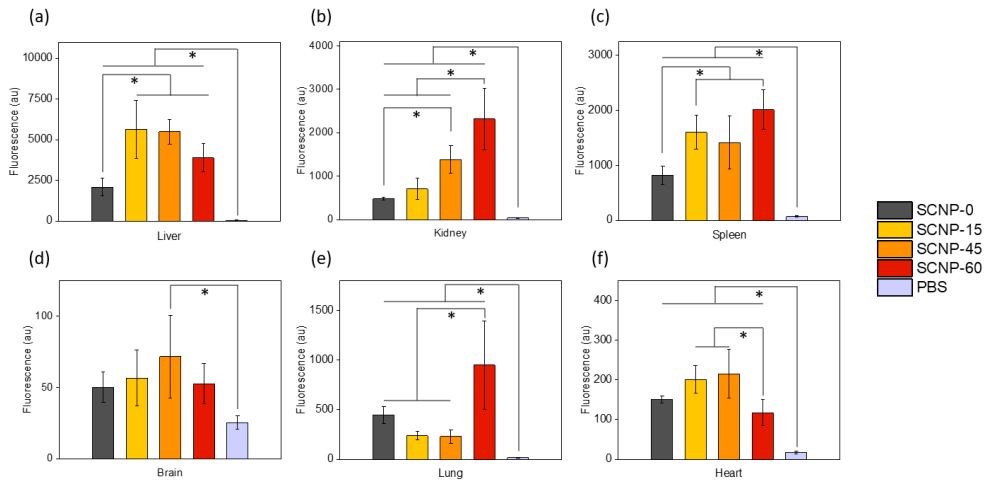


Figure 6.6. *Ex vivo* tissue distribution, $n = 4$ per type of SCNP (or PBS). Fluorescence intensity corrected for mass and intrinsic fluorescence. * indicates $p < 0.05$.

Increasing the surface charge leads to an increased fluorescent signal in the spleen and liver, organs of the reticuloendothelial system (RES), compared to fully amino-glycerol terminated **SCNP-0** (Figure 6.6a and c). Furthermore, the highest charged **SCNP-60** also shows the highest uptake in the lungs (Figure 6.6e). These results are in line with earlier *in vivo* studies with charged nanoparticles. Larger sized positively charged micelles and chitosan NPs both revealed increased uptake in the RES-organs upon increasing surface charge.³⁶⁻³ Similarly as can be seen for our SCNPs in Figure 6.6a and c, lowering the surface charge on ~40 nm block copolymer micelles resulted in lower accumulation in spleen and liver³⁸ High accumulation in RES-organs is indicative of opsonization. This is a result of the NPs attracting complement proteins, which renders them susceptible to phagocytosis. The amount of opsonization of NPs is dependent on the surface charge and hydrophobicity.³⁹ A small increase in brain uptake is observed for **SCNP-45** as compared to the PBS-control (Figure 6.6d). However, due to fluorescence quenching, scattering and signal saturation, the fluorescent imaging is at best semi-quantitative, and the results should be validated by different means, such as radiolabeling.⁴⁰⁻⁴¹

6.6 Conclusion

Scaling up the synthesis of SCNPs in combination with water-compatible functionalization chemistry will dramatically expand the library of functional SCNPs for screening in controlled biomedical applications. Furthermore, despite their small size being close to the renal excretion limit,⁴² the SCNPs are still present in the murine body after 24 h. Even though polyglycerol has been shown to display anti-fouling properties,⁴³⁻⁴⁴ high uptake in the RES-organs is still observed, possibly indicating the formation of complement proteins around the SCNPs. This prompts further research into the interactions of SCNPs with serum proteins, as well as the *in vivo* behavior of differently functionalized SCNPs. Overall, functional SCNPs provide ample opportunities for a plethora of biomedical applications, ranging from targeting cancer cells, to crossing the blood-brain barrier and imaging.

6.7 Acknowledgements

We acknowledge Dr. Ruchi Bansal, Ir. Richell Booiijink and Franck Assayag for their help with the animal experiments.

6.8 Materials and Methods

Tetrahydrofuran (THF, >99%) was purchased from LPS B.V. *N,N*-dimethylformamide (DMF, >99.8%) was purchased from VWR. Triethylamine (TEA, 99%), *N,N*-dimethylethylenediamine (DMEN, 95%), 3-amino-1,2-propanediol (1-aminoglycerol, 97%) and DMSO (anhydrous, 99.9%) were purchased from Sigma-Aldrich. Fluorescent label Cyanine7 (Cy7) amine was purchased from Lumiprobe. All chemicals were used without further purification unless stated otherwise. When stated as dry, solvents were treated with molecular sieves (3 Å) 24 h before usage and stored under nitrogen. Disposable PD-10 desalting columns were purchased from Sigma-Aldrich. ¹⁹F-NMR (376 MHz) spectra were recorded on a Bruker 400 spectrometer. Size exclusion chromatography (SEC) analysis was performed on a Waters e2695 Separations Module equipped with an Agilent PLgel 5 µm MIXED-D 300 × 7.5 mm column and Waters photodiode array detector (PDA 2998), fluorescence detector (FLR 2475) and refractive index detector (RI 2414). DMF with 50 mM LiCl was employed as eluent. Samples for SEC were filtered using a GE Healthcare Whatman SPARTAN 13/0.2 RC 0.2 µm syringe filter prior to measurements.

Synthesis of near-IR SCNPs with charge range

The range of differently positively charged was prepared from a single batch of **PFP-SCNPs**. As an example, for the 15% substituted SCNPs (**SCNP-15**), 40 mg of **PFP-SCNPs** (0.14 mmol PFP, 1 eq.) was dissolved in 3 mL dry THF under nitrogen atmosphere. Triethylamine was added (77 µL, 0.55 mmol, 4 eq.), followed by Cy7-

amine (1.5 mg, 0.002 mmol, 0.01 eq, from a 1.0 wt% stock solution in dry DMF) and the solution was stirred for 24 h at room temperature. *N,N*-dimethylethylenediamine (DMEN) (2.8 mg, 0.02 mmol, 0.15 eq, from a 5.0 wt% stock solution in dry THF) was added and the solution was stirred for 24 h at 45° C. Full conversion was confirmed by ¹⁹F NMR analysis, followed by the addition of 3-amino-1,2,-propanediol (340 mg, 3.7 mmol, 27 eq., 10 wt% solution in DMF) to endcap the remaining reactive PFP-groups. After stirring overnight at room temperature, the mixture was dialyzed against 1 wt% NaCl for 24 hours, followed by another 48 hours against demineralized water. The clear solutions were lyophilized to yield an off-white powder (22 mg, 77% yield). Further purification was performed by (repeated) elution(s) with water from a PD-10 column, until SEC analysis showed no remaining free dye left.

Animals and ethical approval

About 6- to 8-week-old C57BL/6 male mice weighing 18-20 g were obtained from Harlan. All the animal experiments in this study were performed in strict accordance with the guidelines and regulations for the Care and Use of Laboratory Animals, Utrecht University, The Netherlands and comply with the guidelines of ARRIVE and the National Institutes of Health. The animal experimental protocols were approved by the Institutional Animal Ethics Committee of the University of Twente, the Netherlands. Animals were housed in a standard animal housing facility under the conditions of constant temperature of (21 ± 2°C) and humidity (60 ± 5), a 12 h light/12 h dark cycles with ad libitum low-fluorescence diet. Animals were allowed to acclimatize for 2 weeks before the experiment.

In vivo and ex vivo fluorescence imaging of SCNP injected mice

The animals were injected with either PBS, SCNP-0, SCNP-15, SCNP-45 or SCNP-60 with 4 animals per group. Per mouse, 100 µL of a 0.2 mg/mL SCNP solution in PBS (or 100 µL PBS) was intravenously injected via the tail vein. The mice were imaged in the Cy7-mode and white light (body mode) after 30 min, 2 h, 4 h and 24 h using a LI-COR Pearl Trilogy (LI-COR Biosciences) animals imager. After that, the mice were sacrificed, and the organs were imaged. Images were processed using Image Studio Lite 5.2. The regions of interest (ROI's) were kept the same for all different animals and timepoints. For the *ex vivo* imaging, the fluorescence per organ was corrected for the fluorescence intensity of the injected SCNP and the mass of the organ. One-way analysis of variance (ANOVA), followed by Tukey's post hoc test to account for multiple comparisons, was used for data analysis using Origin 2017. P-values < 0.05 were considered as statistically significant.

6.9 References

1. Gruber, A.; Navarro, L.; Klinger, D., Reactive Precursor Particles as Synthetic Platform for the Generation of Functional Nanoparticles, Nanogels, and Microgels. *Advanced Materials Interfaces* **2019**, *7* (5).
2. Yi, Y.; Kim, H. J.; Zheng, M.; Mi, P.; Naito, M.; Kim, B. S.; Min, H. S.; Hayashi, K.; Perche, F.; Toh, K.; Liu, X.; Mochida, Y.; Kinoh, H.; Cabral, H.; Miyata, K.; Kataoka, K., Glucose-linked sub-50-nm unimer polyion complex-assembled gold nanoparticles for targeted siRNA delivery to glucose transporter 1-overexpressing breast cancer stem-like cells. *J Control Release* **2019**, *295*, 268-277.
3. Nam, J.; Kwon, S.; Yu, Y.-G.; Seo, H.-B.; Lee, J.-S.; Lee, W. B.; Kim, Y.; Seo, M., Folding of Sequence-Controlled Graft Copolymers to Subdomain-Defined Single-Chain Nanoparticles. *Macromolecules* **2021**, *54* (18), 8829-8838.
4. Liu, S.; Rong, J.; Liu, R.; Lindsey, J. S., Single-Fluorophore Single-Chain Nanoparticle Undergoes Fluorophore-Driven Assembly with Fluorescence Features Retained in Physiological Milieu. *ACS Applied Polymer Materials* **2021**, *3* (4), 1767-1776.
5. Elzes, M. R.; Mertens, I.; Sedlacek, O.; Verbraeken, B.; Doensen, A. C. A.; Mees, M. A.; Glassner, M.; Jana, S.; Paulusse, J. M. J.; Hoogenboom, R., Linear Poly(ethylenimine-propylenimine) Random Copolymers for Gene Delivery: From Polymer Synthesis to Efficient Transfection with High Serum Tolerance. *Biomacromolecules* **2022**, *23* (6), 2459-2470.
6. Andrade, B.; Knewstubb, S. N.; Harris, K.; Tucker, C. J.; Katz, J. S.; Zimmerman, S. C., Nonionic Surfactant Properties of Amphiphilic Hyperbranched Polyglycerols. *Langmuir* **2020**, *36* (34), 10103-10109.
7. Simon, J.; Wolf, T.; Klein, K.; Landfester, K.; Wurm, F. R.; Mailander, V., Hydrophilicity Regulates the Stealth Properties of Polyphosphoester-Coated Nanocarriers. *Angew Chem Int Ed Engl* **2018**, *57* (19), 5548-5553.
8. Matsumoto, M.; Terashima, T.; Matsumoto, K.; Takenaka, M.; Sawamoto, M., Compartmentalization Technologies via Self-Assembly and Cross-Linking of Amphiphilic Random Block Copolymers in Water. *J Am Chem Soc* **2017**, *139* (21), 7164-7167.
9. Huayameres, S. G.; Lokugamage, M. P.; Rab, R.; Da Silva Sanchez, A. J.; Kim, H.; Radmand, A.; Loughrey, D.; Lian, L.; Hou, Y.; Achyut, B. R.; Ehrhardt, A.; Hong, J. S.; Sago, C. D.; Paunovska, K.; Echeverri, E. S.; Vanover, D.; Santangelo, P. J.; Sorscher, E. J.; Dahlman, J. E., High-throughput screens identify a lipid nanoparticle that preferentially delivers mRNA to human tumors in vivo. *J Control Release* **2023**, *357*, 394-403.
10. Naidu, G. S.; Yong, S. B.; Ramishetti, S.; Rampado, R.; Sharma, P.; Ezra, A.; Goldsmith, M.; Hazan-Halevy, I.; Chatterjee, S.; Aitha, A.; Peer, D., A Combinatorial Library of Lipid Nanoparticles for Cell Type-Specific mRNA Delivery. *Adv Sci* **2023**, e2301929.
11. Feather, L. A. J.; Nadella, V.; Kastner, E.; Perrie, Y.; Hilton, A. C.; Devitt, A., Development of a rapid in vitro pre-screen for distinguishing effective liposome-adjuvant delivery systems. *Sci Rep* **2022**, *12* (1), 12448.
12. Akinc, A.; Zumbuehl, A.; Goldberg, M.; Leshchiner, E. S.; Busini, V.; Hossain, N.; Bacallado, S. A.; Nguyen, D. N.; Fuller, J.; Alvarez, R.; Borodovsky, A.; Borland, T.; Constien, R.; de Fougères, A.; Dorkin, J. R.; Narayanannair Jayaprakash, K.; Jayaraman, M.; John, M.; Kotliansky, V.; Manoharan, M.; Nechev, L.; Qin, J.; Racie, T.; Raitcheva, D.; Rajeev, K. G.; Sah, D. W.; Soutschek, J.; Toudjarska, I.; Vornlocher, H. P.; Zimmermann, T. S.; Langer, R.; Anderson, D. G., A combinatorial library of lipid-like materials for delivery of RNAi therapeutics. *Nat Biotechnol* **2008**, *26* (5), 561-9.
13. Zhao, Z.; Feng, Y.; Xiang, J.; Liu, J.; Piao, Y.; Shao, S.; Tang, J.; Zhou, Z.; Shen, Y., Screening of Zwitterionic Liposomes with Red Blood Cell-Hitchhiking and Tumor Cell-Active Transporting Capability for Efficient Tumor Entrance. *Advanced Functional Materials* **2023**, *33* (16).
14. Ng, C. Z.; Ann Matthews, A.; Sum, R.; Goh, S. M. P.; Xu, A.; Yap, L. W.; Cheong, I., Calibrated liposomal release of the anti-mitotic agent BI-2536 increases the targeting of mitotic tumor cells. *Eur J Pharm Biopharm* **2020**, *157*, 183-190.

15. Galant, O.; Bae, S.; Silberstein, M. N.; Diesendruck, C. E., Highly Stretchable Polymers: Mechanical Properties Improvement by Balancing Intra- and Intermolecular Interactions. *Advanced Functional Materials* **2019**, *30* (18).
16. Galant, O.; Bae, S.; Wang, F.; Levy, A.; Silberstein, M. N.; Diesendruck, C. E., Mechanical and Thermomechanical Characterization of Glassy Thermoplastics with Intrachain Cross-Links. *Macromolecules* **2017**, *50* (17), 6415-6420.
17. Blay, V.; Tolani, B.; Ho, S. P.; Arkin, M. R., High-Throughput Screening: today's biochemical and cell-based approaches. *Drug Discov Today* **2020**, *25* (10), 1807-1821.
18. Inglese, J.; Johnson, R. L.; Simeonov, A.; Xia, M.; Zheng, W.; Austin, C. P.; Auld, D. S., High-throughput screening assays for the identification of chemical probes. *Nature Chemical Biology* **2007**, *3* (8), 466-479.
19. Offenloch, J. T.; Blasco, E.; Bastian, S.; Barner-Kowollik, C.; Mutlu, H., Self-reporting visible light-induced polymer chain collapse. *Polymer Chemistry* **2019**, *10* (33), 4513-4518.
20. Galant, O.; Donmez, H. B.; Barner-Kowollik, C.; Diesendruck, C. E., Flow Photochemistry for Single-Chain Polymer Nanoparticle Synthesis. *Angew Chem Int Ed Engl* **2021**, *60* (4), 2042-2046.
21. Harth, E.; Horn, B. V.; Lee, V. Y.; Germack, D. S.; Gonzales, C. P.; Miller, R. D.; Hawker, C. J., A Facile Approach to Architecturally Defined Nanoparticles via Intramolecular Chain Collapse. *Journal of the American Chemical Society* **2002**, *124* (29), 8653-8660.
22. Kroger, A. P. P.; Hamelmann, N. M.; Juan, A.; Lindhoud, S.; Paulusse, J. M. J., Biocompatible Single-Chain Polymer Nanoparticles for Drug Delivery-A Dual Approach. *ACS Appl Mater Interfaces* **2018**, *10* (37), 30946-30951.
23. Nair, D. P.; Podgórski, M.; Chatani, S.; Gong, T.; Xi, W.; Fenoli, C. R.; Bowman, C. N., The Thiol-Michael Addition Click Reaction: A Powerful and Widely Used Tool in Materials Chemistry. *Chemistry of Materials* **2013**, *26* (1), 724-744.
24. He, L.; Szameit, K.; Zhao, H.; Hahn, U.; Theato, P., Postpolymerization modification using less cytotoxic activated ester polymers for the synthesis of biological active polymers. *Biomacromolecules* **2014**, *15* (8), 3197-205.
25. Niu, J.; Page, Z. A.; Dolinski, N. D.; Anastasaki, A.; Hsueh, A. T.; Soh, H. T.; Hawker, C. J., Rapid Visible Light-Mediated Controlled Aqueous Polymerization with In Situ Monitoring. *ACS Macro Lett* **2017**, *6* (10), 1109-1113.
26. Eberhardt, M.; Mruk, R.; Zentel, R.; Théato, P., Synthesis of pentafluorophenyl(meth)acrylate polymers: New precursor polymers for the synthesis of multifunctional materials. *European Polymer Journal* **2005**, *41* (7), 1569-1575.
27. Gee, K. R.; Archer, E. A.; Kang, H. C., 4-Sulfotetrafluorophenyl (STP) esters: New water-soluble amine-reactive reagents for labeling biomolecules. *Tetrahedron Letters* **1999**, *40* (8), 1471-1474.
28. Zambianchi, M.; Maria, F. D.; Cazzato, A.; Gigli, G.; Piacenza, M.; Sala, F. D.; Barbarella, G., Microwave-Assisted Synthesis of Thiophene Fluorophores, Labeling and Multilabeling of Monoclonal Antibodies, and Long Lasting Staining of Fixed Cells. *Journal of the American Chemical Society* **2009**, *131* (31), 10892-10900.
29. Movilli, J.; Rozzi, A.; Ricciardi, R.; Corradini, R.; Huskens, J., Control of Probe Density at DNA Biosensor Surfaces Using Poly(l-lysine) with Appended Reactive Groups. *Bioconjug Chem* **2018**, *29* (12), 4110-4118.
30. Klykov, O.; Weller, M. G., Quantification of N-hydroxysuccinimide and N-hydroxysulfosuccinimide by hydrophilic interaction chromatography (HILIC). *Analytical Methods* **2015**, *7* (15), 6443-6448.
31. Dahlman, J. E.; Kauffman, K. J.; Xing, Y.; Shaw, T. E.; Mir, F. F.; Dlott, C. C.; Langer, R.; Anderson, D. G.; Wang, E. T., Barcoded nanoparticles for high throughput in vivo discovery of targeted therapeutics. *Proc Natl Acad Sci U S A* **2017**, *114* (8), 2060-2065.

32. Potyrailo, R.; Rajan, K.; Stoewe, K.; Takeuchi, I.; Chisholm, B.; Lam, H., Combinatorial and high-throughput screening of materials libraries: review of state of the art. *ACS Comb Sci* **2011**, *13* (6), 579-633.
33. Weterings, J.; Rijcken, C. J. F.; Veldhuis, H.; Meulemans, T.; Hadavi, D.; Timmers, M.; Honing, M.; Ippel, H.; Liskamp, R. M. J., TMTHSI, a superior 7-membered ring alkyne containing reagent for strain-promoted azide-alkyne cycloaddition reactions. *Chem Sci* **2020**, *11* (33), 9011-9016.
34. Benito, A. B.; Aiertza, M. K.; Marradi, M.; Gil-Iceta, L.; Shekhter Zahavi, T.; Szczupak, B.; Jimenez-Gonzalez, M.; Reese, T.; Scanziani, E.; Passoni, L.; Matteoli, M.; De Maglie, M.; Orenstein, A.; Oron-Herman, M.; Kostenich, G.; Buzhansky, L.; Gazit, E.; Grande, H. J.; Gomez-Vallejo, V.; Llop, J.; Loinaz, I., Functional Single-Chain Polymer Nanoparticles: Targeting and Imaging Pancreatic Tumors in Vivo. *Biomacromolecules* **2016**, *17* (10), 3213-3221.
35. Gracia, R.; Marradi, M.; Cossío, U.; Benito, A.; Pérez-San Vicente, A.; Gómez-Vallejo, V.; Grande, H. J.; Llop, J.; Loinaz, I., Synthesis and functionalization of dextran-based single-chain nanoparticles in aqueous media. *Journal of Materials Chemistry B* **2017**, *5* (6), 1143-1147.
36. Xiao, K.; Li, Y.; Luo, J.; Lee, J. S.; Xiao, W.; Gonik, A. M.; Agarwal, R. G.; Lam, K. S., The effect of surface charge on in vivo biodistribution of PEG-oligocholeic acid based micellar nanoparticles. *Biomaterials* **2011**, *32* (13), 3435-46.
37. He, C.; Hu, Y.; Yin, L.; Tang, C.; Yin, C., Effects of particle size and surface charge on cellular uptake and biodistribution of polymeric nanoparticles. *Biomaterials* **2010**, *31* (13), 3657-66.
38. Yamamoto, Y.; Nagasaki, Y.; Kato, Y.; Sugiyama, Y.; Kataoka, K., Long-circulating poly(ethylene glycol)-poly(D,L-lactide) block copolymer micelles with modulated surface charge. *Journal of Controlled Release* **2001**, *77* (1), 27-38.
39. Hillaireau, H.; Couvreur, P., Nanocarriers' entry into the cell: relevance to drug delivery. *Cell Mol Life Sci* **2009**, *66* (17), 2873-96.
40. Meng, F.; Wang, J.; Ping, Q.; Yeo, Y., Quantitative Assessment of Nanoparticle Biodistribution by Fluorescence Imaging, Revisited. *ACS Nano* **2018**, *12* (7), 6458-6468.
41. Liu, Y.; Tseng, Y. C.; Huang, L., Biodistribution studies of nanoparticles using fluorescence imaging: a qualitative or quantitative method? *Pharm Res* **2012**, *29* (12), 3273-7.
42. Adhipandito, C. F.; Cheung, S. H.; Lin, Y. H.; Wu, S. H., Atypical Renal Clearance of Nanoparticles Larger Than the Kidney Filtration Threshold. *Int J Mol Sci* **2021**, *22* (20).
43. Chen, P. R.; Wang, T. C.; Chen, S. T.; Chen, H. Y.; Tsai, W. B., Development of Antifouling Hyperbranched Polyglycerol Layers on Hydroxyl Poly-p-xylylene Coatings. *Langmuir* **2017**, *33* (51), 14657-14662.
44. Weinhart, M.; Grunwald, I.; Wyszogrodzka, M.; Gaetjen, L.; Hartwig, A.; Haag, R., Linear poly(methyl glycerol) and linear polyglycerol as potent protein and cell resistant alternatives to poly(ethylene glycol). *Chem Asian J* **2010**, *5* (9), 1992-2000.

Samenvatting

Onderzoek in de afgelopen 20 jaar heeft aangetoond dat middels het intramoleculair koppelen van polymeren goed gedefiniëerde enkel-keten polymeer nanodeeltjes (Engels: Single-Chain polymer Nanoparticles, SCNPs) gevormd kunnen worden. Deze deeltjes hebben een grootte van rond de 10 nm, wat vergelijkbaar is eiwitten. SCNPs kunnen worden uitgerust met een grote verscheidenheid aan functionaliteiten, hoewel de functionalisatiestap, en voornamelijk de kwantificatie ervan niet evident is. Dit proefschrift beschrijft een methode voor het vormen van SCNPs met gemakkelijk modificeerbare oppervlaktegroepen, om zo reeksen van functionele nanodeeltjes te kunnen maken en bestuderen voor biomedische toepassingen. Als eerste in **Hoofdstuk 1** beschrijven we de huidige methoden die er zijn om het oppervlak van SCNPs te modificeren.

In **Hoofdstuk 2** beschrijven we de synthese van SCNPs met actieve ester groepen (pentafluorophenyl esters, PFP). Deze actieve esters kunnen op milde en kwantitatieve wijze worden gesubstitueerd door functionele liganden met een amine-groep. In dit hoofdstuk wordt een reeks van SCNPs beschreven met toenemende incorporatie van een protoneerbare tertiaire amine, om zo tot een set SCNPs te komen met een zeta potentiaal die loopt van negatief tot positief. Deze set werd onderzocht op endotheelcellen, waarbij geen significante toxiciteit werd gemeten bij gangbare concentraties, zelfs niet voor de deeltjes met grootste hoeveelheid tertiaire amines. Door middel van flow cytometrie werd aangetoond dat de cellulaire opname sterk afhankelijk is van de oppervlaktefunctionalisatie. SCNPs met een kleine hoeveelheid tertiaire amines vertoonden lage cellulaire opname, met als cellulaire eindbestemming het lysosoom. Deeltjes met een hogere hoeveelheid tertiaire amines vertoonden significant hogere cellulaire opname, waarbij confocale microscopie uitwees dat deze deeltjes terecht kwamen in het cytosol.

De set van SCNPs met toenemende hoeveelheid tertiaire amines wordt in **Hoofdstuk 3** onderzocht in een bloed-hersenbarriere model. Alle SCNPs vertoonden een zeer hoge mate van transcytose, vergeleken met een andere nanostructuren, getest op een vergelijkbaar model. Zoals al beschreven in **Hoofdstuk 2**, vertoonden de deeltjes met de hoogste oppervlakte-lading tevens opname in het cytosol. Deze opname ging ten koste van de transcytose, die licht afneemt naarmate het aantal tertiaire amines op het oppervlak toeneemt. Een gangbare hypothese voor het bereiken van het cytosol door nanostructuren is het

'proton sponge effect'. Na opname in het endosoom ontstaat een influx van protonen in het endosoom, wat zorgt voor een cascade aan instroom van andere ionen. Hierdoor barst het endosoom ten gevolge van de toegenomen osmotische druk en komen de nanostructuren vrij. Om dit te testen, werd de initiële influx van protonen geblokkeerd. Deze blokkade zorgde voor een vermindering van SCNPs in het cytosol, maar volledig voorkomen werd dit niet, wat aangeeft dat het 'proton sponge effect' slechts een deel van de cytosolische afgifte verklaart.

In **Hoofdstuk 4** wordt de functionalisatiestrategie uit **Hoofdstuk 2** gecombineerd met gecontroleerde medicijnafgifte. Hiervoor werd het anti-kanker middel atovaquone geconjugerd aan de SCNPs en het oppervlak gefunctionaliseerd met 15 of 40% tertiaire amines, alsmede met 40% quaternaire ammoniumgroepen. Daar waar de deeltjes met 15 % tertiaire amines een lage mate van cellulaire opname (in HeLa cellen) vertoonden, met co-localisatie in het endosoom, bereikten de 40 % deeltjes het cytosol, zoals al gezien in de **Hoofdstukken 2** en **3**. Interessant genoeg, hoewel de SCNPs met 40 % quaternaire ammonium groepen zeer hoge cel-associatie vertoonden, bleek uit microscopie experimenten dat deze deeltjes vast zaten in het celmembraan en zich dus niet intracellulair bevonden. Daarnaast lieten louter de SCNPs met 40 % tertiaire amines op het oppervlak afname zien van de hoeveelheid HeLa kankercellen. Dit toont duidelijk aan hoe belangrijk de intracellulaire locatie is voor de effectiviteit van anti-kanker middelen.

In **Hoofdstuk 5** hebben we de functionalisatiestrategie uitgebreid door actieve ester chemie te combineren met de koper-gekatalyseerde azide-alkyn-Huisgen-cycloadditie (klikchemie). Hiertoe werden de deeltjes gefunctionaliseerd met een toenemende hoeveelheid amino-alkynen, welke vervolgens werden geconjugerd met een azido-glucose via twee verschillende posities. Toename van alkynen op het oppervlak leidde tot toegenomen hoeveelheid verknoping, wat aangeeft dat de reactiecondities goed gecontroleerd moeten worden. Studies met een model lectine (Concanavaleine A) toonden aan dat de conjugatiepositie bepaalt of er associatie kan plaatsvinden met het lectine. Opname studies op kankercellen (HeLa) lieten zien dat er geen onderscheid is tussen de conjugatiepositie, maar dat de dichtheid bepalend is voor de hoeveelheid opname.

In **Hoofdstuk 6** beschrijven we manieren om de SCNPs productie op te schalen en nieuwe potentiële functionalisatie methodes, om zo grotere sets van deeltjes met uitgebreidere functionalisatiegraden te kunnen synthetiseren. Als laatste beschrijven we een *in vivo* studie, waarbij de deeltjes uit **Hoofdstuk 2** hebben onderzocht in een muismodel. Hieruit bleek dat ondanks de geringe grootte, de deeltjes na 24 uur nog steeds te vinden waren in het lichaam. Toename van de oppervlaktelading leidde tot een verhoogde opname in de lever en milt, wat een indicatie is dat er opsonisatie door macrofagen plaatsvindt.

Summary

Research over the past 20 years has shown that by intramolecularly crosslinking of polymers, well-defined single-chain polymer nanoparticles (**SCNPs**) can be formed. These particles have a size of around 10 nm, which is similar to proteins. SCNPs can be equipped with a wide variety of functionalities, although the functionalization step, and mainly its quantification, is not straightforward. This thesis describes a method for creating SCNPs with easily modifiable surface groups, to synthesize and study sets of functional nanoparticles for biomedical applications. In **Chapter 1**, we first describe the current methods available for modifying the surface of SCNPs.

In **Chapter 2**, we describe the synthesis of SCNPs with active ester groups (pentafluorophenyl esters, PFP). These active esters can be substituted by functional ligands with an amine group in a mild and quantitative manner. In this chapter, a series of SCNPs is described with increasing incorporation of a protonatable tertiary amine, resulting in a set of SCNPs with a zeta potential ranging from negative to positive. This set was studied in endothelial cells, where no significant toxicity was observed at common concentrations, even for particles with the highest amount of tertiary amines. Flow cytometry showed that cellular uptake is strongly dependent on surface functionalization. SCNPs with a small amount of tertiary amines exhibited low cellular uptake, with their cellular fate being the lysosome. Particles with a higher amount of tertiary amines showed significantly higher cellular uptake, and confocal microscopy revealed that these particles reached the cytosol.

Chapter 3 investigates the set of SCNPs with increasing amounts of tertiary amines in a blood-brain barrier model. All SCNPs showed a very high degree of transcytosis compared to other nanostructures tested on a similar model. As described in **Chapter 2**, particles with the highest surface charge also exhibited cytosolic uptake. This uptake however is at the expense of transcytosis, which is slightly reduced upon increasing the number of tertiary amines on the surface. The "proton sponge effect" is a common hypothesis for nanostructures entering the cytosol. After uptake into the endosome, there is an influx of protons, leading to increased osmotic pressure and endosome rupture, releasing the nanostructures. To test this, the initial proton influx was blocked, resulting in a reduction of SCNPs in the cytosol, but complete prevention was not achieved, suggesting that the "proton sponge effect" only partly explains cytosolic delivery.

Chapter 4 combines the functionalization strategy from **Chapter 2** with controlled drug delivery. The anticancer drug atovaquone was conjugated to the SCNPs, and the surface was functionalized with 15% or 40% tertiary amines and 40% quaternary ammonium groups. While particles with 15% tertiary amines showed low cellular uptake (in HeLa cells) with endosomal co-localization, the 40% particles reached the cytosol, as seen in **Chapters 2** and **3**. Interestingly, despite the high cell association of SCNPs with 40% quaternary ammonium groups, microscopy experiments showed that these particles were trapped in the cell membrane and did not reside intracellularly. Furthermore, only SCNPs with 40% tertiary amines on the surface exhibited a decrease in the number of HeLa cancer cells. This clearly demonstrates the importance of intracellular location for the effectiveness of anticancer drugs.

In **Chapter 5**, we expanded the functionalization strategy by combining active ester chemistry with copper-catalyzed azide-alkyne Huisgen cycloaddition (click chemistry). The particles were functionalized with an increasing amount of amino-alkynes, which were then conjugated with azido-glucose via two different positions. Increasing alkynes on the surface led to an increased amount of crosslinking, indicating the need for well-controlled reaction conditions. Studies with a model lectin (Concanavalin A) showed that the conjugation position determined whether association with the lectin could occur. Uptake studies on cancer cells (HeLa) showed no distinction between conjugation positions, but that the density determined the amount of uptake.

Chapter 6 describes ways to scale up SCNPs production and explore new potential functionalization methods, allowing for the synthesis of larger sets of particles with more extensive degrees of functionalization. Finally, we describe an in vivo study in which the particles from **Chapter 2** were investigated in a mouse model. Despite their small size, the particles were still present in the body after 24 hours. Increasing surface charge led to increased uptake in the liver and spleen, indicating opsonization by macrophages.

Dankwoord

En dan eindigen we een dikke vier jaar onderzoek, resulterend in een kleine 140 pagina's, met het met afstand kortste en meest gelezen stukje uit dit boekwerk: het dankwoord. Onderzoek doe je praktisch gezien het grootste gedeelte van de tijd alleen, maar eigenlijk werk je constant samen met alles en iedereen, en zonder een heleboel verschillende mensen die mij hebben bijgestaan was het nooit gelukt. En 3 mol cafeïne.

Allereerst wil ik Jos bedanken. Begonnen met een labcourse, doorgaand in een stage bij Akzo, vervolgens afstuderen en eindigend met dit boekje. Bedankt dat de deur altijd openstond voor raad en daad, korte vragen en overlegjes, die vaak toch wel eindigden in lange overleggen, al dan niet gelardeerd met quotes uit Heat. Jouw betrokken manier van begeleiden met tegelijkertijd heel veel vrijheid heeft er voor gezorgd dat we lekker ons gang konden gaan op het lab, veel dingen hebben kunnen proberen, maar dat er toch uiteindelijk wel resultaten uit kwamen. Bedankt ook voor alle niet werk-gerelateerde adviezen, de congressen (de ESCDD dan ;) en namens de kinderen: bedankt voor de paw patrollers. Jeroen, bedankt voor de supervisie en discussies tijdens de BNT meetings.

I would like to thank my committee members: Prof. dr. Grijpma, dr. Klinger, dr. ir. Lindhoud, prof. dr. Mastrobattista and prof. dr. ir. Palmans for their time for reading my thesis and participating in the defence.

Ik ben extreem blij met mijn paranimfen, twee van de mensen die ik toch ongeveer het allerlangste (pun intended) ken van deze wereld. Pap en Siem, fijn dat jullie vandaag naast mij willen staan en zitten.

Niens, bedankt voor het ontwerpen van een fantastische cover op basis van mijn omschrijving: iets met groen en een zeshoek.

Mijn ganse proefschrift bestaat uit samenwerkingen met Naomi en ik had geen betere partner kunnen bedenken. Vijf jaar lang back-to-back in lab 4; ik heb er erg van genoten. Sorry voor alle overlast van de slechte Nederlandstalige muziek (hoewel ik daar ook wel last van had). En nog steeds onder de indruk van de hoeveelheid experimenten die jij kon verzetten in de tijd dat ik slechts één synthese kon verkloten.

Sandra, du coup, de enige persoon in de academische wereld die zeven studenten tegelijk kan begeleiden. Bedankt voor alle gezelligheid en het luisterende oor als ik (weer) wat te zoeken had. En de ontelbare pogingen mij ergens voor uit te nodigen. ;) Never change!

Door de jaren hebben we een bonte verzameling PhDs/Post-docs en BSc/MSc studenten gehad binnen de JP groep. Allereerst natuurlijk Pia, de mater familias. I remember signing up for your labcourse in the summer of 2016 while visiting Sainte-Enimie, never realizing (of course not) this would eventually lead to this thesis. Thanks for all the fun, teaching me how to stop dwelling on details and how to survive the Dutch Polymer Days. Dan Jonathan, de man met de beste én slechtste muzieksmaak van Oost-Nederland. Was lachen, met toch wel als hoogtepunten Mainz, Schweinshaxe en een avondje onderwerelt. En de formule op mach 10 door lab 4 blazen. Min, was nice having you around, hope you are doing well, although I do not miss your DLS plots ;) Nergiz, nasilsin, I hope the 881 in Turkey tastes as good as here. Laïs, thanks for the work on the BBB! Gigi, mijn respect hoe je uiteindelijk je PhD hebt afgerond. Dan mijn eigen studenten, Jamie, Jurriaan en Anuradha. Ik wens jullie het allerbeste voor de toekomst. En een eervolle vermelding voor Diana, dankzij wie ik nooit meer een lift heb genomen.

Op de afdeling is een groep mensen zonder wie er eigenlijk niets zou gebeuren en dat zijn de technicians. Bedankt Marcel, Richard, Regine, Bianca en Niels voor het draaiende houden van het lab en het toestaan dat ik de storage room kon gebruiken als een soort self-service supermarkt (zonder de kassacontrole gelukkig). De andere groep onmisbaren zijn Nicole en Izabel. Bedankt voor al het administratieve geregel!

Then of course all the people from BNT/MNF/HMOE over the years. I have seen a lot come and go and wish you all the best for the future (and yes, you will finish).

M9, ondertussen alweer zo'n 25 jaar geleden (man o man) dat we bij elkaar in de klas kwamen. Fijn dat jullie in zulke getale aanwezig zijn vandaag.

Thijs, Thomas, Spithaard, Maurits, John, Drukker, Roel, Willum, Tino, Sipco, Wösten, Felix en Flip, niet direct per se de allergrootste bijdrage aan de totstandkoming van dit boekwerk, maar toch zeker een vermelding waardig.

Al mijn familie: Paatsen, Kroezen, van Tuikwerds, de Vliegers, van Dussens, een Schoonen, een Jansen, een Kies en een van der Zee. Bedankt voor alle mentale support en sorry dat ik eigenlijk nooit helemaal goed heb kunnen uitleggen wat ik deed (zelf wist ik het echt wel hoor ;)).

Pap, mam, Marthe, die van alle bovengenoemden het allermeeste hebben betekend.
Ik weet niet eens hoe ik dat moet opschrijven.

Noes, Roos en Guussie, altijd en altijd.

